



Review

A Comprehensive Review of Li-Ion Battery Materials and Their Recycling Techniques

Hee-Je Kim ^{1,*}, TNV Krishna ¹, Kamran Zeb ¹, Vinodh Rajangam ¹, Chandu V. V. Muralee Gopi ², Sangaraju Sambasivam ³, Kummara Venkata Guru Raghavendra ^{1,*} and Ihab M. Obaidat ^{3,*}

¹ School of Electrical Engineering, Pusan National University, Busandaehak-ro 63beon-gil, Geumjeong-gu, Busan 46241, Korea; vamsik.tirumalasetty@gmail.com (T.K.); kami_zeb@yahoo.com (K.Z.); vinoth6482@gmail.com (V.R.)

² Photonics Laboratory, Division of Computer, Electrical, and Mathematical Sciences and Engineering, King Abdullah University of Science and Technology (KAUST), Thuwal Jeddah 23955-6900, Saudi Arabia; naga5673@gmail.com

³ Department of Physics, United Arab Emirates University, Al Ain 15551, UAE; sambaphy@gmail.com

* Correspondence: heeje@pusan.ac.kr (H.-J.K.); kvg.raghavendra999@gmail.com (K.V.G.R.); iobaidat@uaeu.ac.ae (I.M.O.); Tel.: +82-51-510-2364 (H.-J.K.); Fax: +82-51-513-0212 (H.-J.K.)

Received: 15 May 2020; Accepted: 15 July 2020; Published: 17 July 2020



Abstract: In the context of constant growth in the utilization of the Li-ion batteries, there was a great surge in the quest for electrode materials and predominant usage that lead to the retiring of Li-ion batteries. This review focuses on the recent advances in the anode and cathode materials for the next-generation Li-ion batteries. To achieve higher power and energy demands of Li-ion batteries in future energy storage applications, the selection of the electrode materials plays a crucial role. The electrode materials, such as carbon-based, semiconductor/metal, metal oxides/nitrides/phosphides/sulfides, determine appreciable properties of Li-ion batteries such as greater specific surface area, a minimal distance of diffusion, and higher conductivity. Various classifications of the anode materials such as the intercalation/de-intercalation, alloy/de-alloy, and various conversion materials are illustrated lucidly. Further, the cathode materials, such as nickel-rich $\text{LiNi}_x\text{Co}_y\text{Mn}_z\text{O}_2$ (NCM), were discussed. NCM members such as NCM 333, NCM 523 that enabled to advance for NCM622 and NCM81 are reported. The nanostructured materials bridged the gap in the realization of next-generation Li-ion batteries. Li-ion batteries' electrode nanostructure synthesis, performance, and reaction mechanisms were considered with great concern. The serious effects of Li-ion batteries disposal need to be cut significantly to reduce the detrimental effect on the environment. Hence, the recycling of spent Li-ion batteries has gained much attention in recent years. Various recycling techniques and their effect on the electroactive materials are illustrated. The key areas covered in this review are anode and cathode materials and recent advances along with their recycling techniques. In light of crucial points covered in this review, it constitutes a suitable reference for engineers, researchers, and designers in energy storage applications.

Keywords: Li-ion batteries; cathode materials; anode materials; recycling techniques; next-generation Li-ion batteries

1. Introduction

Due to the dramatic evolution in the field of energy storage devices, in recent times, the need for efficient rechargeable batteries has been of paramount importance. Advancements and progress has been made in the development of lightweight batteries. Therefore, many studies are focusing on the sophisticated technologies in manufacturing the batteries for many applications [1]. Further,

scientific research has also enhanced the investigations for batteries' manufacturing units [2]. The Sony Co. made its first kind lithium-ion battery that was dominantly sold for about thirty years. The LIB upheaval in wearable electronics prompted a strong interest in investigations in the following years. In addition to this concern, governments around the world have become more aware of the role of greenhouse gases in climate change and have supported several ingenuities in the field of green energy technologies (solar, wind, etc.) and electric vehicles with energy-saving systems. The future for the LIB expedition has been dominantly decided by wearable electronics, which have recently become more popular. Moreover, environmental concerns are vital in curbing the greenhouse gases, so there has been a need for green energy technologies such as solar, wind, etc., and substituting automotive with electric vehicles will save energy. Researchers these days have introduced many remarkable parameters correlating to battery weight, size, augmented life span, security, and diminished cost that were considered an obligation in the manufacturing of batteries [3–5]. Regarding LIBs, the progression and a wide range of applications with higher specific energy, greater coulombic efficiency, lower self-discharge phenomenon, and many reagents in different versions of electrodes are shown in Figure 1 [6–9].

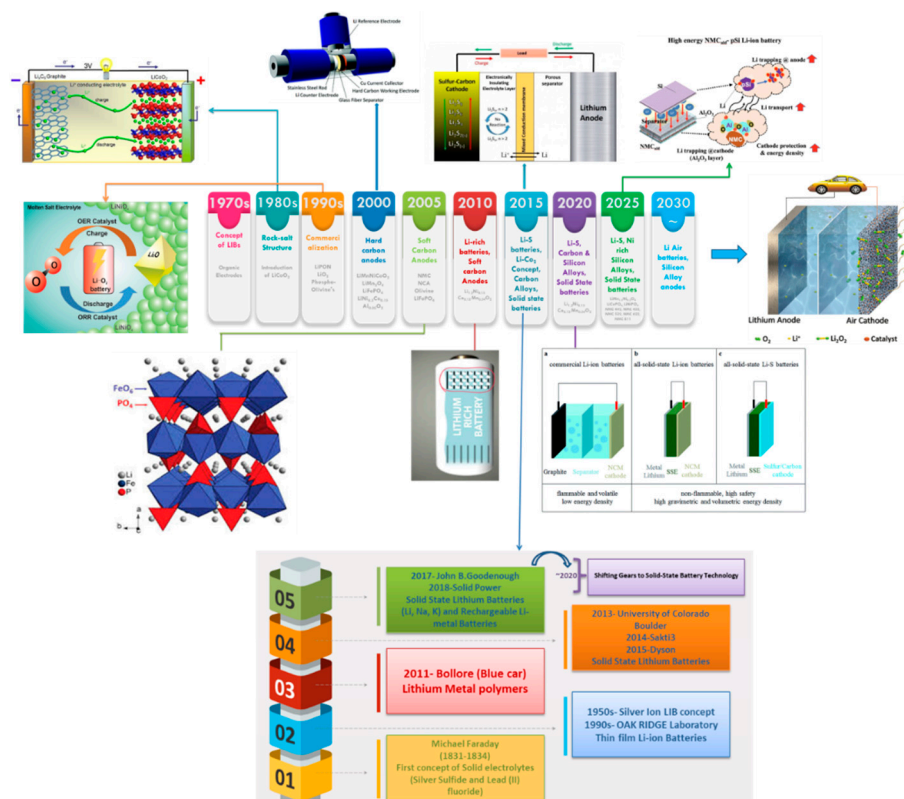
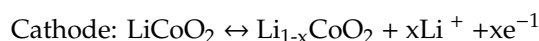
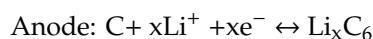


Figure 1. Historical evolution and advances of Lithium-ion battery technologies.

Moreover, there has been a strong trend in the assembly of the next generation superior charge and yielding higher power LIBs shown in Figure 1, which were specially designed for electric vehicles (EVs), hybrid electric vehicles (HEVs), electric appliances, and space applications. For instance, the conventional Li solar batteries have mainly relied on an Li^+ intercalation mechanism (e.g., LiFePO_4 , LiCoO_2 , and LiMn_2O_4) that has relatively lower charging capacities ($<200 \text{ mA}\cdot\text{h}\cdot\text{g}^{-1}$) for targeted application [10,11]. Therefore, attention has shifted to manufacturing technologies for high energy density batteries, namely Li-rich ($\text{Li}_{1.2}\text{Mn}_{0.54}\text{Ni}_{0.13}\text{Co}_{0.13}\text{O}_2$) and Nickel-rich transition metal oxides (e.g., $\text{LiNi}_{0.8}\text{Co}_{0.15}\text{Al}_{0.05}\text{O}_2$ or $\text{Li}[\text{Ni}_{0.8}\text{Co}_{0.1}\text{Mn}_{0.1}]\text{O}_2$), enhanced voltage rotation and Li Air, Li Sulfur, Li CO_2 , organic electrode and solid state batteries. These batteries also have additional benefits, such as higher payloads, lower costs, lower toxicity (compared to LiCoO_2). However, there are critical

issues that can be addressed such as the commercialization concern, electrolyte resolution, phase transition, solid electrolyte interface (SEI) formation, particle surface reconstruction, and volume expansion, charging of the electroactive material, and electrodes during the charging and discharging phenomenon [7,8]. In contrast, a hybrid device that combines both solar cells and LIB and can often be considered as an independent power system has gained a lot of attention recently [12].

The energy density of the LIBs can commonly be improved by high voltage active cathode materials, anode materials, and electrodes. One of the key issues regarding high voltage cathodes and LIBs is the decomposition of the electrolyte at more than 4.2 V Li/Li⁺ [13–19]. Hence, to develop Li-ion conductivity, the stability of the material succeeding the electrolyte can also be considered as a crucial electrochemical parameter in the implementation of next-generation devices that hold higher cell potential. In this regard, much research has been made on augmenting the performance of the LIBs with both organic and inorganic materials [20–33]. The importance of the LIBs can be seen on the cathode side, i.e., transition oxides or phosphates such as LiCoO₂, LiMn₂O₄, LiCo_{1/3}Mn_{1/3}Ni_{1/3}O₂, LiFePO₄, etc., where graphite can mostly be employed as the anode material. By construction, the cathode and anode are separated using a membrane of polypropylene/ polyethylene by electrolyte incorporated with the salts of lithium (i.e., LiPF₆) and organic alkyl carbonates, namely propylene, ethylene, dimethyl carbonate, etc. The separator prevents the electrical contact in between the electrodes, concurrently allowing the Li-ion's diffusion from the cathode to anode during charging and discharging. Eventually, it can be inferred as the anode/cathode Li-ion current that can be transformed into chemical energy and further to electricity. For instance, the LiCoO₂ chemical mechanism can be illustrated by the following reactions:



For electroactive materials to be considered as latent candidates for LIBs, the immediate requirement is to obtain the reversible capacity, excellent ionics, conductivity, good life span, excellent diffusion rate of lithium into active materials, as shown in Figure 2. The most frequently implemented cathodic materials are LiFePO₄, LiMn₂O₄, and LiCoO₂ [31–34], whereas the graphite is a widespread anode material [20–23] since it possesses excellent features such as the flat and low operating potential vs. lithium, low cost, and excellent life cycle. Moreover, the graphite permits the intercalation of only single Li with the 6 carbon atoms that result in the stoichiometry of LiC₆, providing the equivalent reversible specific capacity of 372 mA h g⁻¹. Further, the rate of diffusion for the lithium and carbon materials is between 10⁻¹² and 10⁻⁶ cm² s⁻¹ whereas for graphite it lies in the range 10⁻⁹ to 10⁻⁷ cm²·s⁻¹, leading to the production of energy-efficient batteries [35,36]. Therefore, it is urgent to replace graphite anodes on materials with higher capacity, energy, and power density. Various electrode materials for LIBs have been depicted in Figure 2.

Although lithium metal possesses the highest capacities in anode materials (3860 mA·h·g⁻¹), the major issues with employing the lithium as the anode material are safety issues in secondary batteries. This is because of the formation of dendrites in the lithium metal that could enable an easy path among the cathode and anode [6,37,38]. Hence, obtaining the greater energy and power densities are considered as a huge challenge in selecting the appropriate anode materials that can assure higher capacities and quick diffusion of the Li-ion to the anode side, coupled with greater life span and without safety issues. Much research has been conducted in both the carbon and non-carbon materials to obtain the higher performance of anode in the LIBs. In brief, the carbon and other materials can be inferred with the nanofibers of carbon (450 mA·h·g⁻¹) [39], carbon nanotubes (1100 mA·h·g⁻¹) [40], carbon porous materials (800–1100 mA·h·g⁻¹) [41] graphene (960 mA·h·g⁻¹) [42], silicon (4200 mA·h·g⁻¹) [43], SiO (1600 mA h g⁻¹) [44], tin (994 mA·h·g⁻¹) [45], germanium (1600 mA·h·g⁻¹) [46] and further transition metal oxides (500–1000 mA h g⁻¹) [47–49], etc. In addition, metal nitrides, sulfides, and phosphides [50–52] can also be used as the potential candidates for anodic materials, since they have a higher specific capacity of more than 500 mA h g⁻¹. To obtain the highly efficient anodes,

the coulomb's high expansion, low electron transportation, and low efficiency are considered as the major restrictions.

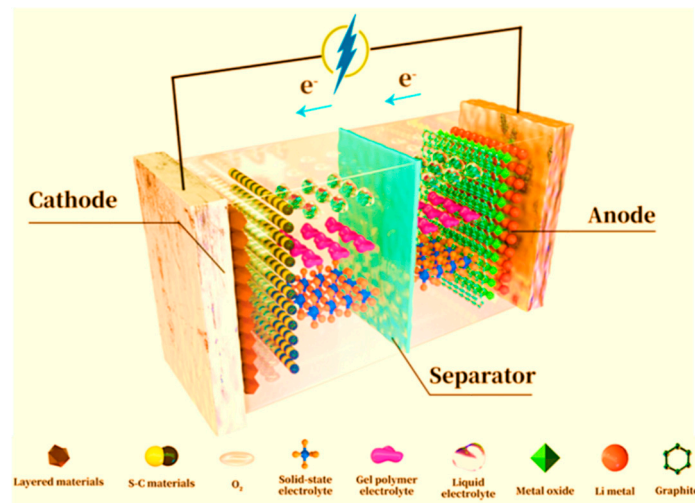


Figure 2. Schematic depiction of lithium insertion/de-insertion mechanism for current rechargeable lithium battery with various electrode materials.

The feasible solution for these kinds of issues is the morphological analysis structures of the above materials. Nano sizing and tailoring morphology can be considered as the key features to rely on novel materials that can be used to reduce the flaws and obtain a breakthrough for efficient technological discovery [53–56]. The major benefits that can be obtained by implementing the nanotechnology in LIBs can be summarized as follows [57–60].

- i. Active materials with a high surface to volume ratio to have more active sites that enhance the lithium storage and obtain a higher specific capacity. The higher flux of Li-ion at the interface of the Li-ions is available by the large surface area comprising the more areal contact with the electrolyte.
- ii. Because some reactions in the electrochemical setup are difficult to generate on a large scale, moving the nanoscale research of anode will overcome these limitations (e.g., bMnO_2).
- iii. Lithium has a good diffusion rate because of its reduced path length, enhancing the power capability of the battery.
- iv. There is a higher rate of electron transportation.

2. Challenges Associated with Li-Ion Batteries

The key challenges associated with the electrode materials of LIBs are enumerated along with their possible elucidations. According to the complications discussed below, the available capacity is supposed to reduce in comparison with the theoretical capacity. This is applicable in fewer instances because of lower energy density. This leads to greater polarization, which becomes intense in charge/discharge cycles along with the deprived life cycle following declining capacities.

2.1. Low Conductivity and Thermal Runway

It is a well-known fact that most electrode materials have minimal conductivities that influence the electron conductivity, resulting in less storage capacity of LIBs. In addition, it is essential that each material employed must possess sufficient capacity in order to compete the collection of electrons and their mobility in the external circuit. Moreover, pertaining to the intrinsic conductivities, many of the electroactive materials do not use the available redox sites since there are no pathways available for the mobility of the electrons between the redox sites and the external circuit [61].

This problem can be overcome to some extent by incorporating the carbon or associated highly conductive agents at the outlining or the inner surface [62]. Furthermore, the power of the battery relies on the internal impedance (inversely) and the emitted heat at the time of operation. The heat emitted in the LIBs is determined by three major factors, namely, Activation (interfacial kinetics), Concentration (species transportation), Ohmic losses (diffusion of electrons). The main reason for the heat emissions is the irreversibility of the battery and the electrochemical behavior. The species concentration also affects the generated heat, which is comparatively lower in well-constructed batteries [63]. Hence, a focus on the appropriate cell chemistry and control over the voltage can fix the thermal issues.

2.2. Morphological and Structural/Phase Changes

Morphology is a key concern in the LIBs, since it can deviate the Li insertion/extraction. It can radically affect the performance and life cycle. In addition, variations in phase or morphology can accumulate more isolated products, causing the electrical contact loss that obliterates the cell operation. The morphological deviations obtain a fresh material surface which is in contact with the electrolyte, reconstructing the solid electrolyte interface layer (SEI) that leads to the irreparable capacity loss [64]. In addition to morphological deviations, different materials display the crystal structure or phase variations through the electrode cycling process. Hence, the constructed crystal structure or phase can be used to enhance the LIBs capacity. The crystal structure variations can cause weaker electronic conductivity and inactive kinetics for Li insertion/extraction, resulting in poor capacities and life cycle [65]. These are intrinsic upon operation conditions. Nanoscience plays a crucial role in the nanostructure evolution that potentially diminishes the structural deviations by refined phase conversion kinetics.

2.3. Volume Changes and Thickness of Solid Electrolyte Interface Film

The variations of material volume by alloying/de-alloying with the Li^+ lead to the severe volume upsurge that causes more electrodes to be under strain. Hence, segregation of the material from the current collector leads to the short circuiting or electrical insulation of the cell. Because of this, the isolation of the Li^+ to access the redox active sites will cause capacity loss and poorer life cycle [66]. This unchangeable capacity loss is considered to be a vital part of battery operation that cannot be completely reduced, but helps to obtain a good control over SEI film thickness by surface chemistry. There are some problems connected with lowering the SEI film's mechanical strength; it cannot sustain any stress, and hence cannot endure pressure or stress. The breakdown of SEI film and fresh electrode surface exposure is dominantly predicted by the structural, morphological and volumetric variations. These results are seen in the electrolyte decomposition and capacity fading [67,68]. The regeneration of the SEI film (insulator by nature) enhances the dispersal path of the Li^+ . Until now, there no decent control mechanisms over the chemical composition, size of the grain, grain thickness and spatial SEI film distribution have been found. Hence, nanostructures affect a large surface area and energies. Controlling these factors or preserving the surface with the inactive metals or carbon coatings will enhance the control on SEI film.

2.4. Issues for Nanomaterials

Because of its compact particle size, the use of nanomaterials can lead to many new challenges, such as high surface area, low packing density and higher cost. A clear nanomaterial approach should address these shortcomings while addressing the challenges of micrometric materials. The formation of a layer of SEI on the electrode surface consumes electrolyte and lithium on the cathode during the battery cycle. Compared to electrodes of micrometer-sized materials, SEI formation on the surface of nanostructured electrodes consumes more electrolyte and lithium due to the larger electrode/electrolyte interface, leading to a lower initial Coulombic Efficiency, and reduces the overall capacity and energy density of the battery. Stable SEI is important for electrode life cycle durability, while specific SEI (electrode/electrolyte surface area) plays an important role in achieving high initial coulombic efficiency.

2.4.1. Cracking and Fracture of Particles and Electrodes

Traditional intercalation-type electrode materials experience minute or less volume variations (<10%) at the time of lithium insertion/extraction phenomenon. However, novel higher-capacity electrode materials generally possess greater variations in volume because of large amounts of lithium intake. The greater variation in the volume at charge/discharge phenomenon has been observed as a key issue in restricting high-capacity electrode materials applications since the late 1990s.

For instance, expansions in the volume of alloy type anodes are seen, for example, 420% for Si, 260% for Ge and Sn, and 300% for P. All are predominantly greater than 10% graphite anodes. Regarding the Li metal anodes, because of their hostless nature, the relative volume change can be virtually infinite. These drastic volume changes define the potential degrading of the active materials and electrodes at the time of cycling, significantly degrading the cycle life.

2.4.2. Solid–Electrolyte Interphase

The operating potential window of anode materials is lower than the reduction potential of organic carbonates, which normally operate in the lithium-based battery electrolytes (around ~1 V; potentials are versus Li^+/Li^0). At the time of battery charging, electrolyte reduction takes place and generates the SEI passive layer on the surface of the anode. The SEI is typically a conducting layer of lithium-ions but electronically an insulator that leads to the SEI growth termination with certain thickness. A stable SEI layer permits the higher coulombic efficiency and stability of an anode that has the merit of passivating the surface. Moreover, considering the repetition of large variations in volume on lithiation and delithiation, the interface of electrolyte/electrode shifts and significant fluctuations makes it a more challenging task to sustain the stable SEI for higher capacity electrodes.

2.4.3. Electron/ion Transport

A higher rate of charge transportation in the individual particles and as a whole electrode is a key to better efficiency. The high conductive paths for the electrons and minimal ion transport distance can help to achieve good capacity retention in order to activate the insulation of materials. When compared with the microscale materials, nanomaterials are smaller. For independent particles, Li-ion insertion/extraction and the transportation of the electrons because of the short transportation distances compared to micro particles. Conductive layer coating on active particles and the embedded particles in conductive matrices are the general routes to enhancing the conductivity for all the individual particles.

2.4.4. Long-Distance Electrode Atom/Molecule Movement

Basically, the traditional insertion type electrodes are stable hosts. They suffer bond breaking and exhibit the minimal structural changes and the lower expansion of volume (<10%) on lithium insertion or extraction. Some high capacitance materials undergo more bond breaking and resemble the huge crystallographic structural variations that are followed by the degradation of the structures. Hence, their usage in the Li based batteries is found to be impossible. These materials with high capacity face serious challenges for active diffusion of atom/molecule at the repeated charge/discharge processes because of the huge structural variation or even the phase variation in the solid, liquid and gas states, causing critical issues that are related to battery performances [69].

3. Anode Materials

3.1. Carbon Based Electroactive Materials

Carbon materials with different features and structures were identified as suitable for LIBs anode materials because of their properties such as easy access, thermal, mechanical, electrochemical stabilities, less price, and higher intercalation of lithium and reversible de-intercalation [70]. These properties

are considered to be crucial because of the materials we consider in the charged electrodes, or in the cathodes (de-lithiated)/anodes (lithiated) that tend to combine rigorously with the electrolytes of aqueous at the temperatures of higher scale. Some side effects shown at room temperature [71,72] such as the LiPF_6 reacting with moisture and tending to form HF. On the other hand, the as-formed HF reacts with any transition electrode material, which can lead to the deterioration of the capacity of the charge cycle. The final result is the slow degradation of both the active electrode material and the electrolyte as well as the formation of a thick passive layer on the electrode surface during cycling. In particular, when it comes to the anode, this layer is known as the Solid Electrolyte Interface (SEI). In this regard, the use of carbon coating on the active materials can provide a way to mitigate the mentioned drawbacks [61]. Carbon has limited activity against the electrolyte with minute potential and no oxidation occurs until the battery voltage starts to rise. Additionally, the high resistance of the HF corrosion can be obtained through the excellent chemical stability of the carbon. Finally, the carbon coating can also stop oxidation of the surface of materials in the atmosphere, especially at the nanoscale. Moreover, the nanostructured active materials possess a greater surface area that can enhance the surface oxidation. So, the carbon coating can significantly diminish the surface degradation at the time of accumulation and capacity reduction during the charging and discharging cycles [73]. A variety of recent anode materials for LIBs is shown in Table 1.

Table 1. Variety of Anode materials for Li-ion Batteries.

References	Anode Materials	Capacity (mA h g ⁻¹)	Merits	Remarks
[74–76]	Hard carbon	200–600	Excellent working potential	Less columbic efficiency
[77–80]	Carbon Nanotubes	1115	Cost-effective	Greater hysteresis voltage
[81]	Graphene	770/1115	Safe to operate	More irreversible capacity
[82]	LiTi_4O_5	176	Safer, Low cost	Lower capacities
	TiO_2	320	Greater power capability, good life cycle	Lower energy densities
[83,84]	Germanium	1623	Greater Specific Capacities, Greater Energy densities, Excellent safety	Lower irreversible capacity, More fading capacity, less life cycle
[85]	Silicon	4213		
[86]	Silicon oxide	1562		
[87]	Antimony	661		
[57]	Tin	992		
[88]	Tin oxide	793		
[88–90]	Metal Oxides (Co_3O_4 , CoO , MoO_2/O_3 , NiO , RuO_2 , Cr_2O_3)	500–1200	Large capacity, energy, Minimal cost, ecofriendly	Lower columbic efficiency, Unstable SEI formation, not good life cycle, more hysteresis potential.
[91–93]	Metal phosphides/nitrides and sulfides	500–1800	Greater capacities, lower potential, the lower polarization	Weak rate capability, short life span, higher production cost.

3.2. Carbon Nanotubes

CNTs are illustrated by the nanostructures of the robust arrangement of carbon nanostructures, obtained from the self-assembly of the phenomenon according to individual growth [94,95]. CNTs are categorized into the single-walled carbon nanotubes (SWCNTs) and multi-walled (MWCNTs) nanotubes. Both are well investigated as anodic and composite nanoarchitectures. When these are implemented with other active anodic materials, they demonstrate greater performance than the

non-CNT composites because of their greater electronic conductivity, excellent thermal and mechanical stabilities, and good rate of adsorption and the transportation facilities [95]. The experimental capacity that was obtained for the CNT was 1116 mA h g^{-1} for the SWCNTs in the stoichiometry of LiC_2 [77–80]. This can include the largest storage capacity of activated carbon-based materials and refers to the intercalation of lithium at stable sites on the surface of the pseudo graphic layers and the central tube. Moreover, experimental confirmation of predictions of theory accompanied by CNTs (lithium) is a big task ahead. Intense CNT research has been conducted on the anodes; several experiments were conducted with many simple methods and pre-treatments, namely acidic and spherical modification of the surface [77,94].

Recently, Di Leo et al. [96] studied SWCNTs that were made by the laser evaporation method and offered the highest performance of the LIBs resembling the enhanced capacities, approximately greater than 1050 mA h g^{-1} , depicted in Figure 3. Greater storage capacity of the lithium and improved battery life is obtained with the various nanostructured materials (such as Ge, Sn, Si, etc.) or oxides of metals (Mo, Ni, Fe, Cr, Cu, Mn) [97,98]. These hybrid systems enabled the CNTs to improve the electrical conductivity and smaller volume changes during the phenomenon of charge and discharge.

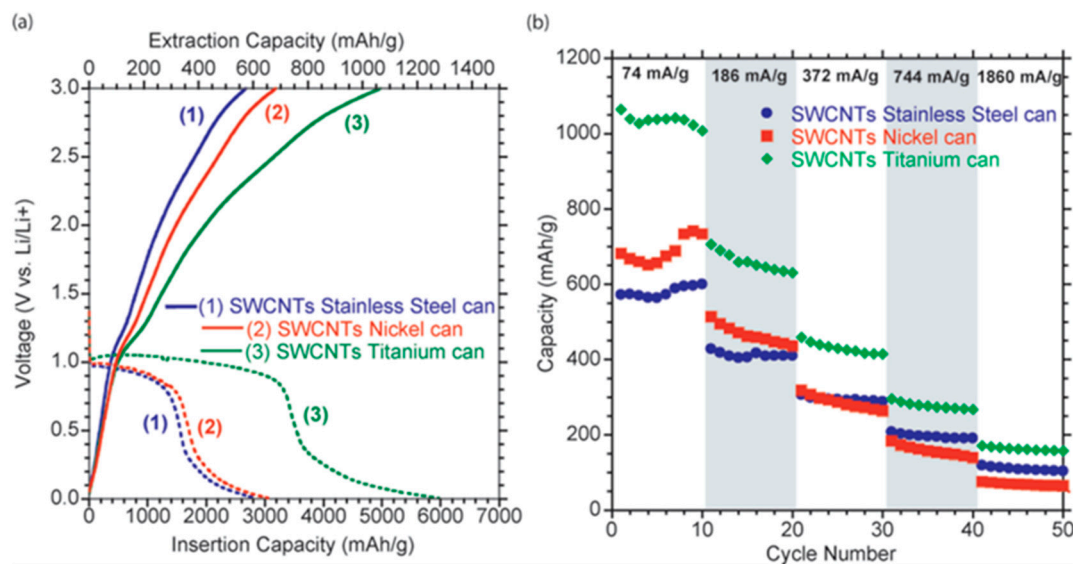


Figure 3. (a) Single-walled carbon nanotube (SWCNT) electrode voltage profile in extraction and initial insertion of the cycle on stainless steel, nickel and titanium coated cells at a current density of 74 mA g^{-1} (b) Cycling stability of all three metal-coated cells at various current densities.

Wu et al. [98] studied the uniform coating of the Fe_3O_4 on micro coated CNTs that lead to an enhanced capacity of more than 799 mA h g^{-1} at 90 cycles with excellent capacity retention [99]. The Mahanthay group elucidated the $\text{MoS}_2/\text{MWCNT}$ composite that showed a stable storage capacity of 1030 mAh g^{-1} in 60 cycles [100]. The above-discussed literature has depicted the potential results when the CNTs were considered to be a crucial part in the battery industry. However, it is a fact that lack of clarity regarding the cost of mass production of CNT still presents a challenge that needs to be addressed for LIB applications.

3.3. Graphene

Graphene consists of a honeycomb network of sp^2 carbons bonded into two-dimensional sheets with nanometer thickness (single-atom thickness). Graphene came into existence in 1987, and has since drawn great attention due to its impressive properties and versatile utilization in various applications, like chemical, biological, physical, and engineering applications [101]. Hence, from graphene, we can obtain excellent electrical conductivity, mechanical strength, good mobility of charge and large

specific areal surface, enabling the graphene to be a possible candidate for LIB applications [102,103]. Graphene's surprising features, such as excellent electrical conductivity, predominant mechanical strength, enhanced mobility of charges, and greater specific surface area, make graphene a suitable electrode material for LIBs. However, the theoretical lithium storage studies of graphene are quite controversial. The amount of lithium adsorbed by the graphene monolayer is low, equivalent to the graphite of 372 mA h g^{-1} [104,105]. If sheets of graphene are combined, this number lies in between 780 mA h g^{-1} and 1116 mA h g^{-1} . These two values are associated with two different descriptions of the interaction between lithium and graphene. In particular, the former assumes absorption of Li-ions on both faces of graphene (Li_2C_6 stoichiometry), while the latter assumes Li trapped at the benzene ring in a covalent bond (LiC_2 stoichiometry). Figure 4 depicts the binding energies of the purely elastic curvature of the carbon nanotube (CNT) wall that enhances binding with a single Li atom. The variation of the diameter leads to the asymptotic approach of the $\epsilon_{\text{Li-graphene}}$ [104].

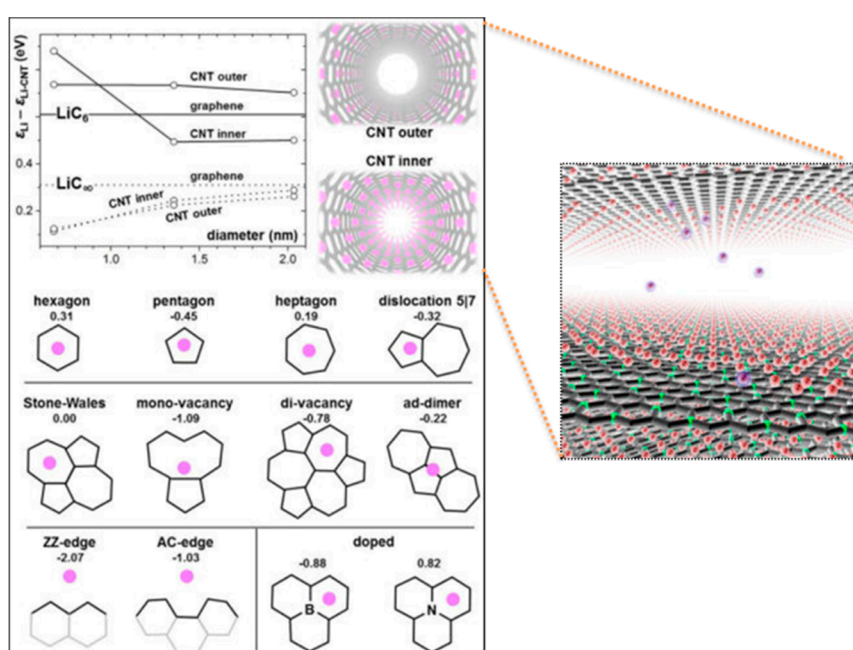


Figure 4. Energies and structures of Li adsorbed on carbon nanotubes (CNTs) and defects. The balls show Li, and the sticks represent C lattice. The numbers are calculated as $\epsilon_{\text{Li}} - \epsilon_{\text{Li-M}}$ in eV. The energy of a single Li atom adsorption on pristine graphene (hexagon) is also shown for comparison. The plots show $\epsilon_{\text{Li}} - \epsilon_{\text{Li-CNT}}$ as a function of diameter for (5, 5), (10, 10), and (15, 15) CNTs, for adsorption on inner or outer surfaces, at high (LiC_6 , solid lines) or low (LiC_∞ , dashed lines) concentrations [104].

This distinction can be identified by the interaction of lithium and graphene. The first step involves the Li-ions' absorption on both sides of the graphene (stoichiometry of Li_2C_6), whereas the second Li ions formed covalent bonds on the benzene ring in a compound (stoichiometry of LiC_2) [106].

3.4. Titanium-Based Oxides Materials

Titanium oxides recently became of paramount importance in the lithium battery since they permit design controls with minimum safety issues. Furthermore, they also have certain interesting properties, namely low toxic nature, and excellent life cycle, and reduced volume change (2–3%) both in cases of insertion and de-insertion of lithium [107–109]. Sometimes, it also depicts a low theoretical capacity starting at $175\text{--}330 \text{ mA h g}^{-1}$ and also a lower possibility of conductivity. Performance (electrochemical) and the ability to insert/remove lithium and titanium-based oxides depend largely on their structure, morphology, and size. In particular, nanostructured titanium oxides have led to better capacity, longer life span, and higher capacity retention when compared to the bulk materials [110] depicted in Figure 5.

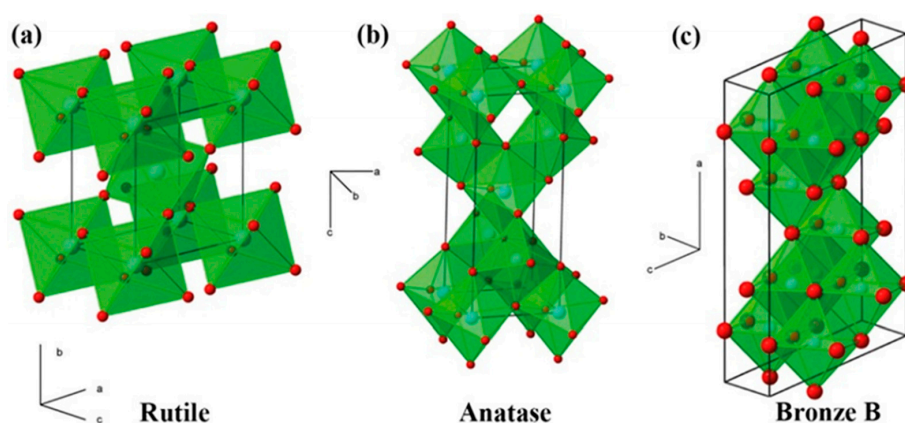


Figure 5. Polyhedral view of (a) rutile, (b) anatase, and (c) bronze B TiO_2 (Reproduced with permission from Ref. [110], Copyright 2013 WILEY-VCH Verlag GmbH & Co. KGaA, Weinheim).

Therefore, great efforts are made in developing anodic materials that rely on titanium oxides nanostructures. Until now, titanium dioxide of different allotropic forms and spinel $\text{Li}_4\text{Ti}_5\text{O}_{12}$ has been intensively investigated for anodic purposes [111,112].

3.5. Spinel $\text{Li}_4\text{Ti}_5\text{O}_{12}$ (LTO)

Spinel $\text{Li}_4\text{Ti}_5\text{O}_{12}$ can be presumed to be the most suitable titanium oxide-based material for lithium storage since it has excellent reversibility in Li-ion with a high operating potential of 1.55 V compared to Li/Li^+ . The insertion/extraction of lithium in the LTO takes place by lithiation of spinel $\text{Li}_4\text{Ti}_5\text{O}_{12}$, which produces $\text{Li}_7\text{Ti}_5\text{O}_{12}$ of rock salt kind. During this process, a greater working voltage causes safety issues. Moreover, the solid electrolyte interface (SEI) formation is affected and the dendrites arousal is prevented, which is a crucial problem for carbon-based anodes that can, however, be overcome [113]. The theoretically low specific capacity of nearly 175 mA h g^{-1} and lower electronic conductivity of nearly $10^{-13} \text{ S cm}^{-1}$ limits the total storage capacity with higher rates of charge and low diffusion of LIBs [114]. This problem can be overcome in two ways. The first is to enhance the conductivity of the LTO implementing treatments of the surface [115,116]. The typical capacity diagram of Li-titanate is as shown in Figure 6.

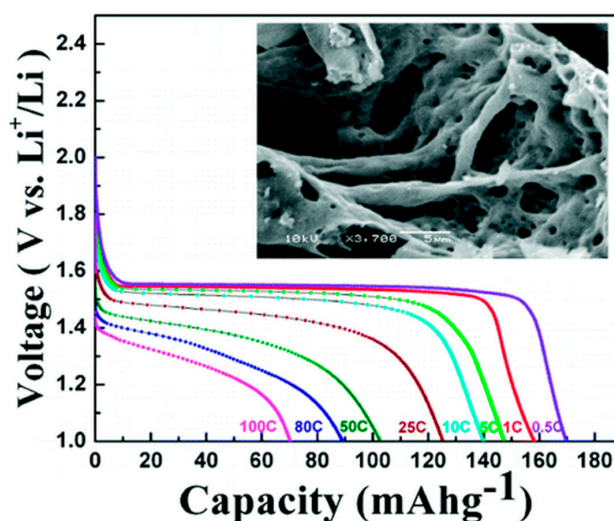


Figure 6. The capacity diagram of various lithium titanate (Reproduced with permission from Ref. [117]).

The second is to improve the diffusion of Li-ions by the reduced nanoscale of the LTO. Nanocrystalline LTO with particle sizes in the range of 20–50 nm was fabricated in a short time (less than 1 min) by a simple combustion method [117]. Shen et al. [118] experimented with a method for directly growing LTO nanoparticles over the surface of titanium foil depicted in Figure 7, which showed an enhancement in the LTO nanowire conductivity by the introduction of the Ti^{+3} ion by implementing hydrogenation [118].

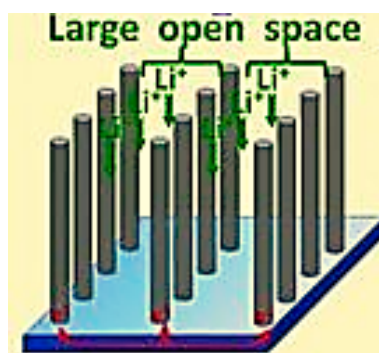


Figure 7. Self-supported $\text{Li}_4\text{Ti}_5\text{O}_{12}$ nanowire arrays with high conductivity architectures.

3.6. Titanium Dioxide (Titania)

Titanium dioxide is a potential electroactive material for anodic uses and LIBs. It is suitable for bulk production and considered to be obtained at low costs. Additionally, titanium has shown good security and stable features at a working voltage of 1.5 V compared to Li/Li^+ . TiO_2 also showed extraordinary characteristics, namely, higher electroactivity, robust oxidizing capacity, chemical stability, great prevalence, and variation in structures [119–121]. These properties make titania a promising candidate as an anodic material in LIB applications, targeted for hybrid electric vehicle applications. Titanium made of 1 M lithium/1 M of TiO_2 has an estimated optimum capacity of 330 mA h g^{-1} and stoichiometry of LiTiO_2 (nearly twice the size of LTO). However, using full storage capacity is still a challenge. Further, the process of intercalation/de-intercalation of lithium in titania usually relies on the crystalline structure, size of the particle, surface, and structure [122–124]. Titania resembles in several allotropic forms, of which brookite (Orthorhombic, Pbca), rutile (tetragonal, P42/mnm), anatase (tetragonal, I41/mnm), and rutile (tetragonal, P42/mnm) [125,126] are the best known (shown in Figure 8). Although titanium anatase is predicted as a form of electroactive nature, the other kind of allotropes, namely brookites and rutile, have also been extensively studied for anodes [127,128].

TiO_2 rutile form was shown to reduce the size of a particle to 15 nm, enabling a greater capacity than 378 mA h g^{-1} during the swift discharge and a consistent specific capacity of 200 mA h g^{-1} (0.6 Li/molecule of rutile TiO_2) for nearly 20 cycles with a current density of 0.05 A g^{-1} . Considering the size of the particle (300 nm), the capacities of the beginning cycles and at the 20th cycle were shown to achieve capacities of 110 and 50 mA h g^{-1} [127]. The ability and enhancement of Li-ion are associated with the nanosizing and large surface properties. The particle size of 6 nm TiO_2 anatase has been reported to have a high capacity of greater than 200 mA h g^{-1} for 20 cycles with a current density of 0.1 A g^{-1} . In addition, the capacity of 125 mA h g^{-1} was achieved with the current rate of 10 A g^{-1} shifting to larger TiO_2 particle size, namely, 15 nm, and 30 nm. Specific capacities were found to be less than 80 and 71 mA h g^{-1} [129]. Particle size reduction facilitates easier intercalation/de-intercalation of lithium and the detection of electrons in the anode by improving the diffusion of ions of Li and decreasing the length of the charge. The Lee research group fabricated the microsphere like anatase TiO_2 with the solvothermal method. These TiO_2 microspheres are devised by the union of 6–8 nm ultrafine nanocrystals of TiO_2 size 4–6 nm structure. The performance of the microspheres of TiO_2 , high lithium storage capacity, a large number of charge/discharge cycles and higher tap density, are depicted by their morphological spherical structures [109].

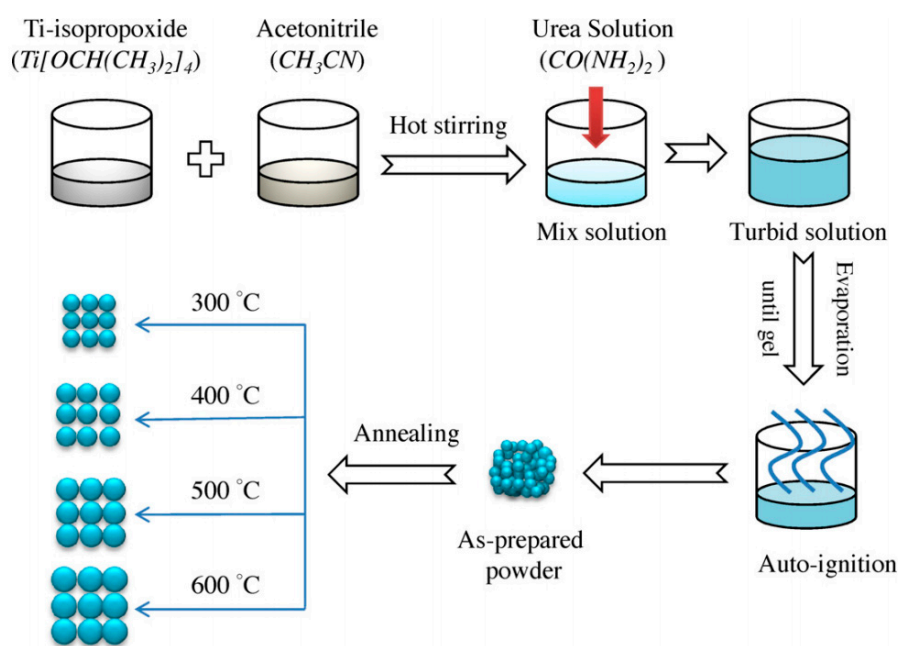


Figure 8. Simple synthesis and particle size effects of TiO₂ nanoparticle anodes for rechargeable lithium ion batteries (Reproduced with the permission from reference [129]).

4. Alloy/De-Alloy Materials

The future LIB is supposed to meet the energy needs of highly efficient EVs and HEV devices and also be used for static applications. Therefore, the capacity is the main basic parameter that needs to be considered in the new anodic active elements. Electroactive materials that can meet the higher capacity requirements are, for instance, germanium, silicon, tin oxide, and silicon monoxide, which take place with the lithium reaction correlated to an alloy/de-alloy phenomenon. Their specific capacities are in the range of 783 mA h g⁻¹ for tin oxide to 4211 mA h g⁻¹ for silicon [130–132]. The Li – Mg alloy has been depicted in Figure 9.

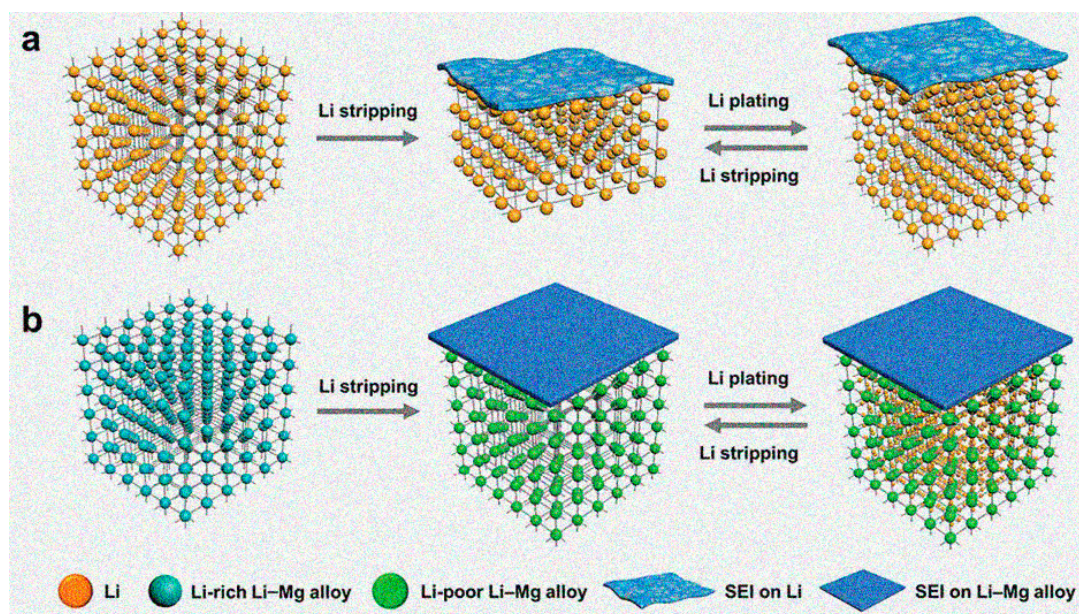


Figure 9. Schematic structure illustration in the bulk and at the surface for (a) Li and (b) Li - Mg alloy anodes during Li stripping/plating process.

While these alloy-based materials can offer higher specific capacities, such as graphite (372 mA h g^{-1}) and LTO (175 mA h g^{-1}), the main disadvantages of short life are the expansion/contraction of a large volume and a more irreversible capacity at the beginning. To overcome these problems, several approaches were followed: reducing the size of the micro particles to the nanoscale and producing compositions with both active lithium and inert materials have the best potential. Considering the next case, active/inactive lithium material is favored as a matrix of conductive buffer between the alloy materials and the source of lithium [133]. Alloy materials exhibited various nanostructures corresponding with diverse morphologies, such as nanotubes and nanowires yield higher capacities with good capacity retention and longer life span [134,135].

4.1. Silicon (Si)

Silicon possesses both the greater gravimetric capacity (4200 mA h g^{-1} , $\text{Li}_{22}\text{Si}_5$) and also the volumetric capacity ($9786 \text{ mA h cm}^{-3}$) in the candidates for the anodic materials [136–139] illustrated in Figure 10.

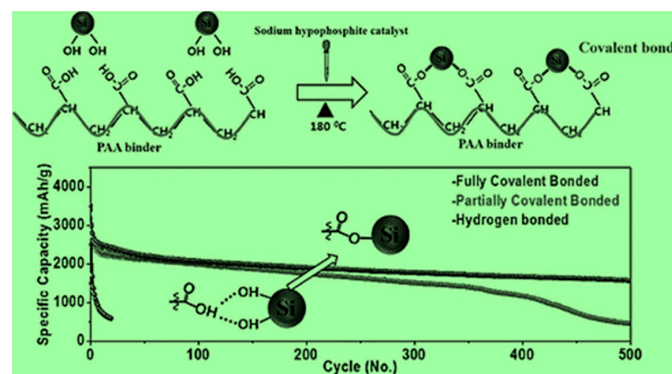


Figure 10. Stable Silicon anode for Lithium-ion batteries by Covalent Bond formation.

Further, the discharge potential of silicon is nearer to the graphite, i.e., $0.4 \text{ V vs. Li/Li}^+$. It is the second most abundant element on earth, so it is cheap and ecological. Hence, it is easy to understand why silicon and its offshoots are regarded as the potential material for the next generation of LIB that manifests strong research from an academic and industrial perspective to fabricate an active anode material. Electrochemical lithiation of Si electrodes was extensively studied by many groups. The high specific capacitance value is by the formation of Li-Si intermetallic binary compounds such as $\text{Li}_{12}\text{Si}_7$, Li_7Si_3 , $\text{Li}_{13}\text{Si}_4$, $\text{Li}_{22}\text{Si}_5$ [137]. The slurry casting phenomenon for MXene sheets with Silicon particles is depicted in Figure 11.

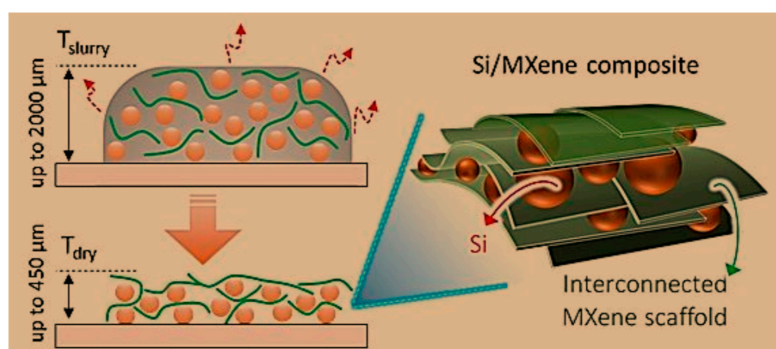


Figure 11. During the slurry-casting process, sheets of MXene material combine with silicon particles to form a network that allows for a more orderly reception of lithium ions, which prevents the silicon anode from expanding and breaking.

Performances of Si NW after anode changes were analyzed by Ge et al. [43] with the direct etching process of silicon wafers of boron-doped structures. Si NW porous structures have excellent electrochemistry and longer life span. After 250 cycles, the reported reverse capacities were 2000, 1600, and 1100 mA h g⁻¹ to 2, 4, and current density of 8 A g⁻¹.

4.2. Silicon Monoxide (SiO)

SiO is presumed to be an alternative for silicon as an anode material because of its high specific capacity (>1600 mA h g⁻¹). Further, coordination of oxygen with lithium involves a minimal volume change in Figure 12 and simultaneously low activation of energy [140–143].

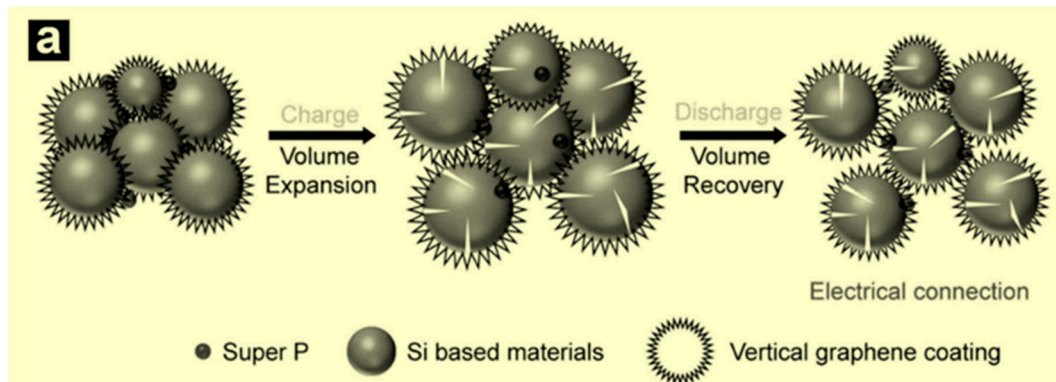
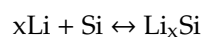
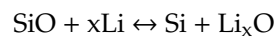
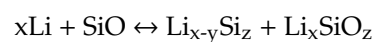


Figure 12. Schematic illustration of the d-SiO/vG during charge/discharge.

The reactions of electrochemistry that occur at the time of the discharge process cause SiO conversion to Si, lithium oxides that can form Si-Li or, the major forms of an alloy of Si-Li and also the silicates of lithium. The reaction mechanism involved is described as:



or



SiO (solid) is not thermally stable at various temperatures. Hence, it is converted into Si and SiO₂ at an enhanced temperature, not a proportionate reaction [144,145].

4.3. Germanium

Germanium is a widespread anode material due to its high lithium capacity (1623 mA h g⁻¹). Li₂₂Ge₅ has corresponding stoichiometry with reversible reactions of alloy/de-alloy [146]. While Ge is higher cost and has lower specific capacity compared to silicon, it possesses impressive benefits of higher electronic conductivity (104 times greater than silicon), greater capacity when compared to graphite anode, and narrower bandwidth potential (0.67 eV). Also, the diffusion of lithium in Ge is 15 and it is observed to be 400 times faster than Si at 360 °C at room temperature. It offers more capacity and more efficient transportation of charge, compared to silicon and graphite [147]. High capacity Ge is as important in high-density applications as electric vehicles. In accordance with the discussion for silicon, the real-time use of Ge as active material in the LIBs is hampered by the greater volume change (300%) at the time of lithium insertion/de-insertion [148]. Nanoarchitectures, such as nanotubes [149], nanowires [147], nanoparticles [150] (Figure 13) could dominantly support change in volume more efficiently when compared to bulk and microstructures.

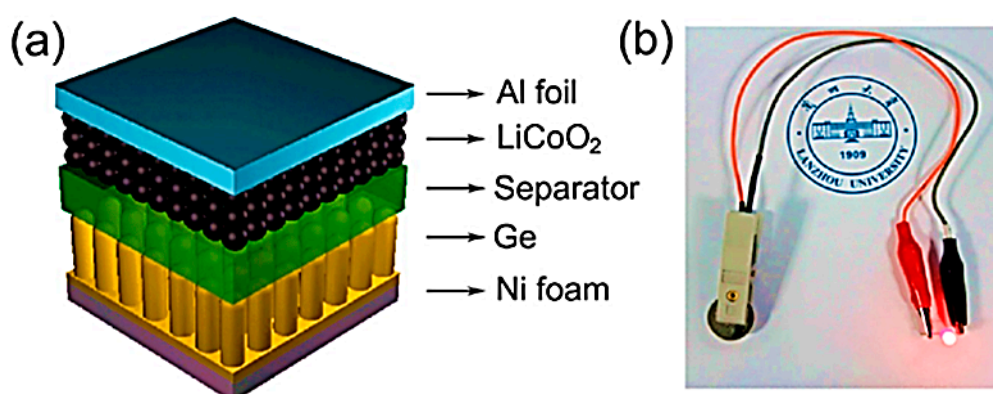


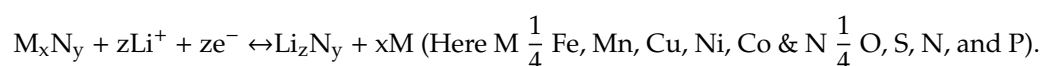
Figure 13. (a) Schematic of the Ge/LCO full-cell. (b) Digital image of a light-emitting diode lighted by the Ge/LCO full-cell.

Dramatic advancements were made with a hybrid nanoparticle compound, which, by using a conductive matrix with simple making methods, was able to identify, for instance, solid pyrolysis [151]. For instance, nanoparticles of Ge had a diameter in the range of 5 nm–20 nm encrypted in nanospheres of carbon of diameter ranging from 50 nm to 70 nm [151]. The nanospheres of carbon were used as a structural buffer in electroactive materials at the time of the insertion/de-insertion of lithium to omit the electrolyte direct contact. The latter aspect prevents Ge accumulation from SEI. The obtained compositions show extremely reversible storage of lithium and higher capacity retention.

Simultaneous features have been identified in the nanoparticles of Ge formed on CVD SWCNTs [152]. Nanoparticles of a crystalline nature with an average dimension of 60 nm were coated on SWCNT in the titanium layer for good capacity retention. The key usage of employing CNTs is the conductivity increase between the current collector and the Ge, along with the rise in lithium diffusion that indicates space for Ge volume expansion in the cycle. The synthesized Ge nanohybrid compound exhibited an excellent anode capacity of about 980 mA h g⁻¹ compared to the lithium metal and 800 mA h g⁻¹ with LiFePO₄ as the cathode. At the same time, comparable reversible capacities were achieved together with excellent longevity and high velocity by mixing nanoparticles of Ge with MWCNTs and the reduced graphene oxide [153].

5. Conversion Materials

This section provides a detailed description of transition metal compounds such as oxides, phosphides, sulfides, and nitrides (M_xN_y; M $\frac{1}{4}$ Fe, Co, Cu, Mn, Ni, and N $\frac{1}{4}$ O, P, S, and N) that are targeted for anode synthesis in LIBs. The electrochemical reaction processes with these compounds of lithium have oxidation/reduction of the transition metal including composition/decomposition of the various compounds of lithium (Li_xN_y; here P, N $\frac{1}{4}$ O, N, and S). Furthermore, the anodes that rely on these compounds have a higher reversible capacity (500–1000 mA h g⁻¹) due to a large number of electrons participating in the conversion reactions [154]. Electrochemical conversion mechanisms can be demonstrated as:



5.1. Tin Oxide (SnO₂)

Tin oxide was originally introduced by the film company Fuji Photo. It established importance in the form of anodes and Li-ion batteries since it possesses a greater capacity and low working potential, that is, 0.6 V vs Li/Li⁺ [154]. The electrochemical reactions of lithium alloys can be inferred in an irreversible first partial step SnO₂ is further reduced to Sn and lithium oxide (SnO₂ + 4Li ↔ Sn + 2Li₂O) that is accompanied by the reversing alloy/dealloying reaction (Sn + 4.4Li⁺ ↔ Li_{4.4}Sn). This general electrochemistry process contains 8.4 Li for one unit of SnO₂ formula. The relevant theoretical capacity

is 1491 mA h g^{-1} , where it is further reduced to 783 mA h g^{-1} when the second extremely reversible step is taken. Therefore, 783 mA h g^{-1} is usually regarded as the actual capacity. Also, there is a strong degradation in the electrodes because of the constant volume change ($> 200\%$) during cycling. Hence, great care was taken to enhance the SnO_2 cycle stability and to decrease the irreversibility of capacity estimated by change in volume. Many porous nanocomposites, nanostructures, and SnO_2 nanostructures have been elucidated to solve the problems mentioned here [155,156], as shown in Figure 14.

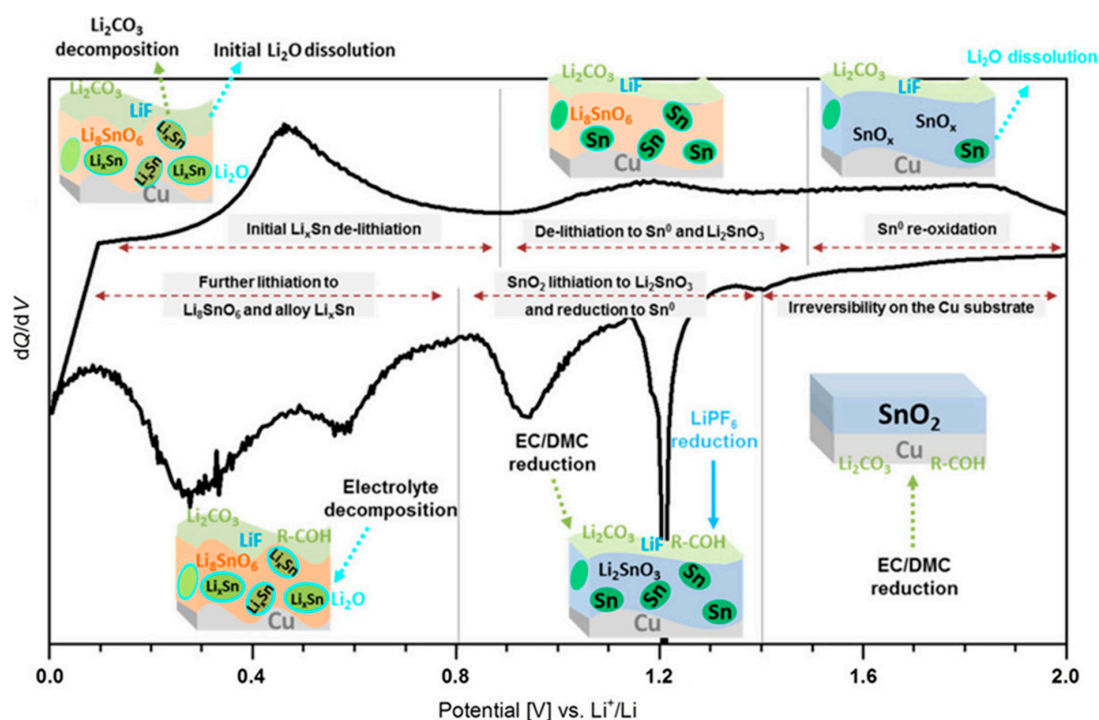


Figure 14. Cyclic voltammogram of a flat SnO_2 model electrode with a schematic representation of the electrode composition, intermediate phases during lithiation, and redox features associated with interfacial reactions with the organic and inorganic part of the electrolyte. EC = ethylene carbonate, DMC = dimethyl carbonate. Reproduced with permission from Ref. [156].

In particular, it was depicted that the porosity of the SnO_2 nanostructures can balance changes in volumes at the time of lithium insertion/de-insertion. Moreover, its porous nature acts as a buffer for greater changes in volume. In this respect, Yin et al. designed mesoporous spherical SnO_2 in the range of 100–300 nm using tin sulfate with a simple and cost-effective solution [157,158]. The as-synthesized SnO_2 spheres exhibited remarkable lithium battery performance with enhanced capacities of 761 and 480 mA h g^{-1} after 50 cycles at corresponding different current densities of 200 mA g^{-1} and 2000 mA g^{-1} .

5.2. Iron Oxide

Iron oxides were tested on rechargeable lithium batteries for low cost, low toxicity, and adequate availability. Iron oxides, both hematite ($\alpha\text{-Fe}_2\text{O}_3$) and magnetite (Fe_3O_4), can participate in reversible lithium conversion reactions and can reach theoretical capacities of 1007 and 926 mA g h^{-1} [159], respectively. Iron oxides, moreover, often have poor cyclic efficiency because of weak conductivity, lower diffusion of Li-ion, higher expansion of volume, and iron agglomeration at the time of charging/discharging. Hence, to exceed the limits described previously, a lot of studies have concentrated on novel strategies for producing nanomaterials of iron oxide, also on their shape, size, and also porous nature [160–164].

More investigations have made on techniques to stabilize their structure and enhance the kinetics of electrochemistry and capacity retention, dominantly through coating with carbon or compositions of carbon of $\alpha\text{-Fe}_2\text{O}_3$ and Fe_3O_4 [165] depicted in Figure 15. The hollow spheres of $\alpha\text{-Fe}_2\text{O}_3$ were made with a simple quasi-emulsion method. Hematite $\alpha\text{-Fe}_2\text{O}_3$ nanotubes were identified with an outer diameter of between 200 and 300 nm with ZnO as the sacrificial format. They were then carbon coated with glucose as a source of carbon [161]. The $\alpha\text{-Fe}_2\text{O}_3$ nanotubes yield exhibited good reversibility of lithium insertion/de-insertion expected specific capacity close to 750 mA h g^{-1} at 150 cycles.

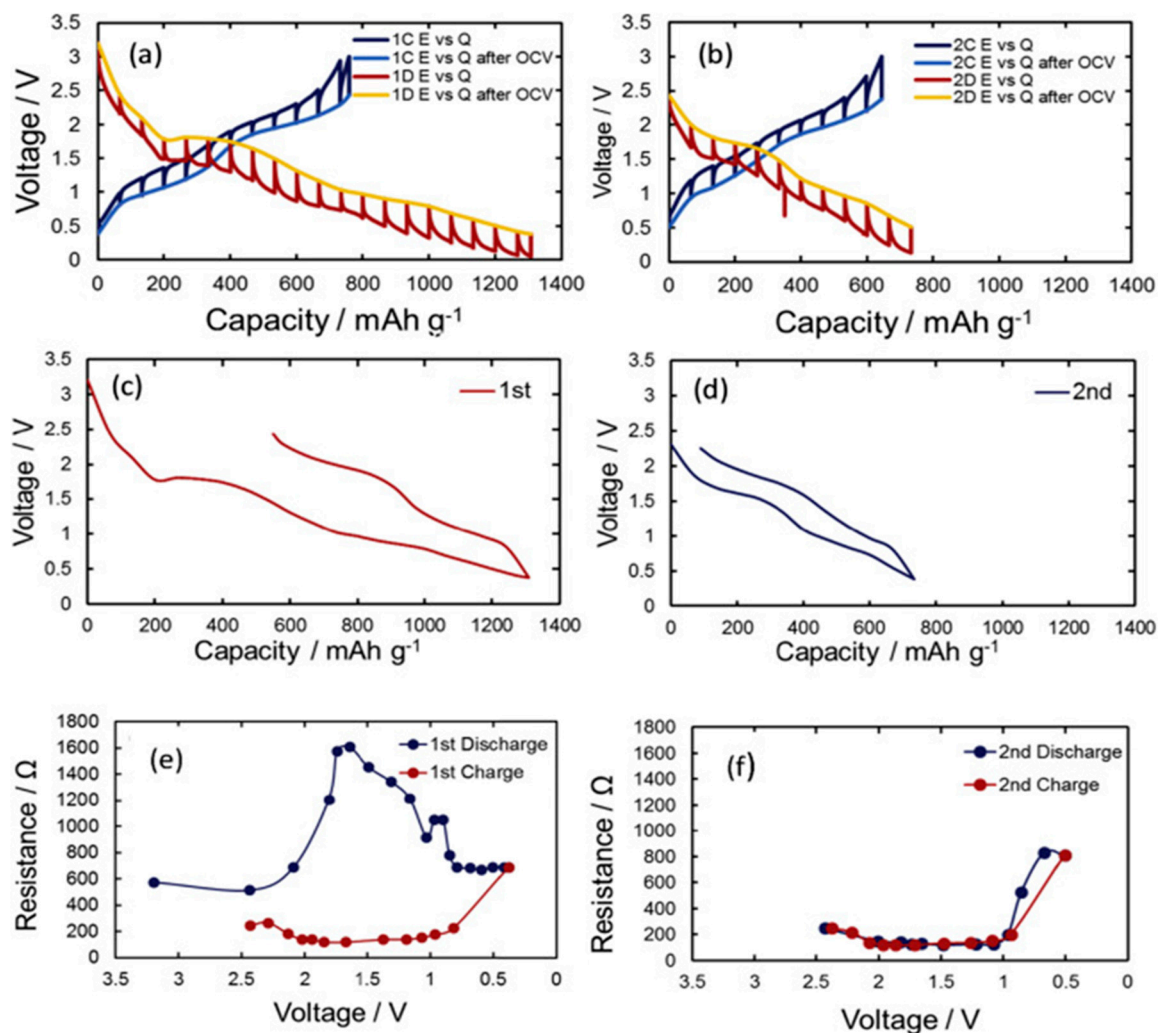


Figure 15. Open Circuit Voltage (OCV) and Closed Circuit Voltage (CCV) curves for the Li/L-BIOX(Biogenous Iron Oxide) cell in both the discharge and charge directions of the (a) first and (b) second cycles. 80 wt% L-BIOX, 10 wt% CNTs, 10 wt% Styrene-Butadiene Rubber/Carboxymethylcellulose (SBR/CMC). Hysteresis of the OCV curves for the first and second discharge-charge is shown in (c) and (d), respectively. Potential (OCV) dependence of cell resistance for the (e) first and (f) second cycles. The intercepts of the semicircle on the real axis at the low-frequency side in is attributed to the total resistance of the cells.

5.3. Cobalt Oxides

There are many recent reports in research on cobalt oxide materials (Co_3O_4 and CoO), which have been employed as anodes for LIBs. Co_3O_4 and CoO have a capacity of 890 and 715 mA h g^{-1} [166–168]. As with other electroactive materials, a variety of cobalt oxides were investigated. Nanostructures, nanowires, nanotubes, and nanocubes have been fabricated in various

fabricating ways, like solid, hydrothermal, microwave chemicals, and wet chemical, that can enhance their efficiency (Figure 16) [169–173]. For instance, Guan et al. [174] used a template-free method that has been developed to produce CoO octahedral nanocages of pure phase with NH_3 as the coordinating etching agent [174].

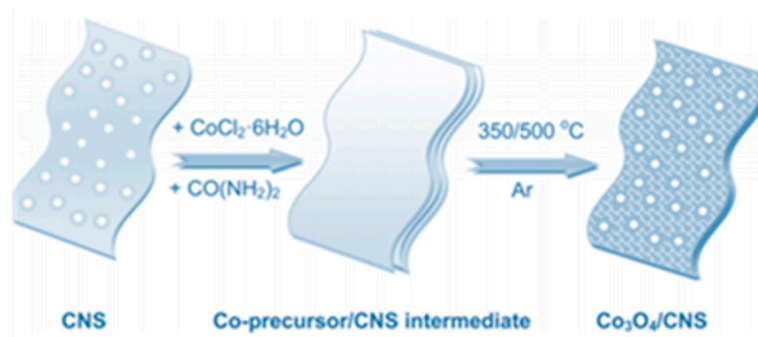
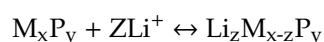


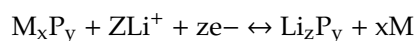
Figure 16. Powder XRD patterns of CNS, $\text{Co}_3\text{O}_4/\text{CNS}$ hybrids, and bare Co_3O_4 .

5.4. Metal Phosphides (MP_x)

Metal phosphides were extensively investigated as anode materials for the applications of lithium batteries of a rechargeable kind [175–179]. There is a reaction with lithium, not only in a conversion reaction scheme but also in an intercalation/de-intercalation reaction, relying on the behavior of many transition metals and the consistency of the phosphorus compound in the electrochemical scenario. MP_x can be divided into two groups. The first is the insertion/deinsertion of lithium without breaking the metaphosphoric compound, the so-called insertion/deinsertion mechanism:



Further, the second group contains a converting mechanism. These kinds of electrochemical reactions break the bonds between the metal and phosphorus, which results in nanosized metal particles and Li phosphides:



Phosphides based on cobalt, iron, copper, tin, and nickel are normally depicted as the other group, like in the conversion phenomenon. However, several studies have shown that MP_x could be involved in the insertion and also in the converting mechanisms in place of conversion mechanisms comparing voltage vs. Li/Li^+ [180]. The metal phosphides can exhibit higher capacities in the range of $500\text{--}1800 \text{ mA h g}^{-1}$. Further, MP_x as an anode exhibits a higher number of electron delocalization, leading to a lower formal state of oxidation and a robust covalent compound of M-Phosphorous. One more benefit is the lower input voltage potential of the MP_x than its counterparts of oxides. Moreover, MP_x normally has lower conductivity and large changes in volume during the charged cycle. The use of MP_x as anodes is worth considering in order to overcome these disadvantages.

5.5. Metal Sulfides (MS_x) and Nitrides (MN_x)

The different kinds of electroactive materials studied in detail for anode applications within LIBs include transition metal sulfides (MS_x) and nitride (MN_x). Tin, antimony, iron, tungsten molybdenum, cobalt, and nickel have gained much attention because of their higher lithium capacity and the morphological benefits of the lithium insertion/deinsertion phenomenon [181–185]. As discussed in the above literature, the reaction mechanisms MS_x and MN_x along with lithium yield in reducing the metal and emerging of lithium-sulfur and lithium nitride, respectively, in the reaction. Wang et al. [186] furnished CoS_x identified polyhedron of phase-controlled made by a solid type of reaction. The fabrication method depends on the high-temperature Co-sulfur powder mechanism with

potassium halide (KX) that acts as a reaction agent [186]. Particularly, Paoella et al. [183] synthesized the nanoplate preparations of Fe_3S_4 with sulfur and thiosulfate, iron salt, octadecylamine, and 3-methyl catechol [183]. However, carbon and graphene gel matrix compositions were reported. Ultra-thin carbon-coatings of nanosheets of FeS ($\text{C} @ \text{FeS}$) were made using the surfactant-favored solution method [187].

In addition to metal sulfides, metal nitrides have also emerged as promising anode materials for LIBs. Some of those which have been investigated are VN , Co_3N , Cu_3N , Fe_3N , CrN , Ni_3N , and Mn_4N [188–192]. Gillot et al. [191] fabricated Ni_3N over several synthesis methods, such as nickel particles, ammonolysis of nickel salts, and thermal breakdown of nickel in the ammonia presence [192]. In particular, the Ni_3N overlap showed the best electrochemical performance with the highest capacity (1200 mA h g^{-1}). In addition, Ni_3N also showed good rate ability with a reversible capacity of 500 mA h g^{-1} held for 10 cycles with the rate of current nearly 1Li per hour. Sun et al. [189] depicted a higher capacity (1200 mA h g^{-1}) with thin Cr_3N films. The Cu_3N nanopowder was reported in a conversion reaction with Li_3N and Cu particles and the resulting leaching capacity in the first cycle was 675 mA h g^{-1} [190]. In addition to the aforementioned anodic nano architectures, an important study includes the usage of conversion of alloy materials characterized by a reversible reaction of conversion followed by a lithium alloy reversible reaction. It is shown that lithium forms various metals alloys, like Al, Sn, Sb, Si, Pb, Zn, In, Ag, Bi, Au, Pt, As, Cd, Ge, and Ga [193–198].

6. Cathode Materials

6.1. Lithium Cobalt Oxide (LiCoO_2)

John B. Goodenough from Oxford University first introduced the efficacy and usage of the lithium cobalt oxide (LCO) in 1980 accompanied by Koichi Mizushima from Tokyo University. This compound is now a major cathode material in the LIBs application. The particle size of this material ranges from micrometers to nanometers. At the time of charging, the cobalt is initially oxidized to +4 state, where the lithium ions have mobility towards the electrolyte, which results in a range of compounds Li_xCoO where $0 < x < 1$. Further, the batteries manufactured from LCO have stable capacities and thermal stability. This enables the LCO with more affinity for thermal runaway when operated at higher temperatures or at the time of overcharging. At greater temperatures, LCO decomposes and generates oxygen. Later, it reacts with the electrolyte. This can be considered as a safety operation because of greater magnitude of exothermic reaction, which can lead to combustion of the adjacent material. Generally, this is observed in many LIB cathodes [199]. Early LIBs used lithium cobalt oxide (LCO) as cathode and graphite as an anode material. LCO has a high tap density, making it an ideal choice for small devices. The battery market has grown tremendously over the last 35 years and is expected to increase even more rapidly within the next years. With the new market segment of electrical vehicles (EV) becoming more important every year, LIB have found an additional application with a huge potential. Even though fuel cells are a natural competitor for LIB, the large commitment necessary to build a hydrogen infrastructure plays into the hands of eager battery suppliers.

In 1975, Whittingham et al. elucidated the first lithium material intercalation (such as TiS_2) [199]. Although this composite exhibited a lithium composite intercalation for one lithium vs, LiTiS_2 and a certain average voltage of $\sim 2 \text{ V}$, it was later removed [200]. A major issue with lithium metal batteries is the improper deposition of lithium on the surface of the anode. In the lithium, dendrites eventually rise from anode to cathode, leading to the short circuit of the internal side and severe failure of the cell. In addition, there must be more lithium to balance lower efficiency [201]. These problems can be reduced to some extent by the transition to lithium alloys rather than metallic lithium, for example, Li/Al , with a plate potential of nearly 0.4 V vs $\text{Li}^+/\text{Li}_{15}$. Moreover, this greater potential prevents the combination with TiS_2 because the cell potential will produce $\sim 1.6 \text{ V}$.

LCO is generally charged in a $\text{Li}_{0.5}\text{CoO}_2$ delithiated state (corresponding to $\sim 4.2 \text{ V}$ vs Li^+/Li) to obtain good cycle stability. The LCO cycle behavior in the range 3–4.5 V usually indicates a rapid

decrease in capacity [202]. Normally it is attributed to irreversible structural changes or severe changes in material volume, as seen in Figure 17 [203].

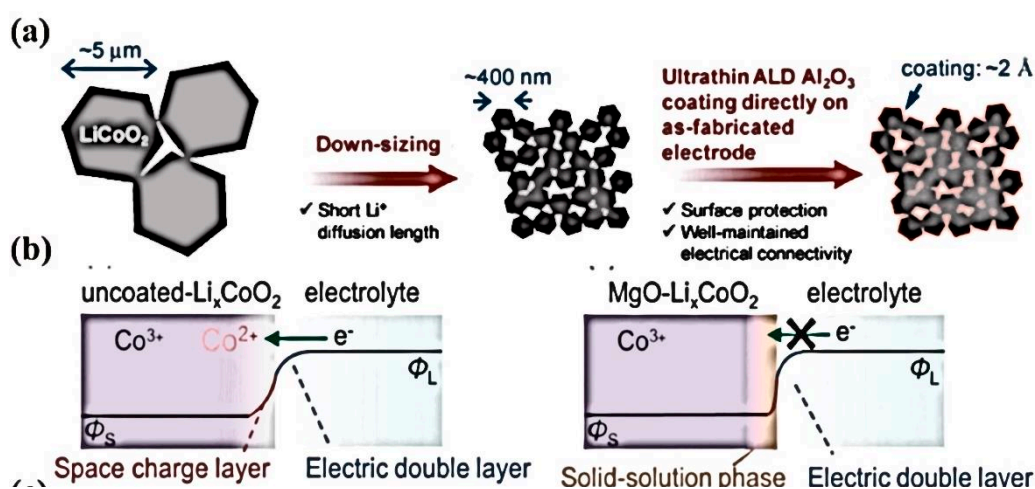


Figure 17. (a) Schematic view of modification mechanism through the ultrathin Al_2O_3 ALD coating (b) Schematic view of the electronic structure of uncoated and MgO-coated LCO/electrolyte interface upon electrolyte immersion (ϕ_s and ϕ_L are the electrochemical potentials of the electrode and electrolyte, respectively).

Dahn et al. [197] demonstrated that an increase in impedance is a more likely reason for poor cycle behavior in the range of 4.5 V, and structural capacity problems run just above 4.5 V [203,204]. Metal oxide coatings have been repeatedly shown to improve the stability of the LCO cycle when operating at > 4.2 V [205–207]. This was ascribed by Dahn to the LCO low surface reactivity with the LiPF_6 based electrolyte solution to obtain LCO coating. Grinding or re-heating the LCO before preparing the cells to clean the surface also exhibited improved cycle stability. In addition, an electrolyte solution based on LiBOB (lithium bis(oxalate) borate) changes has shown significant progress over LiPF_6 . These facts help to develop high voltage LCO cells with a capacity of 180 mA h g^{-1} . A disadvantage of such a method is the poor thermal stability of the delithiated LCO. $\text{Li}_{0.5}\text{CoO}_2$ already exhibits a thermal leak of ~130 °C for which, with delays, $x > 0.5$ in Li_xCoO_2 delithiated states [208].

6.2. Lithium Nickel Oxide (LiNiO_2)

The lithium-ion battery which is widely used as portable power sources with high energy density is greatly being increased due to the development and popularity of portable electronic devices and vehicles. Lithium nickel oxide (LiNiO_2) and their derivatives are promising positive cathode materials for the next generation of lithium-ion batteries. LiNiO_2 potentially offers a higher capacity at about 200 mAh/g. However it is more difficult to synthesize stoichiometric LiNiO_2 because of the loss of lithium from the host structure during high temperature calcination due the high vapor pressure of lithium and fading capacity when charging up to a high voltage (> 4.0V vs Li^+/Li) during deintercalation of the lithium ion, which affects cycling [209].

LiNiO_2 (LNO) was first designed by Dyer in 1954, then it was further extensively researched to replace LCO by Dahn et al. In the 1990s [209–211], nickel was richer in abundance than cobalt, and was found to be cheaper. Also, LNO is isostructural at LCO (R (-) 3 m) and can simply permit lithium intercalation. Contrarily, the synthesis of LNO was found to be difficult due to the trivalent nickel being unstable at high temperatures. Fabrication and synthesis majorly depend on certain parameters (e.g., precursors, oxygen atmosphere, anneal temperature) [212]. Although the stoichiometric LNO preparation is made with the utmost precautions, there is more susceptibility of the material to react under various ambient instances, leading to the formation of inactive LiOH and Li_2CO_3 [209]. The LNOs cycling stability is comparatively poor, which often can be ascribed to the so-called cation

mixing [213]. The nickel and lithium sizes are generally identical and when the lithium layer is depleted at the time of charging, nickel can jump to vacant sites of lithium. In the layered materials, the Lithium intercalation starts from octahedral sites through adjacent tetrahedral sites to the concurrent octahedral site (o-t-o).

Capacity loss can exist in $\text{Li}[\text{Ni}_{1-x-y}\text{Co}_x\text{Al}_y]\text{O}_2$ (NCA) and $\text{Li}[\text{Ni}_{1-x-y}\text{Co}_x\text{Mn}_y]\text{O}_2$ (NCM) because of changes in structures during charge and discharge [214]. Strong electrostatic repulsion increases nickel's charge by the migration of lithium ions. This was impressively shown by the Ceder et al. [215], which resembles the lithium slab distance change that has a strong impact when compared to electric repulsion [215]. In the case of disorder materials, the Lithium slab makes lithium diffusion tedious. When the lithium is fathomed at the time of charging, the materials c lattice will have more expansion, making the adjacent Li diffusion easier. This can be suppressed in the case of the disordered LNO with the outcome of lower capacities and lower capacity retention. The nickel vacancies created at the cation sites can be ionized to create Ni^{3+} ions. For layered cathodes in Li-ion batteries, such as LNO, it is considered that they have the structure of R-3m space group. Removal of lithium from LiNi_xO_2 in the range of $0.4 < x < 0.75$ leads to a monoclinic phase, often attributed to Jahn-Teller distortion, helped by lithium vacancies [209]. Eventually, another hexagonal configuration for $x < 0.4$ was depicted. To make LNO beneficial, many doping techniques were found (e.g., Mg [216] Al [217], Co [218–221], Ga [222], etc.). These materials have in common the facile synthesis of the active materials. One nickel atom generally shares its edges with the tetrahedral site, but when the disorder of the material takes place, two or even more nickel atoms can exist, as depicted in Figure 18 [217].

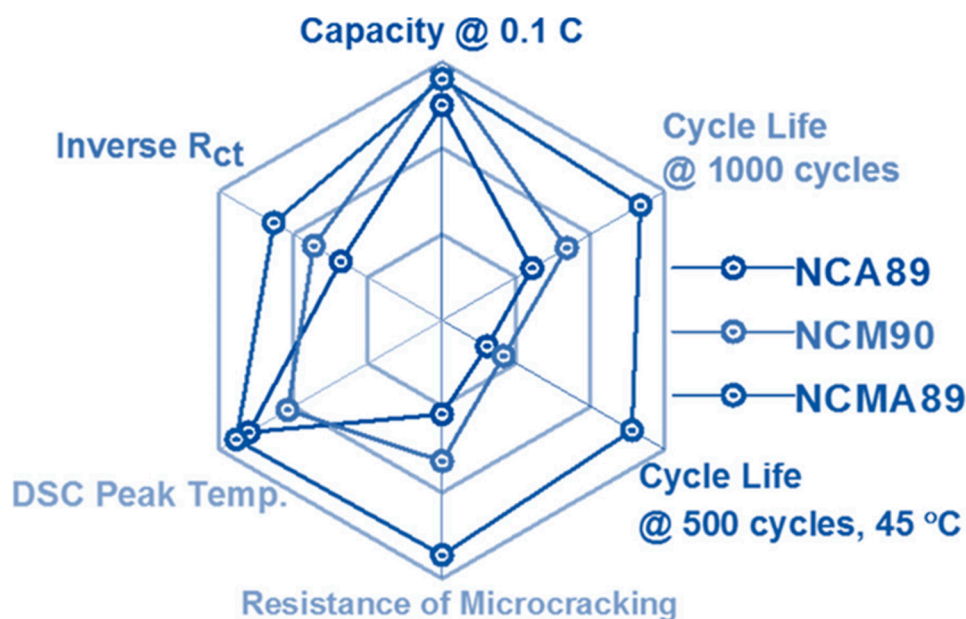


Figure 18. $\text{Li}[\text{Ni}_{1-x-y}\text{Co}_x\text{Al}_y]\text{O}_2$ (NCA) and $\text{Li}[\text{Ni}_{1-x-y}\text{Co}_x\text{Mn}_y]\text{O}_2$ (NCM) cathodes have been the archetypes of current high-energy-density cathodes for Li-ion batteries [217].

Cobalt doping was studied with most care since it was known that LCO already works adequately. LNO and LCO elucidate solid solutions during the range of composition [223]. Furthermore, the low cobalt content exhibits a significant mixture of $\text{Li}^+/\text{Ni}^{2+}$. The $\text{LiNi}_{0.7}\text{Co}_{0.3}\text{O}_2$ compound operates well and there is a possibility that lithium formula is reversible [224].

6.3. Lithium Manganese Oxide; LiMnO_2

Pristine LiMnO_2 (LMO) has gained much attention as a low cost, eco-friendly, and simple alternative to LCO and LNO. Regression is the hard method of LMO since a high-temperature direct synthesis enables the orthorhombic phase (Pmmn) along with corrugated LiO_6 plates [225–227]. o-LMO

was shown to be electrochemically active with initiative capacities up to 200 mA h g^{-1} when circulating over a broad potential of 2.5–4.3V Manganese Spinel LiMn_2O_4 . Besides, two voltage plateaus at ~ 4 and $\sim 3 \text{ V}$ are identified, making it unattractive for applications of commercial usage that need stable voltage [225]. To obtain the stratified LMO, a cation exchange was employed autonomously by Delmas and Bruce in 1996 [228,229]. It was later identified that lower temperature methods of the synthesis, such as hydrothermal methods, also depict the layer material [230]. Because Mn^{3+} is an active material of the Jahn-Teller counterpart, it adopts a monoclinic phase with the space group of C^2/m . The initial high capacity of $\sim 220 \text{ mA h g}^{-1}$ has aroused great interest in the material [231]. Unfortunately, the capacity is not stable, and the initial discharge already has capacities of 150 mA h g^{-1} . A clear difference can be seen from cyclic voltammetry experiments and for the first cycle phase change of layer material, spinel was identified in Figure 19 as the cause of the unwanted capacity loss [231].

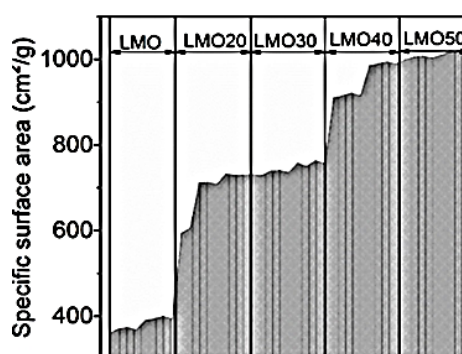


Figure 19. LMO particles size distribution in individual fractions according to the laser diffraction method: The specific surface area of particles in different samples.

Another interesting material that has appeared in the reports on LMO and LNO is combining them both with $\text{LiNi}_{0.5}\text{Mn}_{0.5}\text{O}_2$. The solid solutions were found to have a viable manganese content of up to 0.5 [232]. Higher levels of manganese led to unsafe phases and were not followed up. The electroactive material has a low capacity with increasing levels of manganese content with $\text{LiNi}_{0.5}\text{Mn}_{0.5}\text{O}_2$, which offers the minimum charging and discharging capacity in the series [232]. The material was studied for no more than 10 years until Ohzuku et al. [233], in 2001, reported it to have a stable capacity of 160 mA h g^{-1} for cycles between 2.5–4.3 V [233].

6.4. Combination of LCO, LNO, and LMO to Layered NCM

Working with individually coated composites and their alternative solid solution systems ultimately leads to the advancement of $\text{Li}[\text{Ni}_{1-x-y}\text{Co}_x\text{Mn}_y]\text{O}_2$ ternary materials. Elements depict the decimal of NCM or NMC (for example, NCM523: $\text{LiNi}_{0.5}\text{Co}_{0.2}\text{Mn}_{0.3}\text{O}_2$). Characteristics of the finite elements have enhanced capacity (nickel), excellent rate capability (cobalt), and enhanced safety (manganese). Manganese does not change its oxidation state by +IV at the time of cycling and could serve as a stabilizing buffer of structures. The redox pairs $\text{Ni}^{2+}/\text{Ni}^{3+}$ and $\text{Ni}^{3+}/\text{Ni}^{4+}$ exhibit the most capacity of the material. The existence of cobalt favors in the fabrication that can lead to low cation mixing compounds of stoichiometric. Symmetric NCM333 was studied by Ohzuku et al., who depicted the material cycle between 4.3 5V and gave a capacity of $\sim 150 \text{ mA h g}^{-1}$. Tests with higher breaking voltage (e.g., 4.6 V) have capacities up to 200 mA h g^{-1} , but at a cost due to the stability cycle. NCM333 is simple to fabricate and many techniques have been reported to provide the desired material. Even though the NCM523 is a commercial reality, the higher nickel content presents huge problems that hinder its success. [233,234]

1. A strong Ni^{4+} reagent is mainly used for the completion of the charge that leads to unnecessary side effects with the electrolyte solution, which ultimately leads to the usage of material, diffusion

- of gas, and capacity reduction. In addition, the higher materials, which have greater temperatures with a higher quantity of nickel content will decrease, resulting in more safety issues.
- As with pristine LNO, a high nickel content in the NCM leads to a mixture of Li/Ni cations. That leads to the formation of spinel at the surface and possibly to the formation of the inactive phase Fm (-) 3m and the fatigue capacity.
 - From NCM811, expanded bicycle lanes cause cracks in the secondary particles with the boundaries of grains. This can lead to the continuous increase of the areal surface and thus lead to a higher number of active sites for the parasitic reactions.

6.5. Phosphates for LIBs

Early in 1997, the first phosphate cathode material for LIBs was lithium iron phosphate (LiFePO_4), which has an olivine construction. Since then, major research has been focused on the phosphates in the battery community and also on the chemistry of polyanionic materials. Some phosphate materials are widely employed and are of keen interest, e.g., LiMnPO_4 , LiVOPO_4 , $\text{Li}_3\text{Fe}_2(\text{PO}_4)$, $\text{Li}_3\text{V}_2(\text{PO}_4)$. The major challenge is the comparison between the intrinsic and extrinsic properties (intrinsic transports of materials were limited by the control rate of transportation, electrode synthesis and structural behavior), leading to unprecedented experimental testing, since the electrochemical measurements significantly relied on these parameters [235]. Consider the following Figure 20, illustrating the phosphate composites of Li that make them to stand out in high capacity materials.

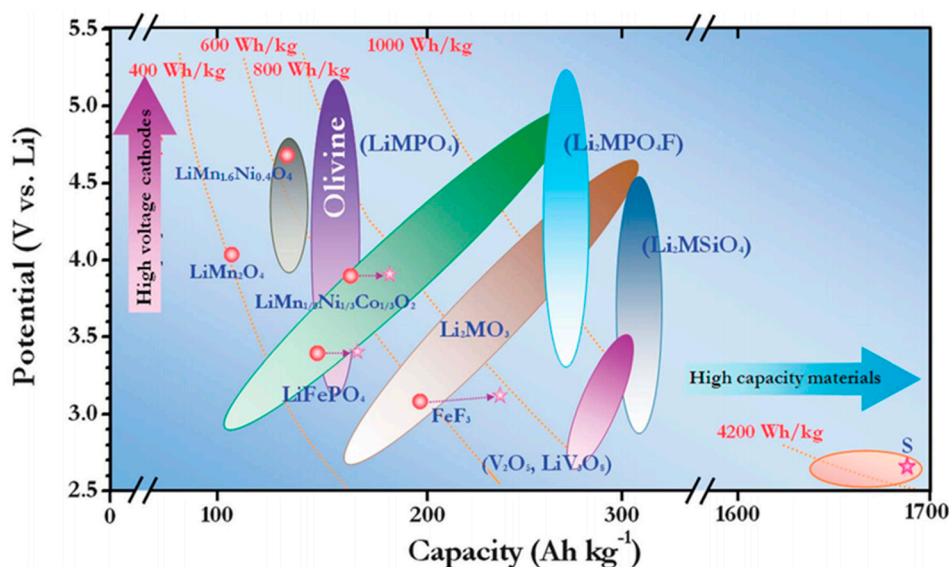


Figure 20. Schematic representation of the plot of Li-ion battery cathode material potentials vs. capacity. LiMPO_4 , Li_2MSiO_4 and $\text{Li}_2\text{MPO}_4\text{F}$, where $\text{M} \frac{1}{4} \text{Fe, Mn, Co, Ni, etc.}$; Li_2MO_3 , where $\text{M} \frac{1}{4} \text{Mn, Mo, Ir, Ru, etc.}$ [236].

Woong et al. [237] illustrated the distorted Li-deficient $\text{Li}_{1-x}\text{V}_2(\text{PO}_4)_3$ phase formation upon third Li-ion removal that affects the adjacent Li-ion insertion that lead to a capacity loss. Furthermore, the authors revealed that the Li-ion insertion during discharge is a two-phase reaction, in contrast to solid-solution reaction and exhibited the excellent electrochemical and stability of the material.

Zheng et al. [238] synthesized the fluorinated cyclic phosphate solvent, 2-(2,2,2-trifluoroethoxy)-1,3,2-dioxaphospholane 2-oxide (TFEP). The authors revealed that this solvent molecule exhibited a fused chemical structure of cyclic carbonates that leads to the formation of stable solid electrolyte interphase and organic phosphates, which can trap hydrogen radicals and prevent combustion.

6.6. Iron Fluoride

In the past decade, huge metal oxides and phosphates have been investigated for high-capacity LIBs. Although many advancements were made, the materials that possess capacity greater than 200 mA h g^{-1} have only rarely been reported. The reason for this is that the interaction process in the material generally involves mono electron diffusion per formula unit that corresponds to a limited capacity [239].

Recently, iron trifluoride has become of paramount importance because of its attractive features such as low cost, non-toxic nature and good thermal stabilities [240]. Additionally, FeF_3 depicted the greater voltage output because of its greater electro-negativity, prominent theoretical capacities and energy densities. Li et al. used a low-temperature ionic-liquid based method [241], $\text{FeF}_{3.0.33}\text{H}_2\text{O}$ depicted at the sixth cycle, the discharge capacity was 154 mA h g^{-1} and after thirty cycles, the capacity decreased to 130 mA h g^{-1} operated at a current density of 14 mA h g^{-1} . The Badway group discovered a method of mechano-chemical phenomenon [242,243]. Carbon metal fluoride nano-composites (CMFNCs) synthesized by this method exhibited a discharge capacity of 500 mA h g^{-1} at a current density of 7.58 mA g^{-1} at 70°C . However, FeF_3 materials that have been shown so far were mostly prepared by solution route and the use of HF was usually inevitable [240].

Chen et al. [244] synthesized the two kinds of iron fluorides, $\text{FeF}_{3.0.33}\text{H}_2\text{O}$ and $\beta\text{-FeF}_{3.3}\text{H}_2\text{O}$, by different chemical routes using $\text{Fe}(\text{NO}_3)_3 \cdot 9\text{H}_2\text{O}$ and NH_4F as precursors and investigated as cathode materials for secondary LIBs. $\beta\text{-FeF}_{3.3}\text{H}_2\text{O}$ was processed using the mechano-chemical process and $\text{FeF}_{3.0.33}\text{H}_2\text{O}$ by a precipitation reaction from ethanol solution. The results showed that the as-prepared $\beta\text{-FeF}_{3.3}\text{H}_2\text{O}/\text{C}$ depicted a better performance and cycling stability. It showed an initial discharge capacity of $199.6 \text{ mA h g}^{-1}$ at a current density of 20 mA g^{-1} as depicted in Figure 21.

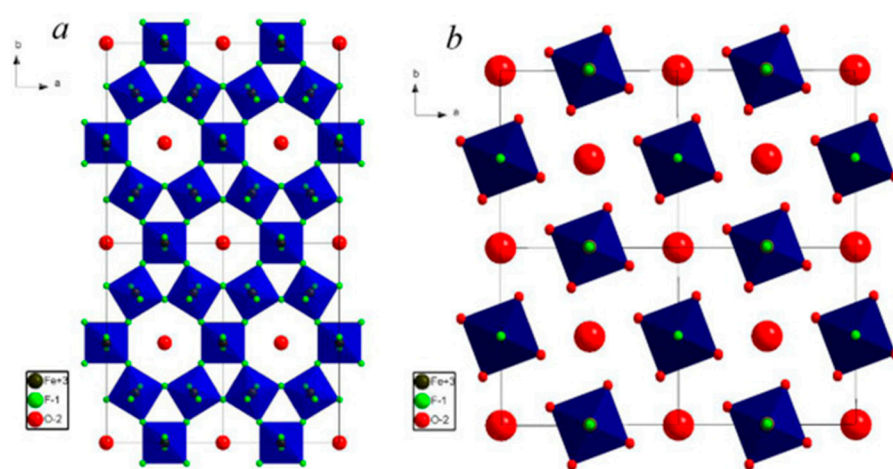


Figure 21. [001] direction projection of four unit cells of phase $\text{FeF}_{3.0.33}\text{H}_2\text{O}$ (a) and $\beta\text{-FeF}_{3.3}\text{H}_2\text{O}$ (b) [244].

6.7. Vanadium Oxides

In the various prominent cathode materials for LIBs, vanadium pentoxide and other vanadium-based oxides have attracted keen interest because of their attractive features like enhanced specific capacity, less cost, facile synthesis and abundant availability from the territory of earth. V_2O_5 (space group: Pmmn ; $a = 11.512 \text{ \AA}$, $b = 3.564 \text{ \AA}$, $c = 4.368 \text{ \AA}$) uses a structure of orthorhombic layers obtained from alternating pairs of V_2O_5 square pyramid sheets interconnected by sharing boundaries, and further, the adjacent layers are weakly bonded by van der Waals forces. The open-layered structures enable V_2O_5 a good host for the Li^+ easy insertion/extraction into their interlayer space. The resulting synthesized capacity of V_2O_5 is certainly a greater value, 294 mA h g^{-1} , and the insertion/extractions

of two lithiums are correspondingly higher than commonly used cathodes (e.g., 148 mA h g⁻¹ for LiMnO₄, 170 mA h g⁻¹ for LiFePO₄, and 140 mA h g⁻¹ for LiCoO₂) [244].

Moreover, the practical use of V₂O₅ has been hindered due to expense of its intrinsic low diffusion of Li⁺ (10⁻¹²–10⁻¹³ cm² s⁻¹), restrained electrical conductivity (10⁻²–10⁻³ S cm⁻¹) and structural instability, which could determinately slow the kinetics of ion/electron transports of LIBs resulting in poor cycling stability and lower performance [245].

Various nanostructures of V₂O₅, such as nanoparticles, nanobelts, nanosheets, nanowires, nanospheres or hierarchical nanostructures have been fabricated for enhancing the electrochemical behavior. Due to the captivating properties and inimitable application, hierarchical nanostructures attained a greater importance in synthesis and application than electrodes for LIBs [244]. Yolk-shell microspheres V₂O₅ and rattle-type hollow microspheres, including those composed of roughly crowded nanoparticles, have been synthesized by Lou et al. [239] and both nanostructures exhibited high specific discharge capacity, good rate capability and excellent cycling stability [246].

Li et al. presented a facile solvothermal method to blend V₂O₅ nanosheet hierarchical structures with diverse thicknesses. By the usage of a voltage regulation charge/discharge scheme, the electrodes exhibited good cycling stability and lower capacity decay of 0.10% per cycle (2.8 to 4.0 V) over 500 cycles [247].

7. Recycling Techniques

7.1. Methods of LIBs Recycling

A detailed procedure with the general purpose of LIBs usually requires two main crucial steps: chemical and physical processes, because of the tedious assembly of LIBs or battery packs, including the variation of electrode materials. It should be noted that if LIBs still have residual energy, this can lead to accidents of fire and also blasting during recycling [248,249]. Due to this, LIBs that have already been used generally need discharging during the process of recycling. The physical processors equip the pre-treatment, screening, crushing, thermal pre-treatment, washing, magnetic separation, etc. [250,251], as well as various processes that allow electrode materials to direct their recovery from the already used LIBs not involving chemical treatment. Chemical processors can be divided into pyrometallurgical and hydrometallurgical processors that typically involve leaching, chemical/electrochemical removal, separation, extraction, and also precipitation [252]. The crucial recovery techniques that are usually implemented are pre-treatment and hydrometallurgical processes employed for spent LIBs, as shown in Figure 22.

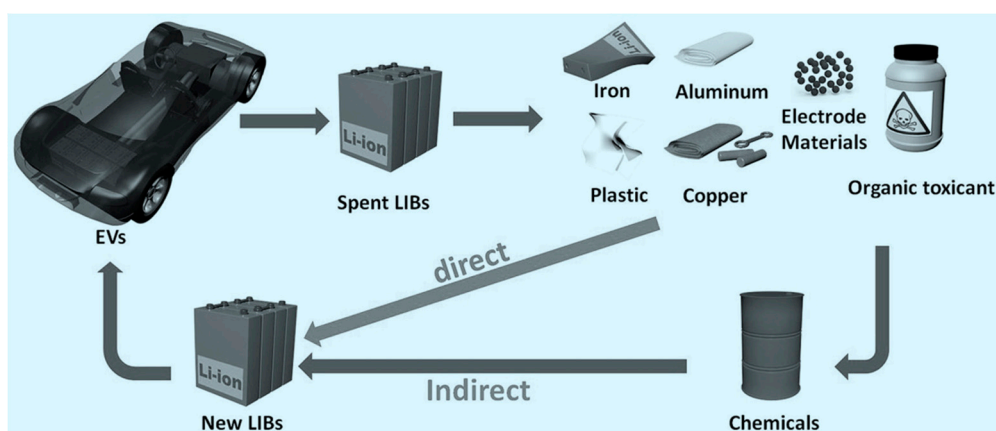


Figure 22. Perspectives for LIBs recycling.

7.2. Pre-Treatment

Normally, the processing is intended to target different components and the materials from used LIBs based on various physical processes such as density, magnetic and shape properties, and conductivity, etc. [250]. Pre-treatments enable metal components, materials, and scrap to separate and produce identical physical properties that result in enhanced recovery rates and lower consumption of energy in the corresponding pyrometallurgical or the hydrometallurgical processes. Few reports have depicted the benefits of pre-treatment and recycling processes for used LIBs (Figures 22 and 23).

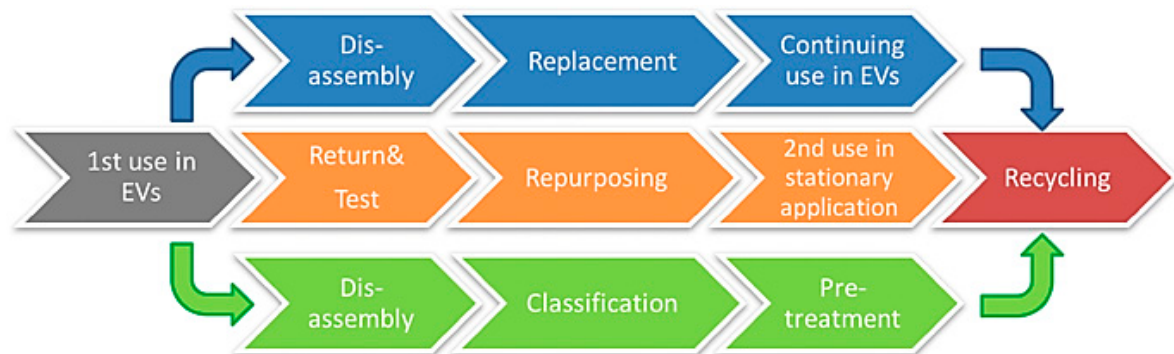


Figure 23. Pre-treatments for lithium-ion recycling process [252,253].

Lee et al. [254] used heat treatment and fragments to fathom and collect LiCoO_2 from used LIBs. To further enhance the energy efficiency of the pre-treatment, Li et al. [255] combined herbal and ultrasonic washing as a pre-treatment process in recycling LIBs. In their activity, the effects of the opening of the grinding screen and the temperature and duration of the ultrasonic wash were investigated. It has been confirmed that a 12 mm aperture screen has the best selectivity to enrich sub residues, and ultrasonic washing at room temperature for 15 min is recommended for separation of LiCoO_2 and the shattered flow collector (Al foil). Li's method is superior in terms of energy efficiency, as reported by Li et al. [253] and Lee et al. [254]. This is because the ultrasonic washing uses less energy when compared to an additional vigorous or heat treatment steps.

7.3. Pyrometallurgical Process

The pyrometallurgical process has been used by the plants of commercial cobalt recycling [256]. For instance, the Umicore research group has synthesized a pyrometallurgical phenomenon, namely that used LIBs are normally treated ores [257]. At the time, the only pre-treatment step is a facile separation of the large battery cells into the single cells. The battery units/cells are then placed in a shelf oven with around three temperatures areas, the preheating zone, the plastic pyrolysis zone, and the melting and reducing zone. In the preheating zone, used LIBs are heated to a temperature less than $300\text{ }^\circ\text{C}$ to provide explosion-resistant vapors of electrolyte. The plastic pyrolysis zone is employed at $700\text{ }^\circ\text{C}$ to burn the LIBs plastic components operated to sustain the temperature and decrease the energy consumption in the melting phase. In the final area, the smelt materials and copper alloy, nickel, cobalt, and iron are formed along with the accumulation of a tray that contains lithium, aluminum, silicon, calcium, and some iron. This process can only recover copper, cobalt, nickel, and some of the iron from the used LIBs. It should be noted that the economic efficiency of this process depends mainly on the price of cobalt and the cobalt content of the batteries. It is widely identified that cobalt is gradually being replaced in automobile LIBs and that cathodic material for LIB is constantly evolving [258,259]. For instance, the cathode material for batteries operated by GM Volt is LiMn_2O_4 , and also the cathode material for A123 batteries can be LiFePO_4 . It is worth mentioning that the industrialized pyrometallurgical process cannot recover lithium if it is expected to be lower than the production of the electric vehicle increases, as depicted in Figure 24 [260,261].

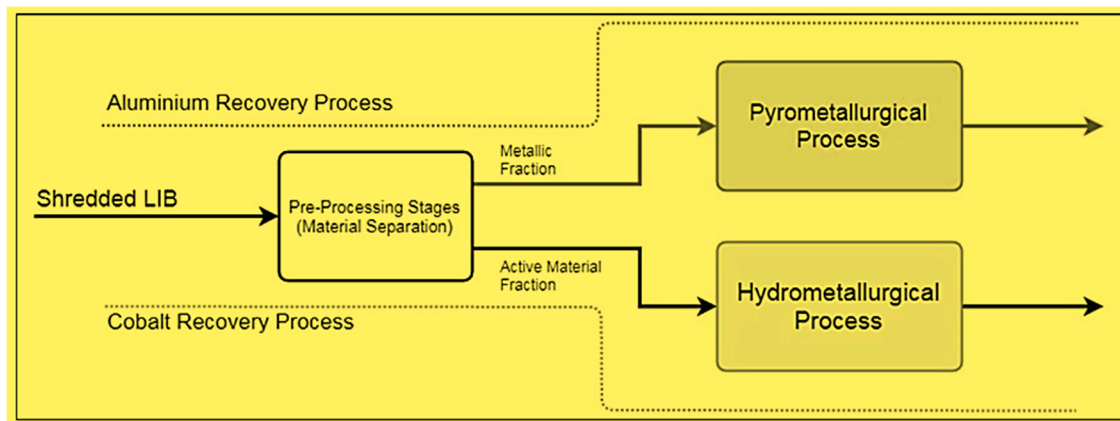
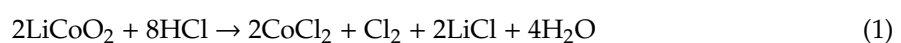


Figure 24. Pyrometallurgical and Hydrothermal Processes.

Therefore, such a traditional pyrometallurgical process is at risk of not making a profit in the future. For the concurrent cobalt and lithium recovery from the used LIBs, Georgi-Maschler et al. [262] reported a particular pyrometallurgical treatment employing an electric arc furnace that could transcend the material fractions of LIBs are used in cobalt alloy and the lithium-containing concentrates. The latter lithium can be recovered as Li_2CO_3 by a hydrometallurgical step. Further, the various material fractions could be obtained for further treatments, such as the fraction of iron-nickel, aluminum, and copper. It should be noted that, before the pyrometallurgical step, four physical processes that allow the individual dismantled components and the fractions of materials collection and used separately, also for the electrolyte. This can enhance the efficiency of complete usage. Moreover, the predicted efficiency (economic) of the procedure depends robustly on the cost of cobalt. The pyrometallurgical process has several demerits, like high energy consumption, material loss, and emission of toxic gases (e.g., furans, dioxins, etc.) [263–265]. Hence, the alternative recycling methods with greater cycling rates, lower consumption of energy, and lower environmental risks are required for a large number of LIBs in future applications.

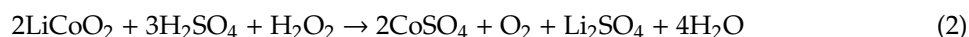
7.4. Hydrometallurgical Process

The hydrometallurgical method is the key to the recycling of used LIBs, as more than half of the reported recycling processes are hydrometallurgical processes [266]. It has effluent (e.g., acid effluent, biodegradation, etc.) and recovery stages (e.g., solvent plant, chemical, and electrochemical deposition, etc.). The hydrometallurgical process is a robust technique for the extraction of metal by LIBs. Nearly 99% of cobalt and lithium can be studied by the process reported by Zhang et al. [267]. More than 98% copper and 97% cobalt were obtained by the hydrometallurgical method [267]. Mousavi et al. [268] reported an ecological method for bio washing that the metals from used LIBs are cured by organic acids. In their activity, 100% copper and lithium, 77% manganese, 75% aluminum, 64% cobalt, and 54% nickel were obtained. Acid liquid action of cathodic materials can be reacted with inorganic release agents such as H_2SO_4 [269–273], HNO_3 [274,275], HCl [276,277], H_3PO_4 [278,279] and some other organic releases like citric acid [280,281] and oxalic acid [282,283]. Compared to the pyrometallurgical method, the leakage of acid can get enhanced recovery efficiency because of the more soluble nature of cathodic electroactive materials and acid solutions. For instance, the reaction of the LiCoO_2 cathodic material in hydrochloric acid can be explained by Equation (1).



During the leaching process of HCL, from the LiCoO_2 powder, Co (III) can be reduced to Co (II) that is lighter in solution in the aqueous phase [284]. The as-obtained solution of the HCl solution is, therefore, an effective solvent for cobalt extraction of used LIBs. Moreover, a major problem with

the leaching of the HCl method is the emission of majorly caustic and dangerous Cl_2 that requires more treatment. To overcome this problem, researchers have proposed a hull of H_2SO_4 . Meanwhile, the H_2O_2 reducing agent was used in this process to reduce Co (III) to Co (II) [285] after Equation (2).



When compared to strong inorganic acids, some mild organic acids have attracted much attention in previous years. Oxalic acid can allow a brief cobalt/lithium recovery from the cathodic LiCoO_2 waste because soldering and precipitation occur simultaneously (CoC_2O_4 formation) at the leaching stage [282]. In this condition, the separation of cobalt from lithium can be done without further processing, such as precipitation of chemicals or extraction of solvent. Also, H_3PO_4 , a mild mineral acid, has not been shown to dissociate and divide at the same time [279]. In the H_3PO_4 annealing process, cobalt can be directly extracted as $\text{Co}_3(\text{PO}_4)_2$ precipitates, lithium and leaves in the effluent. In acidic leaching processes, the leaching efficiency can be significantly influenced by several operational parameters such as temperature, oxygen concentration (or H^+ concentration), leaching time, solid-liquid ratio, and feedstock. To balance the efficiency and reduction of the economy, it is necessary to optimize the leach conditions. Besides, some optimal operating conditions for the removal of materials from the fraction of LIBs used by various acidic cleaners are summarized and recorded.

Bio washing is another type of hydrometallurgical process that uses metabolites secreted by microorganisms to dissolve waste electrode materials and extract valuable metals [286,287]. Some bacteria and fungi may contain metals from used LIBs. Mishra et al. [288] used chemolithotrophic and acidophilic bacteria *Acidithiobacillus ferrooxidans* to treat cathodic LiCoO_2 materials. In the process, the bacteria used elemental sulfur and ferrous ions to produce sulfuric acids and iron ions in the solder medium, which allows the cathodic material to dissolve LiCoO_2 . The use of live biomass makes the leaching process more difficult to control [289]. Xin et al. [290] compared the bioleaching behavior of *Alicyclobacillus* sp. at a different mass density and it was found that the leaching efficiency was significantly affected by the mass density. As can be seen, the leaching efficiency dropped from 52% to 10% for cobalt and from 80% to 37% for lithium, with an increase in mass density from 1% to 4%. A similar result was reported in Mousavi et al. [291] observed in which they investigated the effect of bulk density on metal recovery for *Aspergillus niger* during the bio washing process. This phenomenon can be explained by the sensitivity of the microorganisms to the toxic electrolyte and spent LIBs since a higher mass density would contain more organic electrolytes with LiPF_6 , LiClO_4 , and LiBF_4 .

In the last stage of the hydrometallurgical process, metal separation and recovery must be done by trigger extraction, chemical precipitation, and electrochemical deposition. Solvent extraction is a liquid-liquid extraction process for separating metals in the effluent with extractants. Various extracts were used for Li, Co, Mn, Cu, etc. LIBs were used, such as bis- (2,4,4-trimethylpentyl) phosphinic acid (Cyanex) [292–294], di- (2-Ethylhexyl) phosphoric acid (D2EHPA) [295], Acorga M5640 [296,297], Trioctylamine (TOA) [296], 2-Ethylhexylphosphonic acid Mono-2-Ethylhexyl ester (PC-88 A) [298,299], etc. Chen et al. [295] used co-charged D2EHPA (Co-D2EHPA) to extract Mn from Mn, Co, and liqueur. More than 99% Mn was recovered under conditions as follows. Extraction time 5 min, pH-3.5 equilibrium, the concentration of Co-D2EHPA-15 vol%, and O: 1: Solvent ratio has some advantages such as low energy consumption, good separability, and easy operating conditions. Extracts are expensive, however, which increases processing costs in the recycling industry.

For the chemical precipitation method, precipitators are used to deposit precious metals in the liqueur. For instance, Contestabile et al. [300] used CO_2 balloon gas to convert dissolved lithium to lithium carbonate precipitation. Zhang et al. [266] chose a saturated sodium carbonate solution to precipitate lithium carbonate. In Zhang's work, the precipitation process was carried out at almost 100 °C because the solubility of lithium carbonate in an aqueous solution is inversely proportional to the temperature. After the rain, about 80% of lithium was recovered. Chemical precipitation has the advantages of low energy consumption and cheap cost, but its applications can be exacerbated

by the difficulties of separation and the use of metals by complicated solutions. Electrochemical deposition is an effective way to extract metals from the waste liquid in the form of pure metal or metal hydroxide. Freitas et al. [301] recovered cobalt from used electrodeposition LIBs. Pure cobalt was formed on the surface of the electrode and the highest charge efficiency of 96.9% was reached at pH 5.4. Myoung et al. [302] used an electrochemical deposit to recover cobalt from LiCoO₂ cathode waste. Because of their activity, cobalt was recycled as Co(OH)₂. Because hydroxide ions can be formed at the electrode by electro-reduction of dissolved oxygen and nitrate rations, which leads to an increase in the local surface pH titanium substrate, under suitable pH conditions, cobalt hydroxide could be deposited on the substrate. High purity metals with a high recovery rate can be obtained by electrochemical deposition; however, the energy consumption in this process is significant.

7.5. Direct Physical Recycling Process

The direct process involves the recovery of LIB components that are used without chemical treatments. The characteristic steps of direct physical recovery can be shown in Figure 23 which reflects the direct use of LIB, LiMn₂O₄, as cathode agent [303]. The cells are treated with CO₂, which can remove electrolytes. Subsequently, the CO₂ can be separated following a decrease in temperature and pressure; it is also possible to charge the electrolyte during battery reuse. Subsequently, the cellular components are extracted from physical methods; then the Cathode material is collected and reused with a new battery, probably with some relief.

Chen et al. [303] used direct recycling for LiFePO₄ from the already-employed LIB. Here, LIBs were separated, crushed, and washed in a sealing box without recovering the electrolyte. The LiFePO₄ material recovered without treatment has a low valve density and very low electrochemical performance because of polyvinylidene fluoride (PVDF) binder or material damage after a few charge-discharge cycles. After heat treatment, the cured cathode material showed an improvement in valve density and electrochemical properties. Especially when treated at 650 °C, the cathodic material has almost the same discharge capacity and energy density as fresh at high current densities. Rothermel et al. [304] compared three direct physical recovery processes to recover graphite anode materials obtained from used LIBs depicted in Figure 25. The first method is based on graphite heat treatment without electrolyte recovery. The second is the extraction of the electrolyte by subcritical CO₂ followed by heat treatment. The third process also contains electrolyte extraction and heat treatment, in addition to using supercritical CO₂ as an extract.

Experimental results have shown that electrolysis with subcritical CO₂ was the best recovery method. In the process, the graphite returned as the commercial TIMREX SLP50 synthetic graphite and the electrolyte was recovered by 90%. It should be noted that the residual salt (LiPF₆) can be extracted together with the electrolyte solvents, as long as some functional additives (such as 3:1 acetonitrile/propylene carbonate) are added to the extraction of CO₂ [305].

The advantages of recycling process control are short-path recycling processes, low power consumption, low pollution, and a higher rate of recycling. It is therefore not clear that recycled materials are new and durable. Finally, all of the recycling methods explained above are employed to recycle the LIBs. Due to various technical problems and economies of scale, the systems use different stages of development. Due to the simple operation and high cobalt recycling performance, the pyrometallurgy process was the most important metal in LIBs. With the advancements of battery technology, the internal electrical properties of cobalt are decreasing, while the demand for nickel and manganese is increasing. Lithium storage capacity has been shown to be a key issue, and the use of lithium batteries has been enhanced sharply in the previous years because of the drastic growth of the electricity market. Therefore, repeated cobalt recycling technologies should focus on the functional diffusion of LIB. Further, proper elimination or recovery of ambient elements, such as electrolytes, must be considered when designing recycling applications for LIB use.

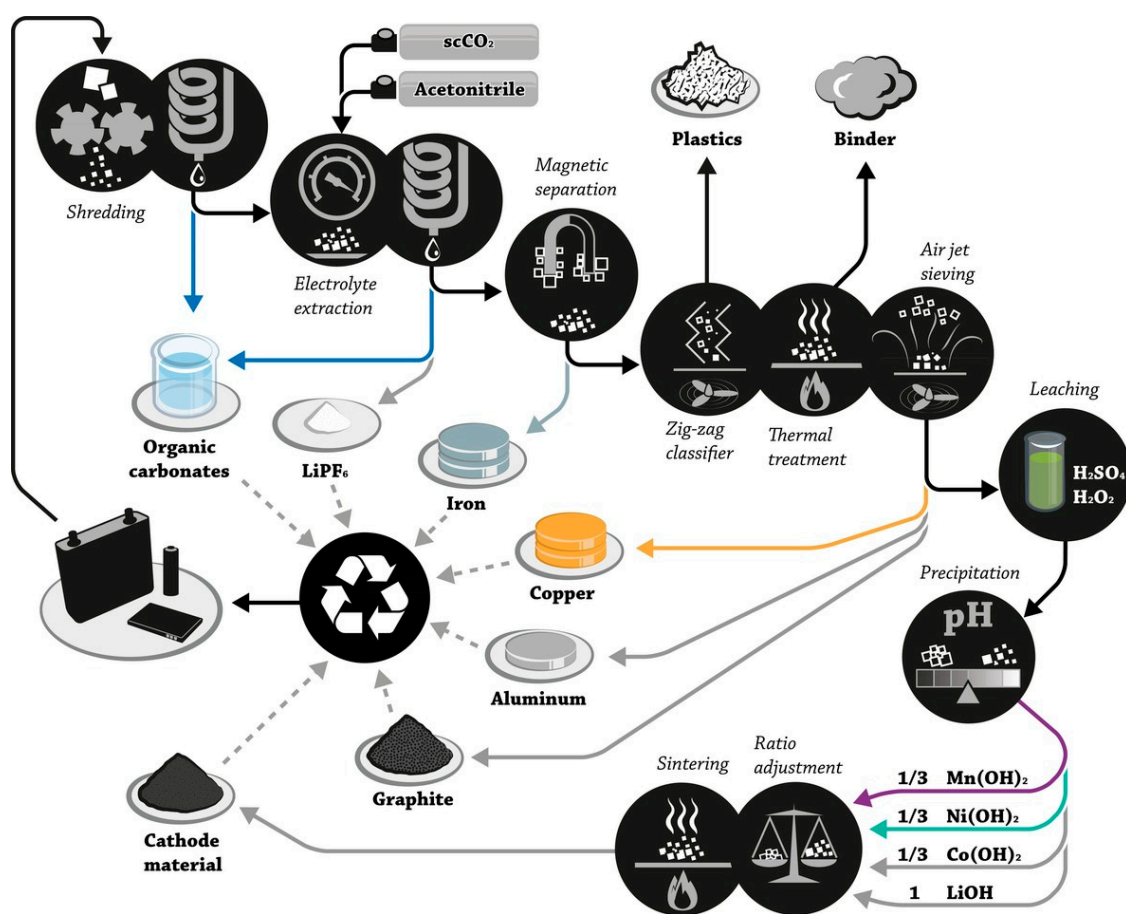


Figure 25. Schematic flowsheet for the LithoRec battery recycling process [304].

Currently, there are low volumes of electric-vehicle batteries that need recycling. When these volumes see an intense upsurge, there are queries about the financial prudence of gauge regarding recycling processes [306]. Pyrometallurgical methods, in particular, suffer from high capital costs, and if full recyclability of LIBs is to be attained, finding other methods is of immediate importance, rather than looking to recycling the spare valued components.

From lead acid battery recycling, there are many lessons to be learned for future LIBs recycling processes. A variety of advances enable electric-vehicle LIB recycling routes to be sparingly more effective [307], like improved cataloging skills, methods for splitting electrode materials, better progression flexibility, strategy for reprocessing, and superior company regulations of batteries. There is a strong chance for an extra refined style to battery recovery over automatic disassembly, keen seclusion of diverse batteries and the smart description, assessment and 'triage' of castoff batteries into streams for remanufacture, re-use and recycling. The possible aids to this are numerous and comprised abridged costs, greater value of recovered material streams, and the near abolition of the risk of injury to human workers.

The proposal of existing battery packs is not augmented for easy disassembly. Use of adhesives, bonding methods and fixtures do not lend themselves to easy disassembly either by hand or machine. All stated present profitable physical cell-breaking procedures use slicing or crushing with subsequent organization of the component materials. This makes the parting of the modules more challenging than if they were presorted, and significantly decreases the profitable value of waste material streams. Numerous tests in this area suggest that remanufacture, re-use and recycling could be useful if measured, promptly in the design process.

For direct recycling where purity of the recuperated materials is obligatory, a route which comprises of less component adulteration throughout the breaking stage is significant. This would

have an advantage in terms of an examination of the cell module chemistry, and the assessment of the state of charge and state of health of the cells earlier, before disassembling the module parts, rather than the manufacture of a combination of all components. Thus far, this parting has only been achieved at a laboratory scale and usually uses physical disassembly techniques that are problematic to scale up sparingly. The shift to better automation and robotic disassembly has the potential to make this process much faster. Matters about the binder still need to be fixed, and acid, alkali, solvent and thermal behaviors all have their positives and negatives. A cell proposal for recovery of materials is extremely alluring, with low-cost water-soluble binders [308,309].

8. Conclusions and Perspectives

In light of the aforementioned literature that shows the intent of tedious research efforts in the advancements of novel electrode materials for LIBs, a wider perception is revealed by nanoscience and technology. Novel methods and a deeper insight into the material science have delivered the chance to design, fabricate, and synthesize the suitable nanoarchitecture of electrodes for the next generation LIBs. Exquisitely tailored Physico-chemical features of nanostructures enable us to achieve high Li-ion flux at the interface of electrode/electrolyte, high storage of lithium, a lower path of diffusion for electrons and Li-ions, and minimal change of anode volume at the time of charging/discharging phenomenon. These unique features, when coupled together, can lead to the enhancement of energy and power density of the devices.

In the current review, recently advanced anode and cathode materials were comprehensively illustrated depending on their reaction mechanism with the lithium. The intuitive analysis of the intercalation and deintercalation materials that include both the carbonaceous and TiO/O₂ materials were discussed. The key observations include specific surface area, crystallinity, orientation, and morphology depicted by the storage capacity of the LIBs. Soft carbon has been of recent interest and hard carbon has had paramount importance in the EV sector. Graphene was elucidated with great detail and it was found that its excellent electrical characteristics made it more feasible for hybrid graphene/metal anodes. CNTs are next-generation LIB anode materials. Further, the alloying materials such as the Si, Ge, SnO, etc., can offer greater capacities and higher energy densities. Various conversion materials such as the metal phosphides/oxides/sulfides/nitrides need to be deeply investigated because of their certain disadvantages such as low capacity retention and higher hysteresis potential.

A variety of NCM members (NCM333, NCM523) are already of commercial interest and the possibilities of enhanced NCM811 and NCM622 will be seen in the near future. The consistent incremental enhancement in nickel has led to a potential increase in storage capacity. Unfortunately, NCM materials with Ni \geq 60% show not only a greater potential but also problems related to LiNiO₂. The major obstacles are the greater reactivity of Ni⁴⁺ at the end of charge, which can lead to lower thermal stability, and other reactions with the electrolyte (see the reactivity of Ni-rich NCM cathodes section). The Li/Ni mixing can disorder the phase and can finally inactive the rock salt phase on the surface of the particle (Cation/NCM cathodes section). Besides, the swift variation in the c parameter at the charge end puts more stress on the material leading to micro-cracks (Micro cracks formation in NCM section). All these challenges warrant more research that needs to be focused on enhancing the charge storage phenomenon. A cumulative approach that includes several treatments might provide the key to nickel rich materials. Structural stability can be enhanced by various dopants, whereas the surface, thermal stability, and minimal side reactions can be achieved by the active materials uniform coating. Eventually, the electrolyte solution itself may be able to be tailored to the needs of the material by suitable additives.

The appropriate recycling of the LIBs is of urgent focus since they contain various useful metals and harmful ingredients. Many recycling techniques that aim to recover the metal substances from the spent LIBs have been illustrated and most of them are industrialized. The key points in the recovery process of these metals and substances are the consumption of lower power and the eco-friendly nature of the technique. Moreover, to meet the efficient recycling and recovery establishment of the spent LIBs, more

research needs to be done, not only confined to the following key points. (1) Identification of spent LIBs in various efficient techniques. (2) Labeling/marketing or indexing the LIBs at the manufacturing plant and recycling plant could favor routing and supervision of the recycling. (3) Designing LIBs from a recycling point of view can avoid complex or irreversible assembling. (4) Standard norms of legislation should be of most importance in the recycling processes. This review article will be of assistance to future work and can be considered to be a convenient reference for the researchers and engineers in choosing the most adequate and suitable electrode materials along with their recycling techniques.

Author Contributions: Conceptualization, K.V.G.R., and H.-J.K.; methodology, T.K. and V.R. validation, C.V.V.M.G. formal analysis K.V.G.R. and K.Z. investigation K.V.G.R., S.S. and V.R.; resources, K.V.G.R. and K.Z. writing—H.-J.K. and K.V.G.R.; supervision, H.-J.K.; project administration, H.-J.K. and I.M.O. All authors have read and agreed to the published version of the manuscript.

Funding: This work was supported by BK21PLUS, Creative Human Resource Development Program for IT Convergence.

Conflicts of Interest: The authors declare no conflict of interest.

References

1. Scrosati, B. History of lithium batteries. *J. Solid State Electrochem.* **2011**, *15*, 1623–1630. [[CrossRef](#)]
2. Whittingham, M.S. Lithium batteries and cathode materials. *Chem. Rev.* **2004**, *104*, 4271–4302. [[CrossRef](#)]
3. Blomgren, G.E. The Development and Future of Lithium Ion Batteries. *J. Electrochem. Soc.* **2017**, *164*, 1. [[CrossRef](#)]
4. Nitta, N.; Wu, F.; Lee, J.T.; Yushin, G. Li-ion battery materials: Present and future. *Mater. Today* **2015**, *18*, 252–264. [[CrossRef](#)]
5. Etacheri, V.; Marom, R.; Elazari, R.; Salitra, G.; Aurbach, D. Challenges in the development of advanced Li-ion batteries: A review. *Energy Environ. Sci.* **2011**, *4*, 3243–3262. [[CrossRef](#)]
6. Tarascon, J.M.; Armand, M. Issues and challenges facing rechargeable lithium batteries. *Nature* **2001**, *414*, 359–367. [[CrossRef](#)]
7. Goodenough, J.B.; Park, K.S. The Li-ion rechargeable battery: A perspective. *J. Am. Chem. Soc.* **2013**, *135*, 1167–1176. [[CrossRef](#)]
8. Goodenough, J.B.; Kim, Y. Challenges for rechargeable Li batteries. *J. Power Sources* **2011**, *196*, 6688–6694. [[CrossRef](#)]
9. Armand, M.; Tarascon, J.M. Building better batteries. *Nature* **2008**, *451*, 652–657. [[CrossRef](#)]
10. Liu, W.; Oh, P.; Liu, X.; Lee, M.J.; Cho, W.; Chae, S.; Kim, Y.; Cho, J. Nickel-Rich Layered Lithium Transition-Metal Oxide for High-Energy Lithium-Ion Batteries. *Angew. Chem. Int. Ed.* **2015**, *54*, 4440–4457. [[CrossRef](#)]
11. Manthiram, A.; Knight, J.C.; Myung, S.T.; Oh, S.M.; Sun, Y.K. Nickel-Rich and Lithium-Rich Layered Oxide Cathodes: Progress and Perspectives. *Adv. Energy Mater.* **2016**, *6*, 1501010. [[CrossRef](#)]
12. Ahmad, S.; George, C.; Beesley, D.J.; Baumberg, J.J.; De Volder, M. Photo-Rechargeable Organo-Halide Perovskite Batteries. *Nano Lett.* **2018**, *18*, 1856–1862. [[CrossRef](#)] [[PubMed](#)]
13. Manthiram, A. Materials challenges and opportunities of lithium ion batteries. *J. Phys. Chem. Lett.* **2011**, *2*, 176–184. [[CrossRef](#)]
14. Goriparti, S.; Miele, E.; De Angelis, F.; Di Fabrizio, E.; Proietti Zaccaria, R.; Capiglia, C. Review on recent progress of nanostructured anode materials for Li-ion batteries. *J. Power Sources* **2014**, *257*, 421–443. [[CrossRef](#)]
15. Von Cresce, A.; Xu, K. Electrolyte Additive in Support of 5 V Li Ion Chemistry. *J. Electrochem. Soc.* **2011**, *158*, 3. [[CrossRef](#)]
16. Dedryvère, R.; Foix, D.; Franger, S.; Patoux, S.; Daniel, L.; Gonbeau, D. Electrode/electrolyte interface reactivity in high-voltage spinel LiMn_{1.6}Ni_{0.4}O₄/Li₄Ti₅O₁₂ lithium-ion battery. *J. Phys. Chem. C* **2010**, *114*, 10999–11008. [[CrossRef](#)]
17. Brédas, J.L.; Norton, J.E.; Cornil, J.; Coropceanu, V. Molecular understanding of organic solar cells: The challenges. *Acc. Chem. Res.* **2009**, *42*, 1691–1699. [[CrossRef](#)]

18. Capiglia, C.; Saito, Y.; Kageyama, H.; Mustarelli, P.; Iwamoto, T.; Tabuchi, T.; Tukamoto, H. 7Li and 19F diffusion coefficients and thermal properties of non-aqueous electrolyte solutions for rechargeable lithium batteries. *J. Power Sources* **1999**, *81*, 859–862. [[CrossRef](#)]
19. Capiglia, C.; Saito, Y.; Kataoka, H.; Kodama, T.; Quartarone, E.; Mustarelli, P. Structure and transport properties of polymer gel electrolytes based on PVdF-HFP and LiN(C₂F₅SO₂)₂. *Solid State Ion.* **2000**, *131*, 291–299. [[CrossRef](#)]
20. Marom, R.; Amalraj, S.F.; Leifer, N.; Jacob, D.; Aurbach, D. A review of advanced and practical lithium battery materials. *J. Mater. Chem.* **2011**, *21*, 9938–9954. [[CrossRef](#)]
21. Nazri, G.A.; Pistoia, G. *Lithium Batteries: Science and Technology*, 1st ed.; Springer: Berlin/Heidelberg, Germany, 2003; ISBN 978-0-387-92675-9.
22. Girishkumar, G.; McCloskey, B.; Luntz, A.C.; Swanson, S.; Wilcke, W. Lithium—Air battery: promise and challenges. *J. Phys. Chem. Lett.* **2010**, 2193–2203. [[CrossRef](#)]
23. Scrosati, B.; Garche, J. Lithium batteries: Status, prospects and future. *J. Power Sources* **2010**, *195*, 2419–2430. [[CrossRef](#)]
24. Ding, N.; Zhou, L.; Zhou, C.; Geng, D.; Yang, J.; Chien, S.W.; Liu, Z.; Ng, M.F.; Yu, A.; Hor, T.S.A.; et al. Building better lithium-sulfur batteries: From LiNO₂ to solid oxide catalyst. *Sci. Rep.* **2016**, *6*, 33154. [[CrossRef](#)] [[PubMed](#)]
25. Kim, T.H.; Park, J.S.; Chang, S.K.; Choi, S.; Ryu, J.H.; Song, H.K. The current move of lithium ion batteries towards the next phase. *Adv. Energy Mater.* **2012**, *2*, 860–872. [[CrossRef](#)]
26. Hu, L.; Zhang, Z.; Amine, K. Electrochemical investigation of carbonate-based electrolytes for high voltage lithium-ion cells. *J. Power Sources* **2013**, *236*, 175–180. [[CrossRef](#)]
27. Sun, X.G.; Liao, C.; Shao, N.; Bell, J.R.; Guo, B.; Luo, H.; Jiang, D.E.; Dai, S. Bicyclic imidazolium ionic liquids as potential electrolytes for rechargeable lithium ion batteries. *J. Power Sources* **2013**, *237*, 5–12. [[CrossRef](#)]
28. Quartarone, E.; Mustarelli, P. Electrolytes for solid-state lithium rechargeable batteries: Recent advances and perspectives. *Chem. Soc. Rev.* **2011**, *40*, 2525–2540. [[CrossRef](#)]
29. Xu, K. Nonaqueous liquid electrolytes for lithium-based rechargeable batteries. *Chem. Rev.* **2004**, *104*, 4303–4418. [[CrossRef](#)]
30. Borup, R.; Meyers, J.; Pivovar, B.; Kim, Y.S.; Mukundan, R.; Garland, N.; Myers, D.; Wilson, M.; Garzon, F.; Wood, D.; et al. Scientific aspects of polymer electrolyte fuel cell durability and degradation. *Chem. Rev.* **2007**, *107*, 3904–3951. [[CrossRef](#)]
31. Liang, Y.; Tao, Z.; Chen, J. Organic electrode materials for rechargeable lithium batteries. *Adv. Energy Mater.* **2012**, *2*, 742–769. [[CrossRef](#)]
32. Song, Z.; Zhou, H. Towards sustainable and versatile energy storage devices: An overview of organic electrode materials. *Energy Environ. Sci.* **2013**, *6*, 2280–2301. [[CrossRef](#)]
33. Goriparti, S.; Harish, M.N.K.; Sampath, S. Ellagic acid—A novel organic electrode material for high capacity lithium ion batteries. *Chem. Commun.* **2013**, *49*, 7234–7236. [[CrossRef](#)] [[PubMed](#)]
34. Gong, Z.; Yang, Y. Recent advances in the research of polyanion-type cathode materials for Li-ion batteries. *Energy Environ. Sci.* **2011**, *4*, 3223–3242. [[CrossRef](#)]
35. Li, C.C.; Wang, Y.W. Importance of binder compositions to the dispersion and electrochemical properties of water-based LiCoO₂ cathodes. *J. Power Sources* **2013**, *227*, 204–210. [[CrossRef](#)]
36. Ramanan, A. Development of Lithium-ion Batteries. *Curr. Sci.* **2019**, *117*, 1416–1418.
37. Liu, J. Addressing the grand challenges in energy storage. *Adv. Funct. Mater.* **2013**, *23*, 924–928. [[CrossRef](#)]
38. Orsini, F.; Du Pasquier, A.; Beaudouin, B.; Tarascon, J.M.; Trentin, M.; Langenhuizen, N.; De Beer, E.; Notten, P. In situ SEM study of the interfaces in plastic lithium cells. *J. Power Sources* **1999**, *81–82*, 918–921. [[CrossRef](#)]
39. Kim, C.; Yang, K.S.; Kojima, M.; Yoshida, K.; Kim, Y.J.; Kim, Y.A.; Endo, M. Fabrication of electrospinning-derived carbon nanofiber webs for the anode material of lithium-ion secondary batteries. *Adv. Funct. Mater.* **2006**, *16*, 2393–2397. [[CrossRef](#)]
40. Wu, Y.P.; Rahm, E.; Holze, R. Carbon anode materials for lithium ion batteries. *J. Power Sources* **2003**, *114*, 228–236. [[CrossRef](#)]
41. Zhou, H.; Zhu, S.; Hibino, M.; Honma, I.; Ichihara, M. Lithium Storage in Ordered Mesoporous Carbon (CMK-3) with High Reversible Specific Energy Capacity and Good Cycling Performance. *Adv. Mater.* **2003**, *15*, 2107–2111. [[CrossRef](#)]

42. Raccichini, R.; Varzi, A.; Passerini, S.; Scrosati, B. The role of graphene for electrochemical energy storage. *Nat. Mater.* **2015**, *14*, 271–279. [[CrossRef](#)] [[PubMed](#)]
43. Ge, M.; Rong, J.; Fang, X.; Zhou, C. Porous doped silicon nanowires for lithium ion battery anode with long cycle life. *Nano Lett.* **2012**, *12*, 2318–2323. [[CrossRef](#)]
44. Cheng, X.B.; Zhang, R.; Zhao, C.Z.; Zhang, Q. Toward Safe Lithium Metal Anode in Rechargeable Batteries: A Review. *Chem. Rev.* **2017**, *117*, 10403–10473. [[CrossRef](#)]
45. Zhuo, K.; Jeong, M.G.; Chung, C.H. Highly porous dendritic Ni-Sn anodes for lithium-ion batteries. *J. Power Sources* **2013**, *244*, 601–605. [[CrossRef](#)]
46. Hwang, I.S.; Kim, J.C.; Seo, S.D.; Lee, S.; Lee, J.H.; Kim, D.W. A binder-free Ge-nanoparticle anode assembled on multiwalled carbon nanotube networks for Li-ion batteries. *Chem. Commun.* **2012**, *48*, 7061–7063. [[CrossRef](#)] [[PubMed](#)]
47. Yuan, C.; Wu, H.B.; Xie, Y.; Lou, X.W. Mixed transition-metal oxides: Design, synthesis, and energy-related applications. *Angew. Chemie Int. Ed.* **2014**, *53*, 1488–1504. [[CrossRef](#)] [[PubMed](#)]
48. Wei, W.; Wang, Z.; Liu, Z.; Liu, Y.; He, L.; Chen, D.; Umar, A.; Guo, L.; Li, J. Metal oxide hollow nanostructures: Fabrication and Li storage performance. *J. Power Sources* **2013**, *238*, 376–387. [[CrossRef](#)]
49. Zhang, L.; Wu, H.B.; Lou, X.W. Iron-oxide-based advanced anode materials for lithium-ion batteries. *Adv. Energy Mater.* **2014**, *4*, 1300958. [[CrossRef](#)]
50. Chen, J. Recent progress in advanced materials for lithium ion batteries. *Materials (Basel)* **2013**, *6*, 156–183. [[CrossRef](#)]
51. Poizot, P.; Laruelle, S.; Grugeon, S.; Dupont, L.; Tarascon, J.M. Nano-sized transition-metal oxides as negative-electrode materials for lithium-ion batteries. *Nature* **2000**, *407*, 496–499. [[CrossRef](#)]
52. Guo, Y.; Li, H.; Zhai, T. Reviving Lithium-Metal Anodes for Next-Generation High-Energy Batteries. *Adv. Mater.* **2017**, *29*, 1700007. [[CrossRef](#)]
53. Sun, Q.; Zhang, X.Q.; Han, F.; Li, W.C.; Lu, A.H. Controlled hydrothermal synthesis of 1D nanocarbons by surfactant-templated assembly for use as anodes for rechargeable lithium-ion batteries. *J. Mater. Chem.* **2012**, *22*, 17049–17054. [[CrossRef](#)]
54. Chen, J.; Xia, X.H.; Tu, J.P.; Xiong, Q.Q.; Yu, Y.X.; Wang, X.L.; Gu, C.D. Co₃O₄-C core-shell nanowire array as an advanced anode material for lithium ion batteries. *J. Mater. Chem.* **2012**, *22*, 15056–15061. [[CrossRef](#)]
55. Ueda, A.; Nagao, M.; Inoue, A.; Hayashi, A.; Seino, Y.; Ota, T.; Tatsumisago, M. Electrochemical performance of all-solid-state lithium batteries with Sn₄P₃ negative electrode. *J. Power Sources* **2013**, *244*, 597–600. [[CrossRef](#)]
56. Hwang, H.; Kim, H.; Cho, J. MoS₂ nanoplates consisting of disordered graphene-like layers for high rate lithium battery anode materials. *Nano Lett.* **2011**, *11*, 4826–4830. [[CrossRef](#)] [[PubMed](#)]
57. Bruce, P.G.; Scrosati, B.; Tarascon, J.M. Nanomaterials for rechargeable lithium batteries. *Angew. Chem. Int. Ed.* **2008**, *47*, 2930–2946. [[CrossRef](#)]
58. Wang, Y.; Li, H.; He, P.; Hosono, E.; Zhou, H. Nano active materials for lithium-ion batteries. *Nanoscale* **2010**, *2*, 1294–1305. [[CrossRef](#)] [[PubMed](#)]
59. Mukherjee, R.; Krishnan, R.; Lu, T.M.; Koratkar, N. Nanostructured electrodes for high-power lithium ion batteries. *Nano Energy* **2012**, *1*, 518–533. [[CrossRef](#)]
60. Wu, F.; Maier, J.; Yu, Y. Guidelines and trends for next-generation rechargeable lithium and lithium-ion batteries. *Chem. Soc. Rev.* **2020**, *49*, 1569–1614. [[CrossRef](#)]
61. Yen, Y.-C.; Chao, S.-C.; Wu, H.-C.; Wu, N.-L. Study on Solid-Electrolyte-Interphase of Si and C-Coated Si Electrodes in Lithium Cells. *J. Electrochem. Soc.* **2009**, *156*, 2. [[CrossRef](#)]
62. Bai, P.; Bazant, M.Z. Charge transfer kinetics at the solid-solid interface in porous electrodes. *Nat. Commun.* **2014**, *5*, 1–7.
63. Liu, J.; Song, K.; Van Aken, P.A.; Maier, J.; Yu, Y. Self-supported Li₄Ti₅O₁₂-C nanotube arrays as high-rate and long-life anode materials for flexible Li-ion batteries. *Nano Lett.* **2014**, *14*, 2597–2603. [[CrossRef](#)] [[PubMed](#)]
64. Bandhauer, T.M.; Garimella, S.; Fuller, T.F. A Critical Review of Thermal Issues in Lithium-Ion Batteries. *J. Electrochem. Soc.* **2011**, *158*, R1. [[CrossRef](#)]
65. Son, M.Y.; Hong, Y.J.; Lee, J.K.; Chan Kang, Y. One-pot synthesis of Fe₂O₃ yolk-shell particles with two, three, and four shells for application as an anode material in lithium-ion batteries. *Nanoscale* **2013**, *5*, 11592–11597. [[CrossRef](#)]

66. Yin, L.; Zhang, Z.; Li, Z.; Hao, F.; Li, Q.; Wang, C.; Fan, R.; Qi, Y. Spinel ZnMn₂O₄ nanocrystal-anchored 3D hierarchical carbon aerogel hybrids as anode materials for lithium ion batteries. *Adv. Funct. Mater.* **2014**, *24*, 4176–4185. [[CrossRef](#)]
67. Wang, C.; Wu, H.; Chen, Z.; Mcdowell, M.T.; Cui, Y.; Bao, Z. Self-healing chemistry enables the stable operation of silicon microparticle anodes for high-energy lithium-ion batteries. *Nat. Chem.* **2013**, *5*, 1042. [[CrossRef](#)]
68. Mahmood, N.; Zhang, C.; Liu, F.; Zhu, J.; Hou, Y. Hybrid of Co₃Sn₂@Co nanoparticles and nitrogen-doped graphene as a lithium ion battery anode. *ACS Nano* **2013**, *7*, 10307–10318. [[CrossRef](#)]
69. Sun, Y.; Liu, N.; Cui, Y. Promises and challenges of nanomaterials for lithium-based rechargeable batteries. *Nat. Energy* **2016**, *1*, 1–12.
70. Li, H.; Zhou, H. Enhancing the performances of Li-ion batteries by carbon-coating: Present and future. *Chem. Commun.* **2012**, *48*, 1201–1217. [[CrossRef](#)]
71. Zhang, H.L.; Liu, S.H.; Li, F.; Bai, S.; Liu, C.; Tan, J.; Cheng, H.M. Electrochemical performance of pyrolytic carbon-coated natural graphite spheres. *Carbon* **2006**, *44*, 2212–2218. [[CrossRef](#)]
72. Yoshio, M.; Wang, H.; Fukuda, K.; Umeno, T.; Abe, T.; Ogumi, Z. Improvement of natural graphite as a lithium-ion battery anode material, from raw flake to carbon-coated sphere. *J. Mater. Chem.* **2004**, *14*, 1754–1758. [[CrossRef](#)]
73. Fu, L.J.; Liu, H.; Li, C.; Wu, Y.P.; Rahm, E.; Holze, R.; Wu, H.Q. Surface modifications of electrode materials for lithium ion batteries. *Solid State Sci.* **2006**, *8*, 113–128. [[CrossRef](#)]
74. Fujimoto, H.; Tokumitsu, K.; Mabuchi, A.; Chinnasamy, N.; Kasuh, T. The anode performance of the hard carbon for the lithium ion battery derived from the oxygen-containing aromatic precursors. *J. Power Sources* **2010**, *195*, 7452–7456. [[CrossRef](#)]
75. Yang, J.; Zhou, X.Y.; Li, J.; Zou, Y.L.; Tang, J.J. Study of nano-porous hard carbons as anode materials for lithium ion batteries. *Mater. Chem. Phys.* **2012**, *135*, 445–450. [[CrossRef](#)]
76. Bridges, C.A.; Sun, X.G.; Zhao, J.; Paranthaman, M.P.; Dai, S. In situ observation of solid electrolyte interphase formation in ordered mesoporous hard carbon by small-angle neutron scattering. *J. Phys. Chem. C* **2012**, *116*, 7701–7711. [[CrossRef](#)]
77. Meunier, V.; Kephart, J.; Roland, C.; Bernholc, J. Ab Initio Investigations of Lithium Diffusion in Carbon Nanotube Systems. *Phys. Rev. Lett.* **2002**, *88*, 075506. [[CrossRef](#)]
78. Schauerma, C.M.; Ganter, M.J.; Gaustad, G.; Babbitt, C.W.; Raffaele, R.P.; Landi, B.J. Recycling single-wall carbon nanotube anodes from lithium ion batteries. *J. Mater. Chem.* **2012**, *22*, 12008–12015. [[CrossRef](#)]
79. Nishidate, K.; Hasegawa, M. Energetics of lithium ion adsorption on defective carbon nanotubes. *Phys. Rev. B Condens. Matter Mater. Phys.* **2005**, *71*, 245418. [[CrossRef](#)]
80. Zhao, J.; Buldum, A.; Han, J.; Lu, J.P. First-principles study of Li-intercalated carbon nanotube ropes. *Phys. Rev. Lett.* **2000**, *85*, 1706. [[CrossRef](#)] [[PubMed](#)]
81. Zhu, J.; Yang, D.; Yin, Z.; Yan, Q.; Zhang, H. Graphene and graphene-based materials for energy storage applications. *Small* **2014**, *10*, 3480–3498. [[CrossRef](#)]
82. Chen, Z.; Belharouak, I.; Sun, Y.K.; Amine, K. Titanium-based anode materials for safe lithium-ion batteries. *Adv. Funct. Mater.* **2013**, *23*, 959–969. [[CrossRef](#)]
83. Rudawski, N.G.; Yates, B.R.; Holzworth, M.R.; Jones, K.S.; Elliman, R.G.; Volinsky, A.A. Ion beam-mixed Ge electrodes for high capacity Li rechargeable batteries. *J. Power Sources* **2013**, *223*, 336–340. [[CrossRef](#)]
84. Chockla, A.M.; Klavetter, K.C.; Mullins, C.B.; Korgel, B.A. Solution-grown germanium nanowire anodes for lithium-ion batteries. *ACS Appl. Mater. Interfaces* **2012**, *4*, 4658–4664. [[CrossRef](#)] [[PubMed](#)]
85. Szczech, J.R.; Jin, S. Nanostructured silicon for high capacity lithium battery anodes. *Energy Environ. Sci.* **2011**, *4*, 56–72. [[CrossRef](#)]
86. Yang, J.; Takeda, Y.; Imanishi, N.; Capiglia, C.; Xie, J.Y.; Yamamoto, O. SiO_x-based anodes for secondary lithium batteries. *Solid State Ion.* **2002**, *152*, 125–129. [[CrossRef](#)]
87. Park, C.M.; Kim, J.H.; Kim, H.; Sohn, H.J. Li-alloy based anode materials for Li secondary batteries. *Chem. Soc. Rev.* **2010**, *39*, 3115–3141. [[CrossRef](#)]
88. Wang, Z.; Zhou, L.; Lou, X.W. Metal oxide hollow nanostructures for lithium-ion batteries. *Adv. Mater.* **2012**, *24*, 1903–1911. [[CrossRef](#)]
89. Jiang, J.; Li, Y.; Liu, J.; Huang, X.; Yuan, C.; Lou, X.W. Recent advances in metal oxide-based electrode architecture design for electrochemical energy storage. *Adv. Mater.* **2012**, *24*, 5166–5180. [[CrossRef](#)]

90. Prosini, P.P.; Carewska, M.; Loreti, S.; Minarini, C.; Passerini, S. Lithium iron oxide as alternative anode for li-ion batteries. *Int. J. Inorg. Mater.* **2000**, *2*, 365–370. [[CrossRef](#)]
91. Lai, C.H.; Lu, M.Y.; Chen, L.J. Metal sulfide nanostructures: Synthesis, properties and applications in energy conversion and storage. *J. Mater. Chem.* **2012**, *22*, 19–30. [[CrossRef](#)]
92. Boyanov, S.; Annou, K.; Villevieille, C.; Pelosi, M.; Zitoun, D.; Monconduit, L. Nanostructured transition metal phosphide as negative electrode for lithium-ion batteries. *Ionics* **2008**, *14*, 183–190. [[CrossRef](#)]
93. Ji, L.; Lin, Z.; Alcoutlabi, M.; Zhang, X. Recent developments in nanostructured anode materials for rechargeable lithium-ion batteries. *Energy Environ. Sci.* **2011**, *4*, 2682–2699. [[CrossRef](#)]
94. Lee, J.T.; Chu, Y.J.; Peng, X.W.; Wang, F.M.; Yang, C.R.; Li, C.C. A novel and efficient water-based composite binder for LiCoO₂ cathodes in lithium-ion batteries. *J. Power Sources* **2007**, *173*, 985–989. [[CrossRef](#)]
95. Yu, Y.; Cui, C.; Qian, W.; Xie, Q.; Zheng, C.; Kong, C.; Wei, F. Carbon nanotube production and application in energy storage. *Asia-Pac. J. Chem. Eng.* **2013**, *8*, 234–245. [[CrossRef](#)]
96. Dileo, R.A.; Castiglia, A.; Ganter, M.J.; Rogers, R.E.; Cress, C.D.; Raffaele, R.P.; Landi, B.J. Enhanced capacity and rate capability of carbon nanotube based anodes with titanium contacts for lithium ion batteries. *ACS Nano* **2010**, *10*, 6121–6131. [[CrossRef](#)] [[PubMed](#)]
97. De Las Casas, C.; Li, W. A review of application of carbon nanotubes for lithium ion battery anode material. *J. Power Sources* **2012**, *208*, 74–85. [[CrossRef](#)]
98. Gu, Y.; Wu, F.; Wang, Y. Confined volume change in Sn-Co-C ternary tube-in-tube composites for high-capacity and long-life lithium storage. *Adv. Funct. Mater.* **2013**, *23*, 893–899. [[CrossRef](#)]
99. Wu, Y.; Wei, Y.; Wang, J.; Jiang, K.; Fan, S. Conformal Fe₃O₄ sheath on aligned carbon nanotube scaffolds as high-performance anodes for lithium ion batteries. *Nano Lett.* **2013**, *13*, 818–823. [[CrossRef](#)]
100. Bindumadhavan, K.; Srivastava, S.K.; Mahanty, S. MoS₂-MWCNT hybrids as a superior anode in lithium-ion batteries. *Chem. Commun.* **2013**, *49*, 1823–1825. [[CrossRef](#)]
101. Stankovich, S.; Dikin, D.A.; Dommett, G.H.B.; Kohlhaas, K.M.; Zimney, E.J.; Stach, E.A.; Piner, R.D.; Nguyen, S.B.T.; Ruoff, R.S. Graphene-based composite materials. *Nature* **2006**, *442*, 282–286. [[CrossRef](#)]
102. Liang, M.; Zhi, L. Graphene-based electrode materials for rechargeable lithium batteries. *J. Mater. Chem.* **2009**, *19*, 5871–5878. [[CrossRef](#)]
103. Brownson, D.A.C.; Kampouris, D.K.; Banks, C.E. An overview of graphene in energy production and storage applications. *J. Power Sources* **2011**, *196*, 4873–4885. [[CrossRef](#)]
104. Liu, Y.; Artyukhov, V.I.; Liu, M.; Harutyunyan, A.R.; Yakobson, B.I. Feasibility of lithium storage on graphene and its derivatives. *J. Phys. Chem. Lett.* **2013**, *4*, 1737–1742. [[CrossRef](#)]
105. Hwang, H.J.; Koo, J.; Park, M.; Park, N.; Kwon, Y.; Lee, H. Multilayer graphynes for lithium ion battery anode. *J. Phys. Chem. C* **2013**, *117*, 6919–6923. [[CrossRef](#)]
106. Pan, D.; Wang, S.; Zhao, B.; Wu, M.; Zhang, H.; Wang, Y.; Jiao, Z. Li storage properties of disordered graphene nanosheets. *Chem. Mater.* **2009**, *21*, 3136–3142. [[CrossRef](#)]
107. Lin, D.; Liu, Y.; Cui, Y. Reviving the lithium metal anode for high-energy batteries. *Nat. Nanotechnol.* **2017**, *12*, 194–206. [[CrossRef](#)] [[PubMed](#)]
108. Hong, Z.; Wei, M. Layered titanate nanostructures and their derivatives as negative electrode materials for lithium-ion batteries. *J. Mater. Chem. A* **2013**, *1*, 4403–4414. [[CrossRef](#)]
109. Moretti, A.; Kim, G.T.; Bresser, D.; Renger, K.; Paillard, E.; Marassi, R.; Winter, M.; Passerini, S. Investigation of different binding agents for nanocrystalline anatase TiO₂ anodes and its application in a novel, green lithium-ion battery. *J. Power Sources* **2013**, *221*, 419–426. [[CrossRef](#)]
110. Yang, Z.; Choi, D.; Kerisit, S.; Rosso, K.M.; Wang, D.; Zhang, J.; Graff, G.; Liu, J. Nanostructures and lithium electrochemical reactivity of lithium titanites and titanium oxides: A review. *J. Power Sources* **2009**, *192*, 588–598. [[CrossRef](#)]
111. Ma, Y.; Ji, G.; Ding, B.; Lee, J.Y. Facile solvothermal synthesis of anatase TiO₂ microspheres with adjustable mesoporosity for the reversible storage of lithium ions. *J. Mater. Chem.* **2012**, *22*, 24380–24385. [[CrossRef](#)]
112. Shen, L.; Yuan, C.; Luo, H.; Zhang, X.; Xu, K.; Xia, Y. Facile synthesis of hierarchically porous Li₄Ti₅O₁₂ microspheres for high rate lithium ion batteries. *J. Mater. Chem.* **2010**, *20*, 6998–7004. [[CrossRef](#)]
113. Mahmoud, A.; Amarilla, J.M.; Lasri, K.; Saadoun, I. Influence of the synthesis method on the electrochemical properties of the Li₄Ti₅O₁₂ spinel in Li-half and Li-ion full-cells. A systematic comparison. *Electrochim. Acta* **2013**, *93*, 163–172. [[CrossRef](#)]

114. Zhu, G.N.; Chen, L.; Wang, Y.G.; Wang, C.X.; Che, R.C.; Xia, Y.Y. Binary $\text{Li}_4\text{Ti}_5\text{O}_{12}$ - $\text{Li}_2\text{Ti}_3\text{O}_7$ nanocomposite as an anode material for Li-ion batteries. *Adv. Funct. Mater.* **2013**, *23*, 640–647. [[CrossRef](#)]
115. Wang, J.; Liu, X.M.; Yang, H.; Shen, X.D. Characterization and electrochemical properties of carbon-coated $\text{Li}_4\text{Ti}_5\text{O}_{12}$ prepared by a citric acid sol-gel method. *J. Alloys Compd.* **2011**, *509*, 712–718. [[CrossRef](#)]
116. Lin, J.Y.; Hsu, C.C.; Ho, H.P.; Wu, S.H. Sol-gel synthesis of aluminum doped lithium titanate anode material for lithium ion batteries. *Electrochim. Acta* **2013**, *87*, 126–132. [[CrossRef](#)]
117. Prakash, A.S.; Manikandan, P.; Ramesha, K.; Sathiya, M.; Tarascon, J.M.; Shukla, A.K. Solution-combustion synthesized nanocrystalline $\text{Li}_4\text{Ti}_5\text{O}_{12}$ as high-rate performance li-ion battery anode. *Chem. Mater.* **2010**, *22*, 2857–2863. [[CrossRef](#)]
118. Shen, L.; Uchaker, E.; Zhang, X.; Cao, G. Hydrogenated $\text{Li}_4\text{Ti}_5\text{O}_{12}$ nanowire arrays for high rate lithium ion batteries. *Adv. Mater.* **2012**, *24*, 6502–6506. [[CrossRef](#)]
119. Wagemaker, M.; Mulder, F.M. Properties and promises of nanosized insertion materials for li-ion batteries. *Acc. Chem. Res.* **2013**, *46*, 1206–1215. [[CrossRef](#)]
120. Roy, P.; Srivastava, S.K. Nanostructured anode materials for lithium ion batteries. *J. Mater. Chem. A* **2015**. [[CrossRef](#)]
121. Meng, X.; Banis, M.N.; Geng, D.; Li, X.; Zhang, Y.; Li, R.; Abou-Rachid, H.; Sun, X. Controllable atomic layer deposition of one-dimensional nanotubular TiO_2 . *Appl. Surf. Sci.* **2013**, *266*, 132–140. [[CrossRef](#)]
122. Deng, D.; Kim, M.G.; Lee, J.Y.; Cho, J. Green energy storage materials: Nanostructured TiO_2 and Sn-based anodes for lithium-ion batteries. *Energy Environ. Sci.* **2009**, *2*, 818–837. [[CrossRef](#)]
123. Kang, J.W.; Kim, D.H.; Mathew, V.; Lim, J.S.; Gim, J.H.; Kim, J. Particle Size Effect of Anatase TiO_2 Nanocrystals for Lithium-Ion Batteries. *J. Electrochem. Soc.* **2011**, *158*, 2. [[CrossRef](#)]
124. Bresser, D.; Paillard, E.; Binetti, E.; Krueger, S.; Striccoli, M.; Winter, M.; Passerini, S. Percolating networks of TiO_2 nanorods and carbon for high power lithium insertion electrodes. *J. Power Sources* **2012**, *206*, 301–309. [[CrossRef](#)]
125. Cheng, H.; Ma, J.; Zhao, Z.; Qi, L. Hydrothermal Preparation of Uniform Nanosize Rutile and Anatase Particles. *Chem. Mater.* **1995**, *7*, 663–671. [[CrossRef](#)]
126. Su, X.; Wu, Q.; Zhan, X.; Wu, J.; Wei, S.; Guo, Z. Advanced titania nanostructures and composites for lithium ion battery. *J. Mater. Sci.* **2012**, *47*, 2519–2534. [[CrossRef](#)]
127. Armstrong, A.R.; Armstrong, G.; Canales, J.; García, R.; Bruce, P.G. Lithium-ion intercalation into TiO_2 -B nanowires. *Adv. Mater.* **2005**, *17*, 862–865. [[CrossRef](#)]
128. Jiang, C.; Honma, I.; Kudo, T.; Zhou, H. Nanocrystalline rutile TiO_2 electrode for high-capacity and high-rate lithium storage. *Electrochem. Solid State Lett.* **2007**, *10*, 5. [[CrossRef](#)]
129. Rai, A.K.; Anh, L.T.; Gim, J.; Mathew, V.; Kang, J.; Paul, B.J.; Song, J.; Kim, J. Simple synthesis and particle size effects of TiO_2 nanoparticle anodes for rechargeable lithium ion batteries. *Electrochim. Acta* **2013**, *90*, 112–118. [[CrossRef](#)]
130. Reddy, A.L.M.; Gowda, S.R.; Shaijumon, M.M.; Ajayan, P.M. Hybrid nanostructures for energy storage applications. *Adv. Mater.* **2012**, *24*, 5045–5064. [[CrossRef](#)]
131. Mekonnen, Y.; Sundararajan, A.; Sarwat, A.I. A review of cathode and anode materials for lithium-ion batteries. In Proceedings of the SoutheastCon 2016, Norfolk, VA, USA, 30 March–3 April 2016.
132. Kong, L.L.; Wang, L.; Ni, Z.C.; Liu, S.; Li, G.R.; Gao, X.P. Lithium–Magnesium Alloy as a Stable Anode for Lithium–Sulfur Battery. *Adv. Funct. Mater.* **2019**, *29*, 1808756. [[CrossRef](#)]
133. Kasavajjula, U.; Wang, C.; Appleby, A.J. Nano- and bulk-silicon-based insertion anodes for lithium-ion secondary cells. *J. Power Sources* **2007**, *29*, 1808756. [[CrossRef](#)]
134. Zhang, H.; Braun, P.V. Three-dimensional metal scaffold supported bicontinuous silicon battery anodes. *Nano Lett.* **2012**, *12*, 2778–2783. [[CrossRef](#)] [[PubMed](#)]
135. Gu, J.; Collins, S.M.; Carim, A.I.; Hao, X.; Bartlett, B.M.; Maldonado, S. Template-free preparation of crystalline Ge nanowire film electrodes via an electrochemical liquid-liquid-solid process in water at ambient pressure and temperature for energy storage. *Nano Lett.* **2012**, *12*, 4617–4623. [[CrossRef](#)] [[PubMed](#)]
136. Wu, H.; Cui, Y. Designing nanostructured Si anodes for high energy lithium ion batteries. *Nano Today* **2012**, *7*, 414–429. [[CrossRef](#)]
137. Zhu, B.; Wang, X.; Yao, P.; Lia, J.; Zhu, J. Towards high energy density lithium battery anodes: Silicon and lithium. *Chem. Sci.* **2019**, *10*, 7132–7148. [[CrossRef](#)]

138. Teki, R.; Krishnan, R.; Parker, T.C.; Lu, T.M.; Datta, M.K.; Kumta, P.N.; Koratkar, N. Nanostructured silicon anodes for lithium Ion rechargeable batteries. *Small* **2009**, *5*, 2236–2242. [CrossRef]
139. Magasinski, A.; Dixon, P.; Hertzberg, B.; Kvit, A.; Ayala, J.; Yushin, G. High-performance lithium-ion anodes using a hierarchical bottom-up approach. *Nat. Mater.* **2010**, *9*, 353–358. [CrossRef]
140. Jung, C.H.; Kim, K.H.; Hong, S.H. Stable Silicon Anode for Lithium-Ion Batteries through Covalent Bond Formation with a Binder via Esterification. *ACS Appl. Mater. Interfaces* **2019**, *11*, 26753–26763. [CrossRef]
141. Song, K.; Yoo, S.; Kang, K.; Heo, H.; Kang, Y.M.; Jo, M.H. Hierarchical SiO_x nanoconifers for Li-ion battery anodes with structural stability and kinetic enhancement. *J. Power Sources* **2013**, *229*, 229–233. [CrossRef]
142. Liu, B.; Abouimrane, A.; Ren, Y.; Balasubramanian, M.; Wang, D.; Fang, Z.Z.; Amine, K. New anode material based on SiO-SnxCoyCz for lithium batteries. *Chem. Mater.* **2012**, *24*, 4653–4661. [CrossRef]
143. Yamada, Y.; Iriyama, Y.; Abe, T.; Ogumi, Z. Kinetics of Electrochemical Insertion and Extraction of Lithium Ion at SiO. *J. Electrochem. Soc.* **2010**, *1*, 157. [CrossRef]
144. Hwa, Y.; Park, C.-M.; Sohn, H.-J. Meeting Abstracts, MA2012-02. 2012, p. 913. Available online: <https://iopscience.iop.org/volume/2151-2043/MA2012-02> (accessed on 8 June 2020).
145. Shi, L.; Pang, C.; Chen, S.; Wang, M.; Wang, K.; Tan, Z.; Gao, P.; Ren, J.; Huang, Y.; Peng, H.; et al. Vertical Graphene Growth on SiO Microparticles for Stable Lithium Ion Battery Anodes. *Nano Lett.* **2017**, *6*, 3681–3687. [CrossRef] [PubMed]
146. Erickson, E.M.; Markevich, E.; Salitra, G.; Sharon, D.; Hirshberg, D.; de la Llave, E.; Shterenberg, I.; Rosenman, A.; Frimer, A.; Aurbach, D. Review—Development of Advanced Rechargeable Batteries: A Continuous Challenge in the Choice of Suitable Electrolyte Solutions. *J. Electrochem. Soc.* **2015**, *162*, 1–14. [CrossRef]
147. Flynn, G.; Palaniappan, K.; Sheehan, M.; Kennedy, T.; Ryan, K.M. Solution synthesis of lead seeded germanium nanowires and branched nanowire networks and their application as Li-ion battery anodes. *Nanotechnology* **2017**. [CrossRef] [PubMed]
148. Liu, X.H.; Huang, S.; Picraux, S.T.; Li, J.; Zhu, T.; Huang, J.Y. Reversible nanopore formation in Ge nanowires during lithiation-delithiation cycling: An in situ transmission electron microscopy study. *Nano Lett.* **2011**, *11*, 3991–3997. [CrossRef]
149. Park, M.H.; Cho, Y.; Kim, K.; Kim, J.; Liu, M.; Cho, J. Germanium nanotubes prepared by using the Kirkendall effect as anodes for high-rate lithium batteries. *Angew. Chem. Int. Ed.* **2011**, *50*, 9647–9650. [CrossRef]
150. Kim, C.H.; Im, H.S.; Cho, Y.J.; Jung, C.S.; Jang, D.M.; Myung, Y.; Kim, H.S.; Back, S.H.; Lim, Y.R.; Lee, C.W.; et al. High-yield gas-phase laser photolysis synthesis of germanium nanocrystals for high-performance photodetectors and lithium ion batteries. *J. Phys. Chem. C* **2012**, *50*, 26190–26196. [CrossRef]
151. Cui, G.; Gu, L.; Zhi, L.; Kaskhedikar, N.; Van Aken, P.A.; Müllen, K.; Maier, J. A germanium-carbon nanocomposite material for lithium batteries. *Adv. Mater.* **2008**, *20*, 3079–3083. [CrossRef]
152. Li, X.; Yang, Z.; Fu, Y.; Qiao, L.; Li, D.; Yue, H.; He, D. Germanium Anode with Excellent Lithium Storage Performance in a Germanium/Lithium–Cobalt Oxide Lithium-Ion Battery. *ACS Nano* **2015**, *9*, 1858–1867. [CrossRef]
153. Chockla, A.M.; Panthani, M.G.; Holmberg, V.C.; Hessel, C.M.; Reid, D.K.; Bogart, T.D.; Harris, J.T.; Mullins, C.B.; Korgel, B.A. Electrochemical lithiation of graphene-supported silicon and germanium for rechargeable batteries. *J. Phys. Chem. C* **2012**, *116*, 11917–11923. [CrossRef]
154. Li, X.; Wang, C. Engineering nanostructured anodes via electrostatic spray deposition for high performance lithium ion battery application. *J. Mater. Chem. A* **2013**, *1*, 165–182. [CrossRef]
155. Kim, H.; Cho, J. Hard templating synthesis of mesoporous and nanowire SnO₂ lithium battery anode materials. *J. Mater. Chem.* **2008**, *18*, 771–775. [CrossRef]
156. Yang, Z.; Du, G.; Guo, Z.; Yu, X.; Li, S.; Chen, Z.; Zhang, P.; Liu, H. Plum-branch-like carbon nanofibers decorated with SnO₂ nanocrystals. *Nanoscale* **2010**, *2*, 1011–1017. [CrossRef]
157. Yin, X.; Chen, L.; Li, C.; Hao, Q.; Liu, S.; Li, Q.; Zhang, E.; Wang, T. Synthesis of mesoporous SnO₂ spheres via self-assembly and superior lithium storage properties. *Electrochim. Acta* **2011**, *56*, 2358–2363. [CrossRef]
158. Ferraresi, G.; Villevieille, C.; Czekaj, I.; Horisberger, M.; Novák, P.; El Kazzi, M. SnO₂ Model Electrode Cycled in Li-Ion Battery Reveals the Formation of Li₂SnO₃ and Li₈SnO₆ Phases through Conversion Reactions. *ACS Appl. Mater. Interfaces* **2018**, *10*, 8712–8720. [CrossRef] [PubMed]
159. Xu, J.S.; Zhu, Y.J. Monodisperse Fe₃O₄ and γ-Fe₂O₃ magnetic mesoporous microspheres as anode materials for lithium-ion batteries. *ACS Appl. Mater. Interfaces* **2012**, *4*, 4752–4757. [CrossRef]

160. Koo, B.; Xiong, H.; Slater, M.D.; Prakapenka, V.B.; Balasubramanian, M.; Podsiadlo, P.; Johnson, C.S.; Rajh, T.; Shevchenko, E.V. Hollow iron oxide nanoparticles for application in lithium ion batteries. *Nano Lett.* **2012**, *5*, 2429–2435. [[CrossRef](#)]
161. Liu, J.; Jiang, R. Expression of heme oxygenase in the corpus cavernosum of castrated rats. *Natl. J. Androl.* **2009**, *15*, 212–217.
162. Kang, N.; Park, J.H.; Choi, J.; Jin, J.; Chun, J.; Jung, I.G.; Jeong, J.; Park, J.G.; Lee, S.M.; Kim, H.J.; et al. Nanoparticulate iron oxide tubes from microporous organic nanotubes as stable anode materials for lithium ion batteries. *Angew. Chem. Int. Ed.* **2012**, *51*, 6626–6630. [[CrossRef](#)]
163. Ma, X.H.; Feng, X.Y.; Song, C.; Zou, B.K.; Ding, C.X.; Yu, Y.; Chen, C.H. Facile synthesis of flower-like and yarn-like α -Fe₂O₃ spherical clusters as anode materials for lithium-ion batteries. *Electrochim. Acta* **2013**, *93*, 131–136. [[CrossRef](#)]
164. Mitra, S.; Poizot, P.; Finke, A.; Tarascon, J.M. Growth and electrochemical characterization versus lithium of Fe₃O₄ electrodes made via electrodeposition. *Adv. Funct. Mater.* **2006**, *16*, 2281–2287. [[CrossRef](#)]
165. Zhu, X.; Wu, W.; Liu, Z.; Li, L.; Hu, J.; Dai, H.; Ding, L.; Zhou, K.; Wang, C.; Song, X. A reduced graphene oxide-nanoporous magnetic oxide iron hybrid as an improved anode material for lithium ion batteries. *Electrochim. Acta* **2013**, *95*, 24–28. [[CrossRef](#)]
166. Furusawa, H.; Konishi, R.; Mori, D.; Horino, H.; Horiba, T.; Takeda, Y.; Takada, J.; Yamamoto, O.; Imanishi, N. Biogenous iron oxide (L-BIOX) as a high capacity anode material for lithium ion batteries. *Electrochim. Acta* **2018**, *281*, 227–236. [[CrossRef](#)]
167. Barreca, D.; Cruz-Yusta, M.; Gasparotto, A.; MacCato, C.; Morales, J.; Pozza, A.; Sada, C.; Sánchez, L.; Tondello, E. Cobalt oxide nanomaterials by vapor-phase synthesis for fast and reversible lithium storage. *J. Phys. Chem. C* **2010**, *21*, 10054–10060. [[CrossRef](#)]
168. Zhang, L.; Hu, P.; Zhao, X.; Tian, R.; Zou, R.; Xia, D. Controllable synthesis of core-shell Co@CoO nanocomposites with a superior performance as an anode material for lithium-ion batteries. *J. Mater. Chem.* **2011**, *21*, 18279–18283. [[CrossRef](#)]
169. Fei, L.; Lin, Q.; Yuan, B.; Naemi, M.; Xu, Y.; Li, Y.; Deng, S.; Luo, H. Controlling morphology and enhancing electrochemical performance of cobalt oxide by addition of graphite. *Mater. Lett.* **2013**, *257*, 421–443. [[CrossRef](#)]
170. Yuan, W.; Xie, D.; Dong, Z.; Su, Q.; Zhang, J.; Du, G.; Xu, B. Preparation of porous Co₃O₄ polyhedral architectures and its application as anode material in lithium-ion battery. *Mater. Lett.* **2013**, *97*, 129–132. [[CrossRef](#)]
171. Wang, F.; Lu, C.; Qin, Y.; Liang, C.; Zhao, M.; Yang, S.; Sun, Z.; Song, X. Solid state coalescence growth and electrochemical performance of plate-like Co₃O₄ mesocrystals as anode materials for lithium-ion batteries. *J. Power Sources* **2013**, *235*, 67–73. [[CrossRef](#)]
172. Li, C.C.; Li, Q.H.; Chen, L.B.; Wang, T.H. Topochemical synthesis of cobalt oxide nanowire arrays for high performance binderless lithium ion batteries. *J. Mater. Chem.* **2011**, *21*, 11867–11872. [[CrossRef](#)]
173. Binotto, G.; Larcher, D.; Prakash, A.S.; Herrera Urbina, R.; Hegde, M.S.; Tarascon, J.M. Synthesis, characterization, and li-electrochemical performance of highly porous Co₃O₄ powders. *Chem. Mater.* **2007**, *12*, 3032–3040. [[CrossRef](#)]
174. Guan, H.; Wang, X.; Li, H.; Zhi, C.; Zhai, T.; Bando, Y.; Golberg, D. CoO octahedral nanocages for high-performance lithium ion batteries. *Chem. Commun.* **2012**, *48*, 4878–4880. [[CrossRef](#)]
175. Wang, H.; Mao, N.; Shi, J.; Wang, Q.; Yu, W.; Wang, X. Cobalt oxide-carbon nanosheet nanoarchitecture as an anode for high-performance lithium-ion battery. *ACS Appl. Mater. Interfaces* **2015**, *7*, 2882–2890. [[CrossRef](#)]
176. Villeveille, C.; Robert, F.; Taberna, P.L.; Bazin, L.; Simon, P.; Monconduit, L. The good reactivity of lithium with nanostructured copper phosphide. *J. Mater. Chem.* **2008**, *18*, 5956–5960. [[CrossRef](#)]
177. Li, L.; Peng, Y.; Yang, H. Phase structure changes of MnP anode material during electrochemical lithiation and delithiation process. *Electrochim. Acta* **2013**, *95*, 230–236. [[CrossRef](#)]
178. Kim, M.G.; Cho, J. Reversible and high-capacity nanostructured electrode materials for li-ion batteries. *Adv. Funct. Mater.* **2009**, *14*, 1497–1514. [[CrossRef](#)]
179. Stan, M.C.; Klöpsch, R.; Bhaskar, A.; Li, J.; Passerini, S.; Winter, M. Cu₃P binary phosphide: Synthesis via a wet mechanochemical method and electrochemical behavior as negative electrode material for lithium-ion batteries. *Adv. Energy Mater.* **2013**, *3*, 231–238. [[CrossRef](#)]

180. Lu, Y.; Tu, J.-P.; Xiong, Q.-Q.; Xiang, J.-Y.; Mai, Y.-J.; Zhang, J.; Qiao, Y.-Q.; Wang, X.-L.; Gu, C.-D.; Mao, S.X. Controllable Synthesis of a Monophase Nickel Phosphide/Carbon (Ni₅P₄/C) Composite Electrode via Wet-Chemistry and a Solid-State Reaction for the Anode in Lithium Secondary Batteries. *Adv. Funct. Mater.* **2012**, *22*, 3927–3935. [CrossRef]
181. Aso, K.; Hayashi, A.; Tatsumisago, M. Synthesis of NiS-carbon fiber composites in high-boiling solvent to improve electrochemical performance in all-solid-state lithium secondary batteries. *Electrochim. Acta* **2012**, *83*, 448–453. [CrossRef]
182. Senoh, H.; Kageyama, H.; Takeuchi, T.; Nakanishi, K.; Ohta, T.; Sakaebe, H.; Yao, M.; Sakai, T.; Yasuda, K. Gallium (III) sulfide as an active material in lithium secondary batteries. *J. Power Sources* **2011**, *196*, 5631–5636. [CrossRef]
183. Paoletta, A.; George, C.; Povia, M.; Zhang, Y.; Krahne, R.; Gich, M.; Genovese, A.; Falqui, A.; Longobardi, M.; Guardia, P.; et al. Charge transport and electrochemical properties of colloidal greigite (Fe₃S₄) nanoplatelets. *Chem. Mater.* **2011**, *16*, 3762–3768. [CrossRef]
184. Sun, Q.; Li, W.J.; Fu, Z.W. A novel anode material of antimony nitride for rechargeable lithium batteries. *Solid State Sci.* **2010**, *12*, 397–403. [CrossRef]
185. Cabana, J.; Ionica-Bousquet, C.M.; Grey, C.P.; Palacín, M.R. High rate performance of lithium manganese nitride and oxynitride as negative electrodes in lithium batteries. *Electrochem. commun.* **2010**, *12*, 315–318. [CrossRef]
186. Wang, Y.; Wu, J.; Tang, Y.; Lü, X.; Yang, C.; Qin, M.; Huang, F.; Li, X.; Zhang, X. Phase-controlled synthesis of cobalt sulfides for lithium ion batteries. *ACS Appl. Mater. Interfaces* **2012**, *8*, 4246–4250. [CrossRef]
187. Xu, C.; Zeng, Y.; Rui, X.; Xiao, N.; Zhu, J.; Zhang, W.; Chen, J.; Liu, W.; Tan, H.; Hng, H.H.; et al. Controlled soft-template synthesis of ultrathin C@FeS nanosheets with high-Li-storage performance. *ACS Nano* **2012**, *6*, 4713–4721. [CrossRef] [PubMed]
188. Fu, Z.W.; Wang, Y.; Yue, X.L.; Zhao, S.L.; Qin, Q.Z. Electrochemical reactions of lithium with transition metal nitride electrodes. *J. Phys. Chem. B* **2004**, *7*, 2236–2244. [CrossRef]
189. Sun, Q.; Fu, Z.W. Vanadium nitride as a novel thin film anode material for rechargeable lithium batteries. *Electrochim. Acta* **2008**, *54*, 403–409. [CrossRef]
190. Pereira, N.; Dupont, L.; Tarascon, J.M.; Klein, L.C.; Amatucci, G.G. Electrochemistry of Cu₃N with Lithium: A Complex System with Parallel Processes. *J. Electrochem. Soc.* **2003**, *159*, A1273. [CrossRef]
191. Das, B.; Reddy, M.V.; Malar, P.; Osipowicz, T.; Subba Rao, G.V.; Chowdari, B.V.R. Nanoflake CoN as a high capacity anode for Li-ion batteries. *Solid State Ion.* **2009**, *180*, 1061–1068. [CrossRef]
192. Gillot, F.; Oró-Solé, J.; Palacín, M.R. Nickel nitride as negative electrode material for lithium ion batteries. *J. Mater. Chem.* **2011**, *21*, 9997–10002. [CrossRef]
193. Landi, B.J.; Ganter, M.J.; Cress, C.D.; DiLeo, R.A.; Raffaele, R.P. Carbon nanotubes for lithium ion batteries. *Energy Environ. Sci.* **2009**, *2*, 638–654. [CrossRef]
194. Besenhard, J.O.; Yang, J.; Winter, M. Will advanced lithium-alloy anodes have a chance in lithium-ion batteries? *J. Power Sources* **1997**, *68*, 87–90. [CrossRef]
195. Whittingham, M.S. Inorganic nanomaterials for batteries. *J. Chem. Soc. Dalton Trans.* **2008**, *40*, 5424–5431. [CrossRef] [PubMed]
196. Winter, M.; Besenhard, J.O. Electrochemical lithiation of tin and tin-based intermetallics and composites. *Electrochim. Acta* **1999**, *45*, 31–50. [CrossRef]
197. Park, C.M.; Sohn, H.J. Quasi-intercalation and facile amorphization in layered ZnSb for Li-ion batteries. *Adv. Mater.* **2010**, *22*, 47–52. [CrossRef] [PubMed]
198. Hewitt, K.C.; Beaulieu, L.Y.; Dahn, J.R. Electrochemistry of InSb as a Li Insertion Host: Problems and Prospects. *J. Electrochem. Soc.* **2001**, *148*, A402. [CrossRef]
199. Whittingham, M.S.; Gamble, F.R. The lithium intercalates of the transition metal dichalcogenides. *Mater. Res. Bull.* **1975**, *10*, 363–371. [CrossRef]
200. Lithium-ion Battery. Available online: https://en.wikipedia.org/wiki/Lithium-ion_battery (accessed on 8 June 2020).
201. Whittingham, M.S. Electrical energy storage and intercalation chemistry. *Science* **1976**, *192*, 1126–1127. [CrossRef] [PubMed]
202. Schipper, F.; Erickson, E.M.; Erk, C.; Shin, J.-Y.; Chesneau, F.F.; Aurbach, D. Review—Recent Advances and Remaining Challenges for Lithium Ion Battery Cathodes. *J. Electrochem. Soc.* **2017**, *164*, A6220. [CrossRef]

203. Jung, Y.S.; Cavanagh, A.S.; Dillon, A.C.; Groner, M.D.; George, S.M.; Lee, S.-H. Enhanced Stability of LiCoO₂ Cathodes in Lithium-Ion Batteries Using Surface Modification by Atomic Layer Deposition. *J. Electrochem. Soc.* **2010**, *157*, 1.
204. Cho, J.; Kim, Y.J.; Kim, T.J.; Park, B. Zero-strain intercalation cathode for rechargeable Li-Ion cell. *Angew. Chem. Int. Ed.* **2001**, *40*, 3367–3369. [[CrossRef](#)]
205. Chen, Z.; Dahn, J.R. Methods to obtain excellent capacity retention in LiCoO₂ cycled to 4.5 V. *Electrochim. Acta* **2004**, *49*, 1079–1090. [[CrossRef](#)]
206. Wang, K.; Wan, J.; Xiang, Y.; Zhu, J.; Leng, Q.; Wang, M.; Xu, L.; Yang, Y. Recent advances and historical developments of high voltage lithium cobalt oxide materials for rechargeable Li-ion batteries. *J. Power Sources* **2020**, *46*, 3006–3059. [[CrossRef](#)]
207. Kim, Y.J.; Cho, J.; Kim, T.-J.; Park, B. Suppression of Cobalt Dissolution from the LiCoO₂ Cathodes with Various Metal-Oxide Coatings. *J. Electrochem. Soc.* **2003**, *150*, 2. [[CrossRef](#)]
208. Cho, J.; Kim, Y.J.; Park, B. Novel LiCoO₂ cathode material with Al₂O₃ coating for a Li ion cell. *Chem. Mater.* **2000**, *12*, 3788–3791. [[CrossRef](#)]
209. MacNeil, D.D.; Dahn, J.R. The Reaction of Charged Cathodes with Nonaqueous Solvents and Electrolytes: I. Li_{0.5}CoO₂. *J. Electrochem. Soc.* **2001**, *148*, 1.
210. Dahn, J.R.; von Sacken, U.; Juzkow, M.W.; Aljanaby, H. Rechargeable LiNiO₂ carbon cells. *J. Electrochem. Soc.* **1991**, *138*, 8. [[CrossRef](#)]
211. Dahn, J.R.; von Sacken, U.; Michal, C.A. Structure and electrochemistry of Li_{1±y}NiO₂ and a new Li₂NiO₂ phase with the Ni(OH)₂ structure. *Solid State Ionics* **1990**, *44*, 87–97. [[CrossRef](#)]
212. Dyer, L.D.; Borie, B.S.; Smith, G.P. Alkali Metal-Nickel Oxides of the Type MNiO₂. *J. Am. Chem. Soc.* **1954**, *76*, 1499–1503. [[CrossRef](#)]
213. Ohzuku, T. Electrochemistry and Structural Chemistry of LiNiO₂(R3m) for 4 Volt Secondary Lithium Cells. *J. Electrochem. Soc.* **1993**, *147*, 1862. [[CrossRef](#)]
214. Zhang, Q.; Uchaker, E.; Candelaria, S.L.; Cao, G. Nanomaterials for energy conversion and storage. *Chem. Soc. Rev.* **2013**, *42*, 3127–3171. [[CrossRef](#)]
215. Li, W.; Reimers, J.N.; Dahn, J.R. In situ x-ray diffraction and electrochemical studies of Li_{1-x}NiO₂. *Solid State Ion.* **1993**, *67*, 123–130. [[CrossRef](#)]
216. Kang, K.; Ceder, G. Factors that affect Li mobility in layered lithium transition metal oxides. *Phys. Rev. B Condens. Matter Mater. Phys.* **2006**, *74*, 094105. [[CrossRef](#)]
217. Kim, U.H.; Kuo, L.Y.; Kaghazchi, P.; Yoon, C.S.; Sun, Y.K. Quaternary Layered Ni-Rich NCMA Cathode for Lithium-Ion Batteries. *ACS Energy Lett.* **2019**, *2*, 576–582. [[CrossRef](#)]
218. Zhang, Y.; Cao, H.; Zhang, J.; Xia, B. Synthesis of LiNi_{0.6}Co_{0.2}Mn_{0.2}O₂ cathode material by a carbonate co-precipitation method and its electrochemical characterization. *Solid State Ionics* **2006**, *177*, 3303–3307. [[CrossRef](#)]
219. Lin, S.P.; Fung, K.Z.; Hon, Y.M.; Hon, M.H. Effect of Al addition on formation of layer-structured LiNiO₂. *J. Solid State Chem.* **2002**, *167*, 97–106. [[CrossRef](#)]
220. Li, J.; Daniel, C.; Wood, D. Materials processing for lithium-ion batteries. *J. Power Sources* **2011**, *196*, 2452–2460. [[CrossRef](#)]
221. Rougier, A.; Saadoune, I.; Gravereau, P.; Willmann, P.; Delmas, C. Effect of cobalt substitution on cationic distribution in LiNi_{1-y}CO_yO₂ electrode materials. *Solid State Ionics* **1996**, *90*, 83–90. [[CrossRef](#)]
222. Zhecheva, E.; Stoyanova, R. Stabilization of the layered crystal structure of LiNiO₂ by Co-substitution. *Solid State Ion.* **1993**, *66*, 143–149. [[CrossRef](#)]
223. Ohzuku, T.; Ueda, A.; Nagayama, M.; Iwakoshi, Y.; Komori, H. Comparative study of LiCoO₂, LiNi₁₂Co₁₂O₂ and LiNiO₂ for 4 volt secondary lithium cells. *Electrochim. Acta* **1993**, *38*, 1159–1167. [[CrossRef](#)]
224. Nishida, Y.; Nakane, K.; Satoh, T. Synthesis and properties of gallium-doped LiNiO₂ as the cathode material for lithium secondary batteries. *J. Power Sources* **1997**, *68*, 561–564. [[CrossRef](#)]
225. Delmas, C.; Pérès, J.P.; Rougier, A.; Demourgues, A.; Weill, F.; Chadwick, A.; Broussely, M.; Pertion, F.; Biensan, P.; Willmann, P. On the behavior of the Li_xNiO₂ system: An electrochemical and structural overview. *J. Power Sources* **1997**, *68*, 120–125. [[CrossRef](#)]
226. Rim, H.; Song, J.; Mumm, D.R. Electrochemical characteristics of LiNi_{0.7}Co_{0.3}O₂ synthesized at 850 C from carbonates or oxides of Li, Ni, and Co. *Ceram. Int.* **2014**, *40*, 3511–3516.

227. Croguennec, L.; Deniard, P.; Brec, R. Electrochemical cyclability of orthorhombic LiMnO_2 characterization of cycled materials. *J. Electrochem. Soc.* **1997**, *144*, 10. [[CrossRef](#)]
228. Davidson, I.J.; McMillan, R.S.; Murray, J.J.; Greedan, J.E. Lithium-ion cell based on orthorhombic LiMnO_2 . *J. Power Sources* **1995**, *54*, 232–235. [[CrossRef](#)]
229. Mishra, S.K.; Ceder, G. Structural stability of lithium manganese oxides. *Phys. Rev. B Condens. Matter Mater. Phys.* **1999**, *59*, 6120. [[CrossRef](#)]
230. Capitaine, F.; Gravereau, P.; Delmas, C. A new variety of LiMnO_2 with a layered structure. *Solid State Ion.* **1996**, *89*, 197–202. [[CrossRef](#)]
231. Armstrong, A.R.; Bruce, P.G. Synthesis of layered LiMnO_2 as an electrode for rechargeable lithium batteries. *Nature* **1996**, *381*, 499–500. [[CrossRef](#)]
232. Chen, R.; Zavalij, P.; Whittingham, M.S. Hydrothermal synthesis and characterization of $\text{K}_x\text{MnO}_2 \cdot y\text{H}_2\text{O}$. *Chem. Mater.* **1996**, *8*, 1275–1280. [[CrossRef](#)]
233. Bruce, P.G.; Armstrong, A.R.; Gitzendanner, R.L. New intercalation compounds for lithium batteries: Layered LiMnO_2 . *J. Mater. Chem.* **1999**, *9*, 193–198. [[CrossRef](#)]
234. Bubulinca, C.; Sapurina, I.; Kazantseva, N.E.; Vilčáková, J.; Cheng, Q.; Saha, P. Fabrication of a flexible binder-free lithium manganese oxide cathode for secondary Li-Ion batteries. *J. Phys. Chem. Solids* **2020**, *137*, 109222. [[CrossRef](#)]
235. Ohzuku, T.; Makimura, Y. Layered lithium insertion material of $\text{LiNi}_{1/2}\text{Mn}_{1/2}\text{O}_2$: A possible alternative to LiCoO_2 for advanced lithium-ion batteries. *Chem. Lett.* **2001**, *30*, 744–745. [[CrossRef](#)]
236. Hautier, G.; Jain, A.; Ong, S.P.; Kang, B.; Moore, C.; Doe, R.; Ceder, G. Phosphates as lithium-ion battery cathodes: An evaluation based on high-throughput ab initio calculations. *Chem. Mater.* **2011**, *23*, 3495–3508. [[CrossRef](#)]
237. Aravindan, V.; Gnanaraj, J.; Lee, Y.S.; Madhavi, S. LiMnPO_4 —A next generation cathode material for lithium-ion batteries. *J. Mater. Chem. A* **2013**, *1*, 3518–3539. [[CrossRef](#)]
238. Oh, W.; Park, H.; Jin, B.-S.; Thangavel, R.; Yoon, W.-S. Understanding the structural phase transitions in lithium vanadium phosphate cathodes for lithium-ion batteries. *J. Mater. Chem. A* **2020**, *8*, 10331–10336. [[CrossRef](#)]
239. Zheng, Q.; Yamada, Y.; Shang, R.; Ko, S.; Lee, Y.Y.; Kim, K.; Nakamura, E.; Yamada, A. A cyclic phosphate-based battery electrolyte for high voltage and safe operation. *Nat. Energy* **2020**, *5*, 291–298. [[CrossRef](#)]
240. Li, T.; Li, L.; Cao, Y.L.; Ai, X.P.; Yang, H.X. Reversible three-electron redox behaviors of FeF_3 nanocrystals as high-capacity cathode-active materials for Li-Ion batteries. *J. Phys. Chem. C* **2010**, *114*, 3190–3195. [[CrossRef](#)]
241. Huang, Q.; Turcheniuk, K.; Ren, X.; Magasinski, A.; Song, A.Y.; Xiao, Y.; Kim, D.; Yushin, G. Cycle stability of conversion-type iron fluoride lithium battery cathode at elevated temperatures in polymer electrolyte composites. *Nat. Mater.* **2019**, *18*, 1343–1349. [[CrossRef](#)]
242. Li, C.; Gu, L.; Tsukimoto, S.; Van Aken, P.A.; Maier, J. Low-temperature ionic-liquid-based synthesis of nanostructured iron-based fluoride cathodes for lithium batteries. *Adv. Mater.* **2010**, *22*, 3650–3654. [[CrossRef](#)]
243. Plitz, I.; Badway, F.; Al-Sharab, J.; DuPasquier, A.; Cosandey, F.; Amatucci, G.G. Structure and Electrochemistry of Carbon-Metal Fluoride Nanocomposites Fabricated by Solid-State Redox Conversion Reaction. *J. Electrochem. Soc.* **2005**, *152*, A107. [[CrossRef](#)]
244. Chen, C.; Xu, X.; Chen, S.; Zheng, B.; Shui, M.; Xu, L.; Zheng, W.; Shu, J.; Cheng, L.; Feng, L.; et al. The preparation and characterization of iron fluorides polymorphs $\text{FeF}_3 \cdot 0.33\text{H}_2\text{O}$ and $\beta\text{-FeF}_3 \cdot 3\text{H}_2\text{O}$ as cathode materials for lithium-ion batteries. *Mater. Res. Bull.* **2015**, *64*, 187–193. [[CrossRef](#)]
245. Ma, Y.; Huang, A.; Zhou, H.; Ji, S.; Zhang, S.; Li, R.; Yao, H.; Cao, X.; Jin, P. Template-free formation of various V_2O_5 hierarchical structures as cathode materials for lithium-ion batteries. *J. Mater. Chem. A* **2017**, *5*, 6522–6531. [[CrossRef](#)]
246. Liu, J.; Xia, H.; Xue, D.; Lu, L. Double-shelled nanocapsules of V_2O_5 -based composites as high-performance anode and cathode materials for Li ion batteries. *J. Am. Chem. Soc.* **2009**, *131*, 12086–12087. [[CrossRef](#)] [[PubMed](#)]
247. Pan, A.; Wu, H.B.; Yu, L.; Lou, X.W. Template-free synthesis of VO_2 hollow microspheres with various interiors and their conversion into V_2O_5 for lithium-ion batteries. *Angew. Chem. Int. Ed.* **2013**, *125*, 2282–2286. [[CrossRef](#)]
248. Li, G.; Qiu, Y.; Hou, Y.; Li, H.; Zhou, L.; Deng, H.; Zhang, Y. Synthesis of V_2O_5 hierarchical structures for long cycle-life lithium-ion storage. *J. Mater. Chem. A* **2015**, *3*, 1103–1109. [[CrossRef](#)]

249. Cong, L.; Lei, K.; Wang, J.; Wang, J.; Meng, H.; Cheng, F.; Chen, J. Progress in surface coating on $\text{LiNi}_{0.8}\text{Co}_{0.15}\text{Al}_{0.05}\text{O}_2$ cathode materials for lithium-ion batteries. *Chin. Sci. Bull.* **2016**, *61*, 2216–2226. [[CrossRef](#)]
250. Zeng, X.; Li, J.; Singh, N. Recycling of spent lithium-ion battery: A critical review. *Crit. Rev. Environ. Sci. Technol.* **2014**, *44*, 1129–1165. [[CrossRef](#)]
251. Doerffel, D.; Sharkh, S.A. A critical review of using the Peukert equation for determining the remaining capacity of lead-acid and lithium-ion batteries. *J. Power Sources* **2006**, *155*, 395–400. [[CrossRef](#)]
252. Xu, J.; Thomas, H.R.; Francis, R.W.; Lum, K.R.; Wang, J.; Liang, B. A review of processes and technologies for the recycling of lithium-ion secondary batteries. *J. Power Sources* **2008**, *177*, 512–527. [[CrossRef](#)]
253. Li, L.; Zhang, X.; Li, M.; Chen, R.; Wu, F.; Amine, K.; Lu, J. The Recycling of Spent Lithium-Ion Batteries: A Review of Current Processes and Technologies. *Electrochem. Energy Rev.* **2018**, *1*, 461–482. [[CrossRef](#)]
254. Shin, S.M.; Kim, N.H.; Sohn, J.S.; Yang, D.H.; Kim, Y.H. Development of a metal recovery process from Li-ion battery wastes. *Hydrometallurgy* **2005**, *79*, 172–181. [[CrossRef](#)]
255. Pagnanelli, F.; Moscardini, E.; Altimari, P.; Abo Atia, T.; Toro, L. Leaching of electrodic powders from lithium ion batteries: Optimization of operating conditions and effect of physical pretreatment for waste fraction retrieval. *Waste Manag.* **2017**, *60*, 706–715. [[CrossRef](#)]
256. Li, J.; Shi, P.; Wang, Z.; Chen, Y.; Chang, C.C. A combined recovery process of metals in spent lithium-ion batteries. *Chemosphere* **2009**, *77*, 1132–1136. [[CrossRef](#)] [[PubMed](#)]
257. Dunn, J.B.; Gaines, L.; Sullivan, J.; Wang, M.Q. Impact of recycling on cradle-to-gate energy consumption and greenhouse gas emissions of automotive lithium-ion batteries. *Environ. Sci. Technol.* **2012**, *22*, 12704–12710. [[CrossRef](#)] [[PubMed](#)]
258. Oliveira, L.; Messagie, M.; Rangaraju, S.; Sanfelix, J.; Hernandez Rivas, M.; Van Mierlo, J. Key issues of lithium-ion batteries—From resource depletion to environmental performance indicators. *J. Clean. Prod.* **2015**, *108*, 354–362. [[CrossRef](#)]
259. Kraysberg, A.; Ein-Eli, Y.; Kraysberg, A.; Ein-Eli, Y. Higher, stronger, better... A review of 5 volt cathode materials for advanced lithium-ion batteries. *Adv. Energy Mater.* **2012**, *2*, 922–939. [[CrossRef](#)]
260. Huang, B.; Li, X.; Wang, Z.; Guo, H.; Shen, L.; Wang, J. A comprehensive study on electrochemical performance of Mn-surface-modified $\text{LiNi}_{0.8}\text{Co}_{0.15}\text{Al}_{0.05}\text{O}_2$ synthesized by an in situ oxidizing-coating method. *J. Power Sources* **2014**, *252*, 200–207. [[CrossRef](#)]
261. Massé, R.C.; Uchaker, E.; Cao, G. Beyond Li-ion: Electrode materials for sodium- and magnesium-ion batteries. *Sci. China Mater.* **2015**, *58*, 715–766. [[CrossRef](#)]
262. Huang, B.; Yang, J.; Li, Y.; Xiao, S.; Chen, Q. Carbon encapsulated Sn-Co alloy: A stabilized tin-based material for sodium storage. *Mater. Lett.* **2018**, *210*, 321–324. [[CrossRef](#)]
263. Velázquez-Martínez, O.; Porvali, A.; van den Boogaart, K.G.; Santasalo-Aarnio, A.; Lundström, M.; Reuter, M.; Serna-Guerrero, R. On the use of statistical entropy analysis as assessment parameter for the comparison of lithium-ion battery recycling processes. *Batteries* **2019**, *5*, 41. [[CrossRef](#)]
264. Chen, X.; Chen, Y.; Zhou, T.; Liu, D.; Hu, H.; Fan, S. Hydrometallurgical recovery of metal values from sulfuric acid leaching liquor of spent lithium-ion batteries. *Waste Manag.* **2015**, *38*, 349–356. [[CrossRef](#)]
265. Chen, J.; Proctor, R.W. Influence of response-effect feedback on learning and performance of a complex key-pressing task: Morin and grant (1955) revisited. *Am. J. Psychol.* **2015**, *128*, 197–208. [[CrossRef](#)]
266. Menad, N.; Björkman, B.; Allain, E.G. Combustion of plastics contained in electric and electronic scrap. *Resour. Conserv. Recycl.* **1998**, *24*, 65–85. [[CrossRef](#)]
267. Zhang, P.; Yokoyama, T.; Itabashi, O.; Suzuki, T.M.; Inoue, K. Hydrometallurgical process for recovery of metal values from spent lithium-ion secondary batteries. *Hydrometallurgy* **1998**, *47*, 259–271. [[CrossRef](#)]
268. Nan, J.; Han, D.; Zuo, X. Recovery of metal values from spent lithium-ion batteries with chemical deposition and solvent extraction. *J. Power Sources* **2005**, *152*, 278–284. [[CrossRef](#)]
269. Bahaloo-Horeh, N.; Mousavi, S.M. Enhanced recovery of valuable metals from spent lithium-ion batteries through optimization of organic acids produced by *Aspergillus niger*. *Waste Manag.* **2017**, *60*, 666–679. [[CrossRef](#)] [[PubMed](#)]
270. Meshram, P.; Pandey, B.D.; Mankhand, T.R. Recovery of valuable metals from cathodic active material of spent lithium ion batteries: Leaching and kinetic aspects. *Waste Manag.* **2015**, *45*, 306–313. [[CrossRef](#)]
271. Jha, M.K.; Kumari, A.; Jha, A.K.; Kumar, V.; Hait, J.; Pandey, B.D. Recovery of lithium and cobalt from waste lithium ion batteries of mobile phone. *Waste Manag.* **2013**, *33*, 1890–1897. [[CrossRef](#)]

272. Zhu, S.G.; He, W.Z.; Li, G.M.; Zhou, X.; Zhang, X.J.; Huang, J.W. Recovery of Co and Li from spent lithium-ion batteries by combination method of acid leaching and chemical precipitation. *Trans. Nonferr. Met. Soc. China Engl. Ed.* **2012**, *22*, 2274–2281. [[CrossRef](#)]
273. Kang, J.; Senanayake, G.; Sohn, J.; Shin, S.M. Recovery of cobalt sulfate from spent lithium ion batteries by reductive leaching and solvent extraction with Cyanex 272. *Hydrometallurgy* **2010**, *100*, 168–171. [[CrossRef](#)]
274. Swain, B.; Jeong, J.; Lee, J.C.; Lee, G.H.; Sohn, J.S. Hydrometallurgical process for recovery of cobalt from waste cathodic active material generated during manufacturing of lithium ion batteries. *J. Power Sources* **2007**, *167*, 536–544. [[CrossRef](#)]
275. Lee, C.K.; Rhee, K.I. Reductive leaching of cathodic active materials from lithium ion battery wastes. *Hydrometallurgy* **2003**, *68*, 5–10. [[CrossRef](#)]
276. Castillo, S.; Ansart, F.; Laberty-Robert, C.; Portal, J. Advances in the recovering of spent lithium battery compounds. *J. Power Sources* **2002**, *112*, 247–254. [[CrossRef](#)]
277. Joulié, M.; Laucournet, R.; Billy, E. Hydrometallurgical process for the recovery of high value metals from spent lithium nickel cobalt aluminum oxide based lithium-ion batteries. *J. Power Sources* **2014**, *247*, 551–555. [[CrossRef](#)]
278. Yao, Y.; Zhu, M.; Zhao, Z.; Tong, B.; Fan, Y.; Hua, Z. Hydrometallurgical Processes for Recycling Spent Lithium-Ion Batteries: A Critical Review. *ACS Sustain. Chem. Eng.* **2018**, *6*, 13611–13627. [[CrossRef](#)]
279. Pinna, E.G.; Ruiz, M.C.; Ojeda, M.W.; Rodriguez, M.H. Cathodes of spent Li-ion batteries: Dissolution with phosphoric acid and recovery of lithium and cobalt from leach liquors. *Hydrometallurgy* **2017**, *167*, 66–71. [[CrossRef](#)]
280. Chen, W.S.; Ho, H.J. Recovery of valuable metals from lithium-ion batteries NMC cathode waste materials by hydrometallurgical methods. *Metals (Basel)* **2018**, *8*, 321. [[CrossRef](#)]
281. Chen, X.; Fan, B.; Xu, L.; Zhou, T.; Kong, J. An atom-economic process for the recovery of high value-added metals from spent lithium-ion batteries. *J. Clean. Prod.* **2016**, *112*, 3562–3570. [[CrossRef](#)]
282. Nayaka, G.P.; Manjanna, J.; Pai, K.V.; Vadavi, R.; Keny, S.J.; Tripathi, V.S. Recovery of valuable metal ions from the spent lithium-ion battery using aqueous mixture of mild organic acids as alternative to mineral acids. *Hydrometallurgy* **2015**, *151*, 73–77. [[CrossRef](#)]
283. Zeng, X.; Li, J.; Shen, B. Novel approach to recover cobalt and lithium from spent lithium-ion battery using oxalic acid. *J. Hazard. Mater.* **2015**, *295*, 112–118. [[CrossRef](#)]
284. Sun, L.; Qiu, K. Organic oxalate as leachant and precipitant for the recovery of valuable metals from spent lithium-ion batteries. *Waste Manag.* **2012**, *32*, 1575–1582. [[CrossRef](#)]
285. Peng, C.; Liu, F.; Aji, A.T.; Wilson, B.P.; Lundström, M. Extraction of Li and Co from industrially produced Li-ion battery waste—Using the reductive power of waste itself. *Waste Manag.* **2019**, *95*, 604–611. [[CrossRef](#)] [[PubMed](#)]
286. Ho, H.J.; Chen, W.S.; Wang, W.Y. Recovery of valuable metals from lithium-ion batteries cathode material by leaching and solvent extraction. In Proceedings of the 14th International Symposium on East Asian Resources Recycling Technology, Hokkaido, Japan, 26–29 September 2017.
287. Anjum, F.; Shahid, M.; Akcil, A. Biohydrometallurgy techniques of low grade ores: A review on black shale. *Hydrometallurgy* **2012**, *117*, 1–12. [[CrossRef](#)]
288. Pant, D.; Joshi, D.; Upreti, M.K.; Kotnala, R.K. Chemical and biological extraction of metals present in E waste: A hybrid technology. *Waste Manag.* **2012**, *32*, 979–990. [[CrossRef](#)] [[PubMed](#)]
289. Mishra, D.; Kim, D.J.; Ralph, D.E.; Ahn, J.G.; Rhee, Y.H. Bioleaching of metals from spent lithium ion secondary batteries using *Acidithiobacillus ferrooxidans*. *Waste Manag.* **2008**, *28*, 333–338. [[CrossRef](#)] [[PubMed](#)]
290. Chen, X.; Kang, D.; Cao, L.; Li, J.; Zhou, T.; Ma, H. Separation and recovery of valuable metals from spent lithium ion batteries: Simultaneous recovery of Li and Co in a single step. *Sep. Purif. Technol.* **2019**, *210*, 690–697. [[CrossRef](#)]
291. Niu, Z.; Zou, Y.; Xin, B.; Chen, S.; Liu, C.; Li, Y. Process controls for improving bioleaching performance of both Li and Co from spent lithium ion batteries at high pulp density and its thermodynamics and kinetics exploration. *Chemosphere* **2014**, *109*, 92–98. [[CrossRef](#)]
292. Golmohammadzadeh, R.; Faraji, F.; Rashchi, F. Recovery of lithium and cobalt from spent lithium ion batteries (LIBs) using organic acids as leaching reagents: A review. *Resour. Conserv. Recycl.* **2018**, *136*, 418–435. [[CrossRef](#)]

293. Mantuano, D.P.; Dorella, G.; Elias, R.C.A.; Mansur, M.B. Analysis of a hydrometallurgical route to recover base metals from spent rechargeable batteries by liquid-liquid extraction with Cyanex 272. *J. Power Sources* **2006**, *159*, 1510–1518. [[CrossRef](#)]
294. Torkaman, R.; Asadollahzadeh, M.; Torab-Mostaedi, M.; Ghanadi Maragheh, M. Recovery of cobalt from spent lithium ion batteries by using acidic and basic extractants in solvent extraction process. *Sep. Purif. Technol.* **2017**, *186*, 318–325. [[CrossRef](#)]
295. Pranolo, Y.; Zhang, W.; Cheng, C.Y. Recovery of metals from spent lithium-ion battery leach solutions with a mixed solvent extractant system. *Hydrometallurgy* **2010**, *102*, 37–42. [[CrossRef](#)]
296. Chen, X.; Ma, H.; Luo, C.; Zhou, T. Recovery of valuable metals from waste cathode materials of spent lithium-ion batteries using mild phosphoric acid. *J. Hazard. Mater.* **2017**, *326*, 77–86. [[CrossRef](#)]
297. Cerpa, A.; Alguacil, F.J. Separation of cobalt and nickel from acidic sulfate solutions using mixtures of di(2-ethylhexyl)phosphoric acid (DP-8R) and hydroxyoxime (ACORGA M5640). *J. Chem. Technol. Biotechnol.* **2004**, *79*, 455–460. [[CrossRef](#)]
298. Suzuki, T.; Nakamura, T.; Inoue, Y.; Niinae, M.; Shibata, J. A hydrometallurgical process for the separation of aluminum, cobalt, copper and lithium in acidic sulfate media. *Sep. Purif. Technol.* **2012**, *98*, 396–401. [[CrossRef](#)]
299. Chen, L.; Tang, X.; Zhang, Y.; Li, L.; Zeng, Z.; Zhang, Y. Process for the recovery of cobalt oxalate from spent lithium-ion batteries. *Hydrometallurgy* **2011**, *108*, 80–86. [[CrossRef](#)]
300. Wang, F.; He, F.; Zhao, J.; Sui, N.; Xu, L.; Liu, H. Extraction and separation of cobalt(II), copper(II) and manganese(II) by Cyanex272, PC-88A and their mixtures. *Sep. Purif. Technol.* **2012**, *93*, 8–14. [[CrossRef](#)]
301. Contestabile, M.; Panero, S.; Scrosati, B. A laboratory-scale lithium battery recycling process. *J. Power Sources* **1999**, *92*, 65–69. [[CrossRef](#)]
302. Freitas, M.B.J.G.; Garcia, E.M. Electrochemical recycling of cobalt from cathodes of spent lithium-ion batteries. *J. Power Sources* **2007**, *171*, 953–959. [[CrossRef](#)]
303. Myoung, J.; Jung, Y.; Lee, J.; Tak, Y. Cobalt oxide preparation from waste LiCoO₂ by electrochemical-hydrothermal method. *J. Power Sources* **2002**, *112*, 639–642. [[CrossRef](#)]
304. Chen, J.; Li, Q.; Song, J.; Song, D.; Zhang, L.; Shi, X. Environmentally friendly recycling and effective repairing of cathode powders from spent LiFePO₄ batteries. *Green Chem.* **2016**, *18*, 2500–2506. [[CrossRef](#)]
305. Rothermel, S.; Evertz, M.; Kasnatscheew, J.; Qi, X.; Grützke, M.; Winter, M.; Nowak, S. Graphite Recycling from Spent Lithium-Ion Batteries. *ChemSusChem* **2016**, *9*, 3473–3484. [[CrossRef](#)]
306. Grützke, M.; Mönnighoff, X.; Horsthemke, F.; Kraft, V.; Winter, M.; Nowak, S. Extraction of lithium-ion battery electrolytes with liquid and supercritical carbon dioxide and additional solvents. *RSC Adv.* **2015**, *5*, 43209–43217. [[CrossRef](#)]
307. Wang, X.; Gaustad, G.; Babbitt, C.W. Targeting high value metals in lithium-ion battery recycling via shredding and size-based separation. *Waste Manag.* **2016**, *54*, 203–214. [[CrossRef](#)] [[PubMed](#)]
308. Diekmann, J.; Hanisch, C.; Froböse, L.; Schällicke, G.; Loellhoeffel, T.; Fölster, A.-S.; Kwade, A. Ecological Recycling of Lithium-Ion Batteries from Electric Vehicles with Focus on Mechanical Processes. *J. Electrochem. Soc.* **2017**, *164*, A6184. [[CrossRef](#)]
309. Harper, G.; Sommerville, R.; Kendrick, E.; Driscoll, L.; Slater, P.; Stolkin, R.; Walton, A.; Christensen, P.; Heidrich, O.; Lambert, S.; et al. Recycling lithium-ion batteries from electric vehicles. *Nature* **2019**, *575*, 75–86. [[CrossRef](#)]

